A FRAMEWORK FOR THE RECONSTITUTION OF MEMBRANE PROTEINS

Inauguraldissertation

Zur Erlangung der Würde eines Doktors der Philosophie
vorgelegt der
Philosophisch-Naturwissenschaftlichen Fakultät der Universität Basel

von

Roland Goers

aus Aachen, Deutschland

Basel, 2018

Genehmigt von der Philosophisch-Naturwissenschaftlichen Fakultät
auf Antrag von

Prof. Dr. Wolfgang Meier
(Universität Basel)
Fakultätsverantwortlicher/Dissertationsleiter

Prof. Dr. Daniel Müller
(Eidgenössische Technische Hochschule Zürich)
Korreferent

Prof. Dr. Martin Spiess
(Dekan)

Basel, den 24.04.2018

DON’T TRY.

CHARLES BUKOWSKI

I THINK IT IS IMPORTANT FOR SOFTWARE TO AVOID IMPOSING A COGNITIVE STYLE ON WORKERS AND THEIR WORK.

EDWARD TUFTE

ROLAND GOERS

A FRAMEWORK FOR THE RECONSTITUTION OF MEMBRANE PROTEINS

Summary

Over the last decade, several artificial devices, imitating functionalities found in nature, have emerged in the field of synthetic biology. Often they resemble cellular vesicles which carry out a defined function and where molecular transport is mediated via specific membrane proteins. This work describes the creation of a framework for the reconstitution of membrane proteins into synthetic membranes. The study of membrane proteins in terms of their structure (*e.g.* protein crystallization) and their detailed functionality requires the isolation and re-insertion into a non-native environment. A process called reconstitution which is considered delicate. Beside the commonly used phospholipids, which are part of the natural cell membrane, a membrane environment can be created by the use of amphiphilic block copolymers. Driven by self-assembly, these molecules can be used as a platform for nano-devices, as they can be decorated with active molecular compounds and the resulting membrane can incorporate membrane proteins. Various factors and their interplay and dependencies affect the outcome of the reconstitution of membrane proteins into synthetic membranes. Identifying the key factors and predicting their effect *a priori* is a challenging task. Reliable and systematic approaches are available for lipid based systems but, up to now, not for polymeric ones. A well-established method in the fields of chemical and process engineering is design of experiments. This statistical tool provides a way to do experimental planning systematically and assess the effects and interactions of factors on a measurable response. Within this thesis, this framework was applied to the reconstitution of the light-driven proton pump proteorhodopsin into membranes for the first time. As proteorhodopsin provides a vectorial transport of protons across a membrane, its orientation is critical for its use as an energy generator in a synthetic system. Six factors were studied: the polarization of the membrane, the pH value during reconstitution, the lipid to protein ratio, the salt concentration in the buffer, the amount of detergent used and the effect of the addition of the ionophore valinomycin. Two insertion pathways were identified for proteorhodopsin: *i)* charge assisted and *ii)* detergent mediated. Both of them result in functional proteoliposomes which exhibit the formation of a proton gradient upon illumination. The conditions of the reconstitution decide which path will be taken, as detergent concentrations around 0.5 % will induce the detergent mediated pathway and the combination of a polarized membrane

together with higher detergent concentrations around 1 % will induce the charge assisted pathway. It is noteworthy that this study provides evidence that the detergent mediated one is dominant, as at 0.5 % detergent, an increased membrane charge does not affect the result. Transferring the knowledge gained towards polymeric systems, the second part of this study aims to investigate and compare the reconstitution of proteorhodopsin into polymer and lipid vesicles. As data from successful reconstitutions into polymersomes is rare, a lipid based system was used as a benchmark. Similar to the former chapter presented here, statistical modeling takes a significant part. Efficient one-step screening and optimization designs were employed to examine the assembly process of both membrane types together with proteorhodopsin. It could be revealed that both systems react differently to changing parameter combinations. The assembly of proteopolymersomes has stronger pH dependency compared to proteoliposomes and the addition of detergent does not show the membrane saturation effect known from liposomes. Probing the resulting proteovesicles for proton pumping activities, it was revealed that their performance is comparable, even though polymer membranes are not able to host the same numbers of proteorhodopsin molecules as lipid ones. Due to the applied statistical modeling, the derived equations could be used for mathematical optimization which predicted a set of parameters for reconstitution which are predicted to yield large, uniform and highly functional proteovesicles. Indeed, the results obtained from the verification of these factor settings were close to the predictions. The study provides experimental and modeling evidence for different reconstitution mechanisms depending on the membrane type. By making use of them, proteorhodopsin can be used to provide energy in an artificially created vesicular environment. Depending on the desired application, the membrane base can be composed of biocompatible lipids or robust block copolymers, providing a novel flexibility to researchers. Altogether, this thesis serves as an example of thoroughly designed procedure which fulfills the requirements of reproducibility and predictability. It can pave the way for creation of a toolbox which makes the expansion into the field of hybrid materials (lipid/polymer/protein) as well as more complex systems as molecular factories possible.

Contents

List of Figures

List of Tables

Abbreviations

OG n-Octyl-β-D-Glucopyranoside

DM n-Decyl-β-D-Maltopyranoside

DDM n-Dodecyl-β-D-Maltopyranoside

DLS Dynamic light scattering

BR Bacteriorhodopsin

PR Proteorhodopsin

AFM Atomic force microscopy

cmc critical micelle concentration

DOE Design of experiments

DSD Definitive screening design

OFAT One-factor-at-a-time

DOPC 1,2-Dioleoyl-sn-glycero-3-phosphocholine

DOTAP 1,2-dioleoyl-3-trimethylammonium-propane

FCS Fluorescence correlation spectroscopy

IPTG β-D-1-thiogalactopyranoside

LPR Lipid to protein ratio

PPR Polymer to protein ratio

TEM Transmission electron microscopy

PdI Polydispersity index

PDMS Poly(dimethylsiloxane)

PMOXA Poly(2-methyl oxazoline)

To my family, my love and my friends.

Thanks to you, I truly am standing on the shoulders of giants.

Acknowledgements

First, I would like to thank the committee for evaluating my thesis.

Prof. Dr. Wolfgang Meier for being my supervisor during the four years I pursued my doctoral studies and providing me a great workspace.

Prof. Dr. Daniel Müller for taking over the position as my co-examiner and also for providing personal advice.

Both allowed me to work freely and develop my own approaches, making mistakes and taking over responsibility.

Prof. Dr. Cornelia Palivan for taking over the chair.

Prof. Dr. Dimitrios Fotiadis for the valuable discussions and having me in his labs for four months, teaching me the foundations of membrane proteins and how to handle their frustrations.

Gabriele Persey, who never rejected any sample for measurement, no matter how late it arrived.

Myrto Kyropoulou for the endless support, carrying me through this and being at my side.

My colleagues for providing a nice working atmosphere and fruitful discussions. Especially Martina Garni and her father, Hans-Peter Garni, for their help in developing the fluorescence assay and the not so scientific coffee breaks. Sven Kasper for the polymer synthesis. Johannes Thoma and Noah Ritzmann for their scientific help and developing the PR fusion protein. I wish you all the best for your future! Gesine Gunkel-Grabole for endless proof reading and useful advice.

My students, especially Ina Andrea Ontiveros, Claudio Alter and Alfredo Di Silvestro, who taught me the responsibility of being a supervisor. This work is also your work.

My family and friends who supported me during my studies and motivated me to achieve my goals.

The Swiss Nanoscience Institute for funding my research, Claudia Wirth and Audrey Fischer, Daniela “Dani” Tischhauser and Maya Greuter for providing a smooth administration.

Even though unknown to me, I would like to thank the communities of stackexchange.com, the free software and open source communities for creating software like R and providing amazingly helpful support.

1
Introduction

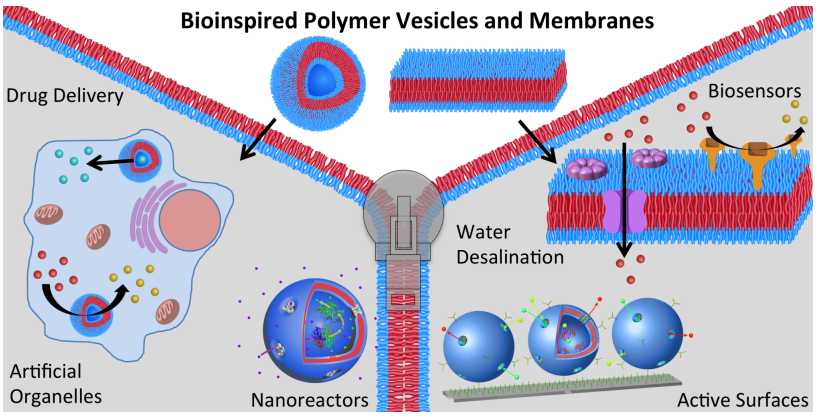

Figure 1.1: Conceptual overview of bioinspired polymer vesicles and polymer membranes highlighting some possible applications of such assemblies. Figure taken from Palivan et al. [1].

This chapter is partially reprinted and has been published Cornelia G. Palivan, **Roland Goers**, Adrian Najer, Xiaoyan Zhang, Anja Car, and Wolfgang Meier. Bioinspired polymer vesicles and membranes for biological and medical applications. *Chemical Society Reviews*, 45(2):377–411, 2016.

Within this chapter, the reader is going to be introduced into the necessary background of the bottom-up approach in synthetic biology. As the work is focused on the creation of nanometer sized vesicles with a desired functionality, the building blocks will be introduced first. Therefore, amphiphilic phospholipids and block copolymers and their self-assembly process will be shown first. Additionally, the potential modifications of these membranes will be shown briefly, which provide a certain functionality. Membrane proteins and their reconstitution into artificial membranes will be discussed afterwards, highlighting currently known differences between lipid and polymer based systems. The reader will be introduced to the concepts of statistical modeling and design of experiments and up-to-date examples from synthetic biology will be shown. The chapter concludes with the underlying vision of this work.

Understanding and mimicking structures and functions found in nature for the design of novel materials and active supramolecular assemblies led to various methods and materials useful in domains such as materials science, chemistry, electronics, and medicine[2,3,4]. Fabrication of molecular bioinspired materials can be realized either by a *top-down* approach, breaking down a complex structure into its components, or a *bottom-up* approach, in which simple components are assembled to produce more advanced supramolecular structures. The latter approach, requires a deep understanding of individual

molecular building blocks and their structures, assembly properties, and dynamic behaviours in order to manufacture nanomaterials. A step further involves the combination of biomolecules, such as enzymes, proteins, or nucleic acids with synthetic materials, for example block copolymers, in order to create new, complex bio-synthetic materials[5]. Specificity and efficiency of biological molecules in addition to robustness and the possibility of tailoring polymeric materials serve for the design of materials/systems with improved properties and functionality. In this respect, polymer supramolecular structures generated by self-assembly of amphiphilic copolymers are of particular interest because these architectures provide a large variety of topologies that permit the insertion/encapsulation/attachment of biomolecules[6,7]. In addition, their properties can be adjusted by chemical modification to support the match with biological molecules, while preserving the characteristics of synthetic materials, such as stability and mechanical robustness[8]. The driving forces that bind building blocks together during self-assembly are weak and noncovalent interactions favoured by chemical complementarity and structural compatibility as key parameters. Amphiphilic copolymers, based on hydrophilic and hydrophobic blocks spontaneously self-assemble in solution in a manner similar to natural lipids, and generate 3D supramolecular assemblies, such as micelles, tubes, worm-like structures and vesicles[9,10], or 2D planar membranes[8]. Of particular interest are vesicles, so called polymersomes, because they offer three topological regions for the location of biomolecules: their inner aqueous cavity, the surrounding membrane, and the external surface exposed to the environment[9]. In the case of polymer membranes (free-standing films, supported membranes, membrane-mimetic brushes) the decoration with biomolecules can be achieved by physical adsorption, insertion, and covalent binding[4,8,11]. In various natural metabolic-, signalling- or transport- processes, the presence of physical or chemical stimuli influence the whole pathway by blocking or unblocking specific molecules/reactions (*e.g.* in the cell cycle[12] or bacterial communication[13]). In addition, biopolymers such as proteins and nucleic acids are all basic stimuli-responsive components of living systems, and often remain stable over wide ranges of external variables, but undergo abrupt and drastic conformational changes at critical points. In this respect, an approach is to design stimuli-responsive polymer assemblies that are able to change their architecture or properties in the presence of stimuli, and therefore to release a cargo, or to allow a specific *in situ* reaction *on demand*[14,15,16].

1.1 *Membrane environment*

The process of molecular self-assembly as a strategy for obtaining programmable colloidal nanostructures, is mediated by weak, noncovalent bonds, such as hydrogen bonds, hydrophobic interactions, van der Waals interactions, and ionic bonds[18]. These weak

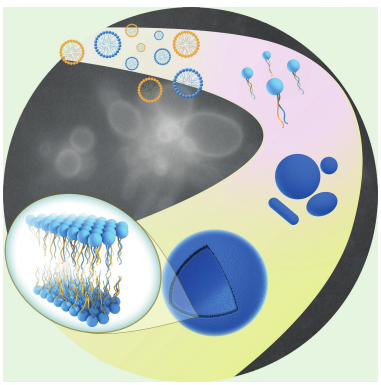

Figure 1.2: Schematic presentation of a the various stages of the molecular assembly process of phospholipids. Figure taken from Brea et al. [17].

interactions act together, and govern the structural conformation of biomacromolecules, and the formation of synthetic supramolecular assemblies, as well as influencing their interactions. By observing the processes by which macromolecules are assembled in nature[19], scientists are generating a variety of architectures by self-assembly of amphiphilic molecules either as spherical objects (3D) or as planar membranes (2D).

Amphiphilic phospholipids are the main components which form the bilayer of the cellular membrane. Introduced into a aqueous environment, they will spontaneously assemble into supramolecular structures as micelles, hollow vesicles or hexagonal shapes[22]. Their molecular structure and shape is the main reason for this phenomena. Two hydrophobic acyl chains linked to a hydrophilic phosphorous group via glycerol is the general scaffold of the molecular class. Driven by hydrophobic interactions and the need to cover their hydrophobic tails, they form agglomerates which minimize the interaction with surrounding water molecules. Various hydrophobic head groups are part of the classification of phospholipids, such as phosphatidylglycerol (PG) and phosphatidylcholine (PC)[22]. The other part is the structure of the hydrophobic tail, its degree of saturation of the fatty **acid** and its length (typical between 14 and 20 C atoms)[23,22]. Taken together, these two factors determine the final assembly in an aqueous environment. Cone shaped phospholipids will assemble into a hexagonal pattern, inverse cone shaped ones into micelles and cylindrical shaped ones into a bilayer[22,21]. The before mentioned PC and PG are part of the cylindrical shape and thus also commonly found in cellular membranes. Various other molecules are found within the cell membranes as steroid and steroid-like molecules (*e.g.* cholestorol). Their particular architectures in combination with active compounds support a large variety of applications. For the structural and functional study of membrane proteins, as well as their application in synthetic biology, a transfer into a native-like environment is required. So far, this has been achieved by transferring them into a lipid membrane, which resemble the natural lipid membrane of cells[24,25,26]. In the past, the needed lipids had to be extracted from nature, but nowadays a wide variety of synthetic lipids is commercially available[24]. In the last decade, a promising synthetic alternative to lipids has emerged: block copolymers. They are composed of a hydrophobic and a hydrophilic block (diblock type) being close to nature's lipids, or of two hydrophilic blocks sandwiching a hydrophobic block in the middle (triblock type)[1,27,28].

The chemical nature of the amphiphilic copolymers is a prerequisite for artificial membranes to support activity by producing membranes/compartments with appropriate properties to allow preservation of the structure, integrity, and activity of biomolecules in a synthetic environment or to mimic biomembrane responses[10,11,38,39]. The molecular properties of each block, and of the overall copolymer chain, such as molecular weight, polydispersity and hydrophobic to hydrophilic block ratio, strongly affect the supramolecular assemblies.

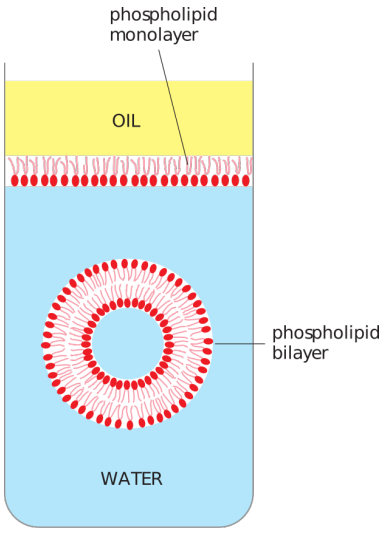

Figure 1.3: Formation of a membrane by amphiphilic phospholipid molecules. From Alberts[20].

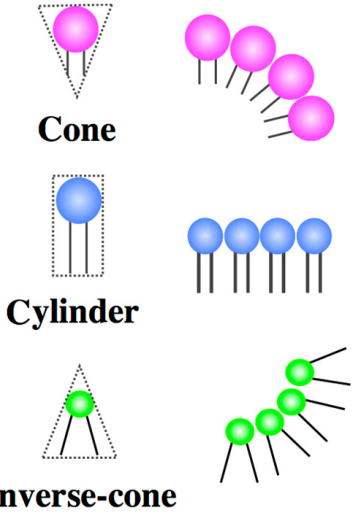

Figure 1.4: Schematic representations of cone-, cylinder- and inverse-cone-shaped lipids. From Sakuma and Imai[21].

Membrane property	Polymersomes	Liposomes[29]
Membrane thickness [nm]	3[30]–40[31]	3–5
Lateral diffusion coefficient [$\mu m^2\ s^{-1}$]	0.0024[32]–6.0[33]	3.8[29]–12.5[33]
Water permeability [$\mu m\ s^{-1}$]	0.8[34]–526[35]	15–150
Bending modulus [kT]	25[36]–74330[31]	11–30
Stretching modulus [mN m^{-1}]	15[37]–2350[31]	250±2

Table 1.1: Specific membrane properties achievable with polymersomes and in comparison to some typical values for liposomes. From Palivan et al.[1].

The most common amphiphilic copolymers used in combination with biomolecules consist of hydrophilic blocks, such as poly(acrylic acid), PAA, poly(ethylene oxide), PEO, poly(ethylene glycol), PEG, poly(2-methyl oxazoline), PMOXA, or poly[L-isocyanoalanine(2-thiophen-3-yl-ethyl)amide], PIAT, and a hydrophobic block, such as polystyrene, PS, poly(butadiene), PB, or poly(dimethylsiloxane), PDMS[16,40,41,42]. Abbreviations of the polymers mentioned in this review can be found in Table 1.2.

More details regarding the synthesis and properties of amphiphilic copolymers used to form supramolecular assemblies can be found in very recent reviews and book chapters[43,41,42]. Mechanical properties of polymersome membranes largely depend on the type of copolymer used to form the membrane and the length of the hydrophobic block and therefore membrane thickness plays a key role in the stability of the assembly[44,45,29,33]. Furthermore, addition of naturally occurring molecules, such as *e.g.* phospholipids into polymer vesicle membranes, further modifies mechanical properties of polymersomes[46], whilst additional membrane protein insertion can increase membrane permeability[34,35]. Therefore, the type of polymersome with optional biomolecules (*e.g.* phospholipids, proteins, peptides) can be carefully chosen to fulfil certain needs for specific applications. Ranges of some typical properties for purely synthetic polymersomes are summarized in Table 1.1 demonstrating that they can be specifically tuned using artificial block copolymer vesicles. It also highlights one main advantage compared to liposomes, namely physicochemical versatility. It has to be noted that many of these properties are measured on polymer-based giant unilamellar vesicles (GUVs) using *e.g.* micropipette aspiration[47]. For more details on physical properties of polymersomes, readers are referred to reviews on this subject matter[29,48,49]. In the case of polymersomes or polymer membranes with stimuli-responsive properties, the selection of the polymers must either have the response associated with one of the blocks, or allow the introduction of specific molecules that reply to a stimulus, and therefore induce a change in the overall architecture/properties of the supramolecular assembly[14].

Abbreviation	Polymer
PAA	Poly(acrylic acid)
PB	Poly(butylene)
PBD	Poly(butadiene)
PBzMA	Poly(benzyl methacrylate)
PCL	Poly(caprolactone)
PDEAEM	Poly(2-(diethylamino)ethyl methacrylate)
PDMAEMA	Poly(2-(dimethylamino)ethyl methacrylate)
PDMIBM	Poly(3,4-dimethyl maleic imido butyl methacrylate)
PDMS	Poly(dimethylsiloxane)
PDPA	Poly(2-(diisopropylamino)-ethyl methacrylate)
PEG	Poly(ethylene glycol)
PEGMA	Poly(ethylene glycol)methacrylate
PEO	Poly(ethylene oxide)
PEtOz	Poly(2-ethyl-2-oxazoline)
PFMMA	Poly(ferrocenylmethyl methacrylate)
PGA	Poly(glutamic acid)
PGMA	Poly(glycidyl methacrylate)
PHEMA	Poly(2-hydroxyethyl methacrylate)
PIAT	Poly(L-isocyanoalanine(2-thiophen-3-yl-ethyl)amide)
PLA	Poly(lactic)acid
PMA	Poly(4,5-dimethoxy-2-nitrobenzyl methyl methacrylate acid)
PMAA	Poly(methacrylic acid)
PMCL	Poly(γ-methyl-ϵ-caprolactone)
PMMA	Poly(methyl methacrylate)
PMOXA	Poly(2-methyl oxazoline)
PMPC	Poly(2-methacryloyloxyethyl phosphorylcholine)
PNBA	Poly(4,5-dimethoxy-2-nitrobenzyl methacrylate)
PnBMA	Poly(n-butylmethacrylate)
PNIPAM	Poly(N-isopropylacrylamide)
PNVP	Poly(N-vinyl-pyrrolidone)
PS	Poly(styrene)
PSA	Poly(sulfobetaine methacrylate)
PSBMA	Poly(11-mercaptoundecyl sulfonic acid)
PtBMA	Poly(tert-butyl methacrylate)
PTMC	Poly(trimethylene carbonate)
PVA	Poly(vinyl alcohol)
PVP	Poly(vinylpyridine)

Table 1.2: Common polymer blocks and their abbreviations. From Palivan et al.[1].

1.1.1 *Modified and responsive membranes*

Responive polymer membranes VARIOUS AMPHIPHILIC COPOLYMERS WITH stimuli-responsive properties are found in recent reviews[14,50], and selected examples are included in the next sections. Stimuli-responsiveness favours a better localization of the system in a desired biological compartment, and controlled release of a payload at the location of a pathological event, or rapid imaging of the pathological event. The requirements for bioinspired membranes/vesicles in the case of *ex vivo* applications are mainly restricted to enhancing system performance by optimizing the functionality of entrapped / encapsulated / attached active compounds in various environmental

conditions (pH, ionic strength, temperature, etc.).

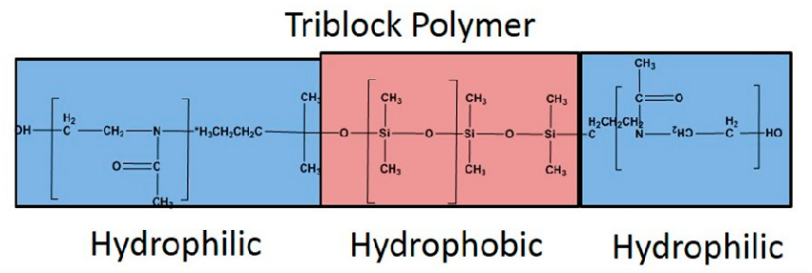

Figure 1.5: Schematic presentation of the PMOXA–PDMS–PMOXA tri-block structure. From Bain et al. [51].

A complex scenario of requirements characterizes *in vivo* applications, which start with the use of polymers that fulfil health safety standards by the U.S. Food and Drug Administration (FDA) and the European Medicines Agency (EMA) up to the biocompatibility and biodegradability of all the components of synthetic systems under biological conditions[42]. In addition, synthesis strategies for amphiphilic copolymer blocks and especially the preparation methods for the supramolecular assemblies should avoid organic solvents, which normally lower the enzymatic activity or denature proteins. Properties, such as charge, flexibility, thickness and membrane density have to be tailored for a desired application. For example, a charged surface is required to attach biomolecules to polymer membranes by electrostatic interactions, and a factor that can influence the circulation time of systems inside the body[52,53]. The flexibility of membranes plays an essential role in the insertion of biomolecules and preservation of their functionality[54] as it will be discussed in sections below. Therefore the selection of a particular amphiphilic copolymer and the supramolecular assembly generated by self-assembly has to match both the specificity of the biomolecules, and the intrinsic conditions of the desired application. Polymersomes, as hollow spherical compartments delimitated by a membrane of block copolymer, have the advantage of a dual carrier role – they can serve as hosts to hydrophilic molecules inside their cavities or to hydrophobic molecules in their membranes[9,55]. Due to the low entropy of mixing of polymers, polymersomes possess higher chemical and physical stability than their lipid-based compartments (liposomes), whilst low immunogenicity similar to liposomes can be achieved, thus meeting essential requirements for advanced technological applications[55,56]. In addition, their chemical versatility makes it possible to tune properties, such as wall thickness, polarity, toxicity or stimuli-responsiveness[50]. In a further step to designing functional systems, polymersomes serve as compartments for *in situ* reactions at the nanoscale, and for the development of nanoreactors, nanodevices, and artificial organelles[16]. Compared to drug delivery systems, where the payload is released mainly by degradation of the polymersomes or by stimuli-responsive change of shape, the concepts of nanoreactors and artificial organelles require a preserved architecture to simultaneously protect the active compounds (enzymes, proteins, mimics), and allow their actions *in*

situ [16,57].

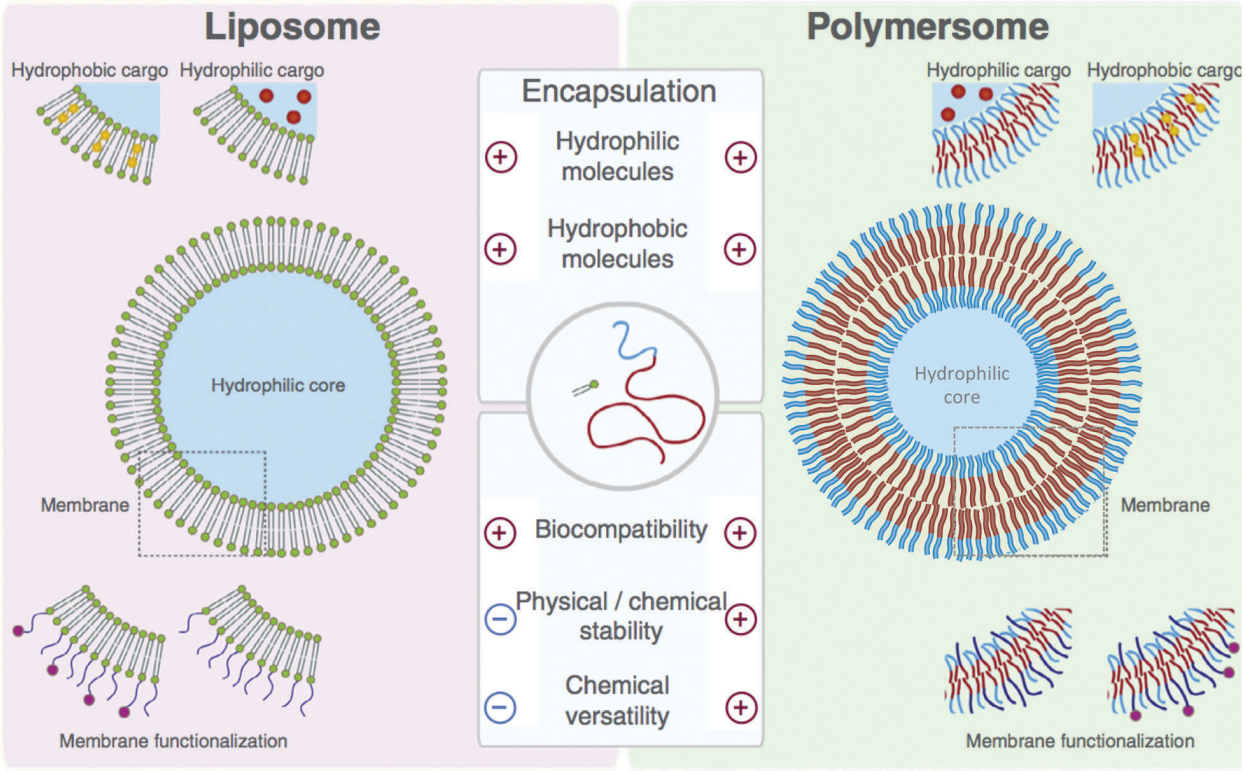

Figure 1.6: Schematic presentation of the cargo-loading concepts in case of liposomes (left) and polymersomes (right). Both systems are able to transport and deliver hydrophobic cargo in their membrane as well as hydrophilic in the aqueous core. The membrane of both vesicles can furthermore be modified to enhance targeting and recognition. In contrast to liposomes, polymersomes exhibit increased physicochemical stability and offer more ways to modify its building blocks. From Palivan et al. [1].

In this respect, reactions inside polymersomes, or multicompartment-polymersomes require the polymersomes to possess specific properties: *i)* sufficient encapsulation of active compounds, *ii)* membrane impermeability for encapsulated compounds, *iii)* permeability for substrates/products, and *iv)* stability in various environmental conditions characteristic for desired applications. Two topological regions need to be considered for a polymer membrane to act as matrix for accommodating a biomolecule: the mono- or bilayer, and the surface exposed to the environment. Each domain has to mimic the properties of a biological membrane to serve as a template for biomolecules [8,58]. Increased mechanic stability either in polymersomes or as planar membranes, results from the formation of thicker membranes, which can be 2 – 10 times that of phospholipid bilayers. This leads to a large mismatch between the membrane thickness and the size of the biomolecules, which could significantly affect the insertion, mobility and functionality of the biomolecules. Theoretical calculations have indicated that synthetic membranes are capable of adjusting their thickness to the size of the membrane inclusion / protein with a hydrophobic mismatch of 1.3 nm [59]. However, recent studies have shown that biomolecules (biopores or membrane proteins) remain functional in membranes up to 6 times thicker than the height of biomolecules [60,34,61,62,28]. Insertion of biomolecules, ranging from short peptides that self-assemble into pores [62] to large transmembrane ion channel porins [34,28] represents an approach for increasing

membrane permeability that is similar to cell membranes. Moreover, very recently the properties of polymer membranes have been varied via polymer libraries in order to establish their effects on the lateral mobility of inserted biomolecules, and to understand which membrane properties are crucial for successful biomolecule insertion[54]. The other topological domain of a membrane is its surface, the properties of which are essential for interactions with biological molecules via molecular recognition, or conversely, to avoid interactions that could lead to decreased circulation times of polymeric carriers in the blood stream. Molecular recognition at surfaces as a key biological process that is accomplished by specific affinity tags is now the focus for potential industrial and medical applications, such as the purification and immobilization of biomolecules[63], labelling of proteins[64], and 2D-crystallization[65,66]. In order to study recognition processes at a molecular level, an efficient approach is to introduce simplified systems, as for example metals that serve as coordination centres with different ligands to provide open coordination sites to favour stable immobilization of biomolecules similar to those in nature[67,68]. Specific molecules involved in molecular recognition interactions (biotin-streptavidin, antibody-antigen, Me-NTA-his tag proteins, etc.) have been used to decorate polymer membranes for targeting approaches or for immobilization of nanoreactors on solid supports[69,70]. In the next sections we describe how the decoration of polymer membranes/compartments with biomolecules is achieved to create hybrid membranes/systems with improved properties and functionality.

Modified polymer membranes In addition to the use of intrinsic stimuli-responsive polymers, another strategy for designing responsive polymersomes is based on the incorporation of naturally responsive biomolecules (proteins, enzymes, DNA, etc.) into such synthetic matrices. Because of their similarity to cellular membranes, vesicles composed of phospholipids, called liposomes, have been the focus of research for decades[71,72,73]. However, despite good biocompatibility they lack long-term structural stability[29,72,73] and these drawbacks have hindered their industrial use and limited their medical applications. In order to create compatible polymersomes, it is possible to incorporate enzymes, which can perform desired reactions in the interior compartment, and/or surface modifications to enhance molecular recognition[8,74]. Furthermore, it is possible to reconstitute membrane proteins in the membrane, or to covalently bind biological moieties to membrane forming polymers. Since membrane proteins play a crucial role in fundamental cell processes, ranging from transportation, gradient formation, to signalling[75,76,25,77], an improved understanding is required to create systems with complex functionalities, such as artificial organelles and nanoreactors. Furthermore, these systems aim to mimic cellular membranes, its compartments or protocells. In the following sections, the current approaches to create polymersomes

with decoration of biomolecules are presented. By chemically coupling biomolecules to block copolymers, systems have been achieved that can be triggered or possess enhanced stability in biologically relevant conditions. Further, recognition and targeting can be greatly improved when ligands are presented on the vesicle surface. Several techniques are known to attach and expose biomolecules on the surfaces of polymersomes, which can be categorized based on pre- or post-modification of vesicles[78]. Modification of polymers with biomolecules before self-assembly simplifies the procedure, but its impact on the self-assembly and cargo loading have to be evaluated carefully. In contrast, post-modification of vesicles adds additional steps to the vesicle preparation procedure and in certain cases the functional molecule serving for biomolecule attachment may be hidden in the membrane after the preparation procedure of vesicles and thus decrease the functionalization efficiency. For pre-modification of polymers, biomolecules are either attached to the hydrophilic block of block copolymers before self-assembly[78] or are used as one of the hydrophilic[79] or hydrophobic blocks[80,81]. Examples of attached biomolecules are polysaccharides, such as dextran and heparin[79,82], polypeptides[80,83], and water soluble green fluorescent protein[84]. Modification of a hydrophilic polymer block with peptides has resulted in the production of a new class of chimeric polymersomes, called pepsomes. Depending on the polypeptide, systems were responsive to stimuli, such as pH change, and the presence of glucose[80,81]. Block copolymers composed of the thermoresponsive polymer PNIPAM and the green fluorescent protein variant amilFP497 assemble into polymersomes when heated above 37°C[84]. Combining this novel bioconjugate with the fluorescent anticancer drug DOX and the light harvesting protein phycoerythrin 545 (PE545), resulted in the generation of a system that allows spatial localization of the encapsulated cargo within the polymersome by using fluorescence lifetime imaging and Förster resonance energy transfer (FLIM-FRET)[84]. Polypeptides with carbohydrate moieties have been developed for delivery with enhanced biocompatibility[82,85]. Their exposed peptides are recognized by specific proteins and enable improved cellular recognition[85] and drug release due to enzymatic cleavage[82]. Another polymeric platform that was introduced are polyion complexes composed of PEO-*block*-polypeptide, which are able to self-assemble into a vesicular structure (PICsomes). The PICsomes exhibited sufficient stability in physiological conditions even without crosslinking, and furthermore are sufficiently permeable for diffusion of small substrates through the membrane[86]. This allowed their use as a reaction compartment by encapsulating an enzyme for which the substrate and product could diffuse through the membrane. Further improvements in the ability of polymersomes to interface with biomolecules have been demonstrated by the attachment of Cu(II)-trisNTA to PB-*b*-PEO[68,87,88]. The metal-functionalized polymers preserved their ability to assemble into vesicles, and allowed specific binding of His-tag modified proteins to the polymersome surface[87]. Because of the well-established protocols

for His-tag modification of proteins, this approach could potentially serve as a platform for further protein decoration of polymersomes. In contrast to the examples described above, targeting of colon cancer cells has been achieved by linking fibronectin mimetic peptides to vesicles after formation of vesicles in an aqueous environment[89]. In a similar study, tumour cell targeting was enhanced by linking a synthetic peptide to the polymer[90].

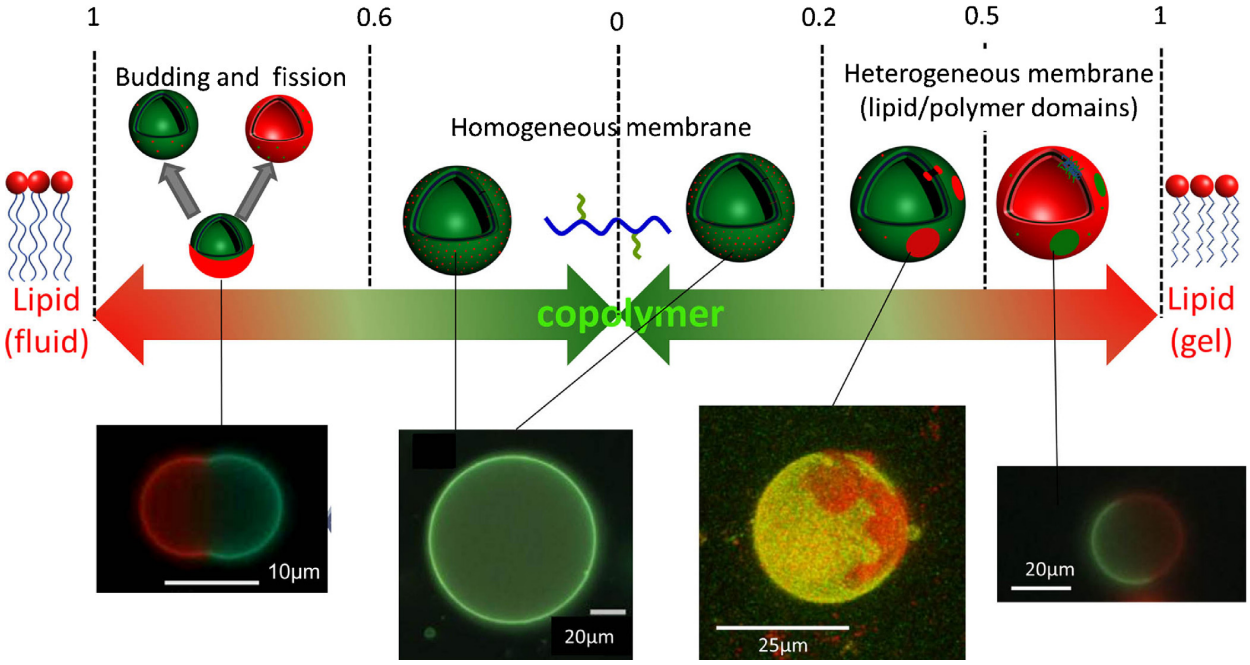

Figure 1.7: Overview of the different hybrid vesicular structures that can be obtained according to the molar composition (polymer/lipid molar ratio) and thermodynamic phase of the phospholipid. Sketches on the top lines illustrate the different cases obtained by study of the epi- or confocal fluorescence microscopy images. From Le Meins et al.[91].

Lipid polymer hybrid membranes After discussing the particular characteristics of lipids and polymers as building blocks for synthetic membranes, a logical step is the study of their mixture towards the assembly of hybrid membranes. Even though the two materials rely on similar self-assembly mechanisms, the differences in membrane thickness, stability, fluidity,chemical versatility and permeability are strong (see table 1.1, p. 23). The ability to intermix with each other is hindered especially by differences in molecular weight, block length and the resulting hydrophobic mismatch. Mixing a PDMS-*b*-PEO diblock copolymer with the lipid POPC at a ratio of 25/75 resulted into the formation of polymeric domains inside lipid vesicles[92]. The different membrane curvature of the two domains resulted in the observation of a vesicle budding process over time. This ultimately lead to the formation of two separate vesicles, one polymer based and one lipid based[92]. On the other hand, inverting the ratio between polymer and lipid (75 % POPC and 25 % PDMS-*b*-PEO) led to homogeneous hybrid vesicles[92,93]. A main advantage of such a hybrid system is that the lipid domain would be the natural and preferable acceptor of a membrane protein, whereas the polymer would provide

a robust scaffold for the structure. This way would take advantage of the stability of block copolymers and the biocompatibility of the lipid membrane. A successful study has been made on planar hybrid membranes and showed the preference of the membrane protein towards the lipid domain[94].

1.2 *Membrane proteins*

Membrane proteins fulfill vital tasks in cells, being it cellular communication, transport of substrates in and out of the cells, adhesion and movement of the cells or generating electrochemical gradients necessary for various metabolic processes. About a quarter of the genome of various organisms encodes for membrane proteins[95,25]. Combination of the number of predicted membrane proteins by bioinformatics with their functions in cells explains the still increasing interest of science and industry in their structure and function. One of the main motivation is to use the generated knowledge in the development of new drugs but also in designing novel devices in synthetic biology as described in section 4[96,23,74]. Nevertheless, ideas for possible applications and profound knowledge about membrane proteins are still diverging at a large scale. The known structures of membrane proteins in protein data bases is less than 1% and the number is even lower in terms of mechanistic information. In case of eukaryotic cells, the structure of only two membrane proteins has been revealed: aquaporin and rhodopsin[95,26]. The light sensitive rhodopsin protein family is one of the most interesting ones, as their members fulfill quite different tasks but still share very similar structural features, depending on the organism they originate from. They are divided into two subfamilies: type I and type II rhodopsins, whereby type I rhodopsins are called microbial rhodopsins and type II animal rhodopsins. Both families share structural features, like the seven transmembrane -helices and the requirement of retinal, a light absorbing cofactor[97]. However, the sequences of the two families share practically no similarity and it is believed that both may have developed independently and distribution of the corresponding gene has taken place via horizontal gene transfer. Type II rhodopsins are only found in higher eukaryotes, utilize 13-*cis*-retinal in their binding pocket and function as G-protein-coupled-receptors (GPCRs) responsible for vision in the human eye. Type I rhodopsins are found among bacteria, algae and fungi and utilize all-*trans*-retinal. They function as light-driven transporters or photoreceptors as shown in figure 1.8. Their function as chloride ion pumps or receptors is detailed elsewhere[98], the present work focuses on their ability to pump protons[97,99,100].

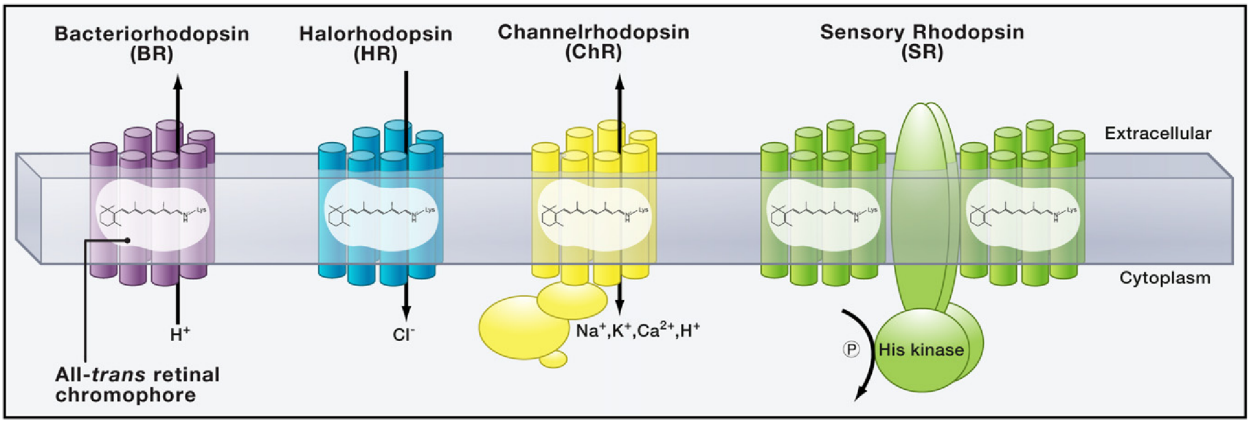

Figure 1.8: Overview of type I rhodopsins. BR pumps protons from the interior to the exterior of the cell, building up a proton gradient. HR actively transports chloride ions into the cell and ChR conducts cations in both directions, but always along an electrochemical gradient. SR activates its attached His kinase upon illumination. Figure taken from Zhang et al. [97].

1.2.1 *Light driven proton pumps*

Many bioenergetic processes in cells depend on the presence of electrochemical gradients. The probably best-known is the proton motive force (pmf) which drives the synthesis of ATP via the enzyme ATP-synthase. Bacteriorhodopsin (BR), a type I rhodopsin, was discovered in *Halobacterium halobium* in 1971 and works as a light-driven proton pump and allows the survival under low oxygen conditions [101]. BR has been studied intensely over the last decades regarding its structure, function and possible applications in biotechnology and novel devices. Even though it now serves as a model for proton pumps due to high resolution crystal structures and understanding of the proton pumping mechanism, its application has never left the proof of concept scale. One of the reason for this shortcoming is, that it has not been possible so far to express it as a recombinant protein. Thus its production in large quantities and its modification on a DNA level has not been achieved, because the tools for genetic and protein engineering are not as sufficiently developed for *H. halobium* than for *Escherichia coli* for example [100,75]. In 2000, Béjà and coworkers discovered a type I rhodopsin in the genome of an uncultivated marine bacterium which became known by the name Proteorhodopsin (PR) [99]. PR shares structural and functional similarities with BR, most importantly it is also able to pump protons. Indeed phylogenetic analysis revealed that PR represents its own branch compared to BR and a horizontal gene transfer is likely to have happened [100]. The family of proteorhodopsins is now one of the largest known rhodopsin families, with over 4000 members discovered so far. They are divided in two categories: blue light-absorbing (λmax 490 nm) and green light-absorbing (λmax 520 nm), according to the absorption maximum of the bound retinal [100,102]. The two distinct absorption maxima are believed to be adapted to the water depth the microorganisms are living in and the phototrophy mediated by PR has a substantial impact on energy and CO_2 flux in the oceans [103,104]. Besides their similarities in structure and function, there are distinct differences

which will be explained in detail in the following and are important to understand for their use in synthetic devices.

1.2.2 *Bacteriorhodopsing and proteorhodopsin*

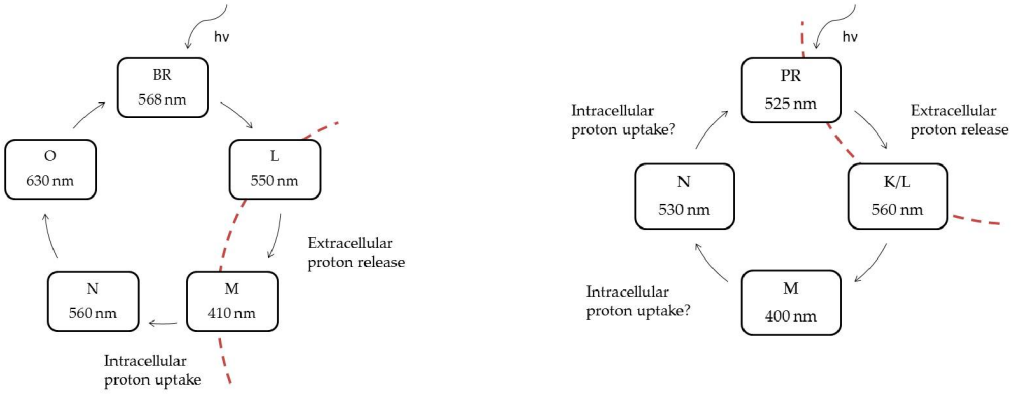

Figure 1.9: Schematic presentation of the photocycle of BR and PR. The numbers refer to the absorption wavelength of the corresponding step and the dashed red line indicates the extracellular proton release and uptake[97,102].

Photocycle THE ABILITY TO TRANSLOCATE protons from the interior of a cell to its outside is the main function of BR and PR. In order to achieve this goal, a series of conformational changes take place as a photon is absorbed by all-*trans*-retinal. This process is called photocycle and displayed in Figure 1.9 for both BR and PR. In case of BR, the absorption of a photon with a wavelength of 568 nm starts the cycle (Figure 1.9, top) which in the following causes a series of photochemical reactions to take place and induces isomerization of all-*trans*- retinal to 13-*cis*-retinal. Each step in this sequence (L, M, N and O) has a characteristic absorption maximum and decay time, caused by the different isomerization states of the bound retinal and its environment. The proton is released during the transition from the L to the M state on the extracellular side and taken up on the cytoplasmic side during the transition from the M to the N state[97]. The photocycle of PR (Figure 1.9, bottom) looks very similar, however, the absorption maximum in the beginning (λ = 525 nm) and during the single steps of the cycle are different. The proton release happens during the transition of PR to the K/L state and the uptake, still a question of debate, during the transition of the M to the N state or from the N to the dark-state PR[102]. The reason for this difference lies in the amino acid sequences of the two proteins. By comparing these two sequences of the two proteins, it becomes obvious that they do not align well and they probably evolved independently[105]. BR has a sequence length of 262 amino acids and PR one of 249 amino acids. However, certain features are conserved in the sequence, especially the residues involved in proton transfer. The proton transfer is caused by the photoisomerization of all-*trans*-retinal, which is bound covalently at position Lys216, forming the retinal Schiff base (RSB). This binding

pocket is highly conserved and found in both proteins[105,97]. Upon the induced conformational change, a proton is transfered to Asp85 (proton acceptor) and released onwards. A new proton is taken up by Asp96 (proton donor) and reprotonates the RSB and the cycle repeats[97]. The residues Asp85 and Asp96 are replaced by Glu108 (Asp96 in BR) and Asp97 (Asp85 in BR) in PR. The spectral properties are heavily influenced by the ionic environment of the RSB and its protonation state. The red-shift of the absorption maximum from 568 nm (BR) to 525 nm (PR) is due the different pKa values of the residues. With a pKa of 7.7, Asp97 is more basic than its counterpart Asp85 in BR with a pKa of 2.5[106,107]. The pKa values also dictate the pH range in which the two proteins are functional. PR seems to be adapted to its marine environment and functions best at a pH around 8, whereas BR can function at more acidic pH values around 6, which is not the case for PR[107]. Hence, depending on the chosen light-driven proton pump, the working range of a proto-cell would be limited in terms of pH range and illumination wavelength.

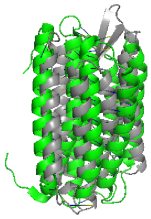

Figure 1.10: Alignment of the three dimensional structures of BR (grey) and PR (green). Graphic created using the software PyMol, utilizing the structural data provided by the Protein Data Bank (PDB) entries 1MoK (BR) and 2L6X (PR).

Molecular Structure Besides these differences in secondary structure (see section 1.2.2), the tertiary structure of the two proteins is highly similar. High resolution crystal structures are available for BR, but not for PR so far. Due to their similar functions, the predictions from homology modeling have been accurate so far[26,108]. As can be seen from Figure 1.10, BR and PR have a similar structure. Both are composed of the characteristic seven transmembrane -helices, which accounts for most of the protein. The RSB is located in the center of the structure where also the proton transition takes place. The arrangement of the transmembrane helices leads to a surprising stability in terms of membrane proteins. Unfolding experiments using single-molecule force spectroscopy (SMFS) of BR revealed that the atomic interactions between the helices lead to pairwise extraction, namely helix E and D, then C in a step-by-step and B in a all-or-none manner. This behavior was also observed in case of PR and is proposed to be the inverse of the folding into the membrane[104,109].Imaging done via atomic force microscopy (AFM) was able to give an insight into the packaging of BR and PR in a membrane environment. In its native membrane environment, the so called purple membrane of *H. salinarium*, the single BR molecules assemble in a trimeric pattern (see Figure 1.11 a). Three trimers are organized in a hexagonal lattice structure with a side length of about 6 nm and cover a membrane area of about 17 nm^2 [109]. It is known from literature that this assembly is required for BR to function properly. Lipid-protein, as well as the protein-protein, interactions in the trimer have an impact on the photocycle, slowing it down when missing[95,110]. PR (Figure 1.11 b) assembles in a different pattern. AFM imaging revealed a donut-like shape of the assembled PR molecules in a hexagonal lattice with a side length of about 9 nm, covering a surface of about 33 nm^2. In contrast to BR, PR assembles into penta- or hexamers in a radial man-

ner. It has been suggested that the higher amount of PR molecules is necessary to compensate the slower photocycle of PR compared to BR and the radial distribution accommodates the polarization of incident light in the ocean[104]. Like BR, the photocycle of PR requires this form of assembly and membrane-protein interactions, as a distinct slow-down of the photocycle has been observed in PR monomers[102]. Calculations indicate that both proteins are present at a similar level, 2.4·104 molecules per cell, when expressed in *E. coli* (PR) or in the purple membrane (BR)[103]. In order to function properly in a synthetic environment, the structure and molecular arrangement has to be conserved during the assembly process.

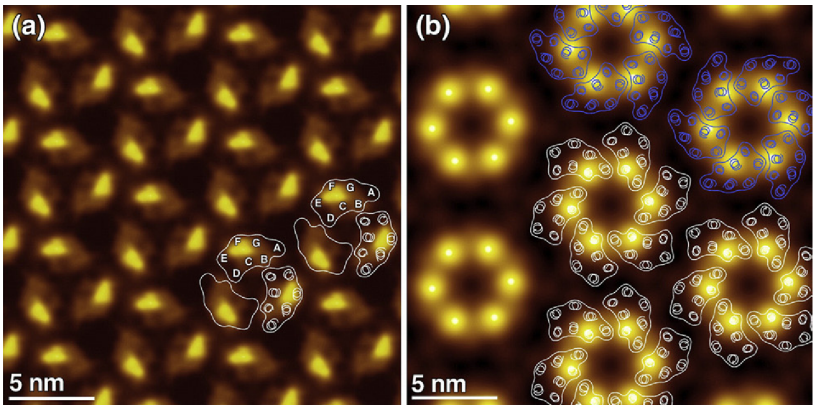

Figure 1.11: AFM topography of BR (a) and PR (b). BR is packed in the purple membrane and the trimeric assembly is outlined in white. PR assembles in radial hexamers and PR molecules are outlined in white and blue, indicating two possible orientations. Figure taken from Klyszejko et al. [104].

1.3 *Membrane protein reconstitution*

1.3.1 *Approaches*

THERE ARE FOUR BASIC strategies concerning the reconstitution of proteins into liposomes which have been used over the decades. Those are mechanical means, freeze-thawing, organic solvents and detergents[25,110].

Mechanical means THE BASIC PRINCIPLE OF reconstituting membrane proteins into vesicles by mechanical means is that heterogeneous mixture of multilamelar membranes is brought to a homogeneous population by the application of some mechanical force. Usually in the presence of a membrane protein. Common ways are by sonication and high pressure (*e.g.* via french press). However, the high energy input usually leads to fast and irreversible denaturation of the membrane proteins[110].

Freeze-thawing SIMILAR TO MECHANICAL METHODS, freeze-thawing also starts off at preformed vesicles which undergo together with the membrane protein several rapid freezing and thawing cycles. During

the freezing process, water molecules crystallize on the membrane interface and break up the organization of the membrane. During thawing the reassembly is taking place and provides the membrane protein a chance to integrate into the membrane[110]. This method can be combined with sonication and does not stress the membrane protein much but is prone to strong randomization of the membrane proteins' orientation[110].

Organic solvents AMPHIPHILIC MOLECULES LIKE PHOSPHOLIPIDS usually have a good solubility in organic solvents like chloroform or ethanol. Diluting the organic mixture dropwise into water leads to spontaneous formation of micelles and vesicles as the membrane molecules need to protect the hydrophobic parts. If membrane proteins are present during that process, their hydrophobic core incorporates into the forming structures. The biggest drawback of that method is the need to solubilize the membrane protein in an organic solvent. Only extremely stable membrane proteins like OmpF survive that process. Furthermore, it proves to be hard to remove the residual traces of the organic solvent which can influence the functionality of the formed structures[110].

1.3.2 Detergent mediated reconstitution

AS MOST OF THESE methods lead to the degradation and denaturation of many membrane proteins and at the same time, membrane proteins are commonly purified by the use of detergents the most successful and frequently used strategy for proteoliposomes preparation is the detergent-mediated technique[25,26]. Here, the protein is first solubilized with lipids and the appropriate detergent in order to form a solution of lipid-protein-detergent and lipid-detergent micelles. Next, the detergent is removed, resulting in vesicle formation with inserted protein[110]. In 1995, Rigaud et al.[110] published a strategy to reconstitute membrane proteins by a stepwise solubilization of preformed liposomes (Figure 1.15). This technique allows experimental monitoring of the mechanism by which the protein interacts with lipid membrane. The results indicate that the reconstitution of proteins into liposomes can be described as a three stage process: In stage I, the monomeric detergent molecules saturate the liposome membrane while the structure of the vesicle remains intact. A structural transition occurs in stage II, as the detergent-saturated liposomes start to dissolve into binary detergent-phospholipid micelles. In stage III, the transition is completed and only micelles are present. The detergent removal process can be seen as the mirror image of the solubilization process[25]. The basic idea of this strategy is to add the protein add different solubilization steps and perform the detergent removal to induce the reconstitution. The result of each point is measured and analyzed and thus an optimal composition for the functional

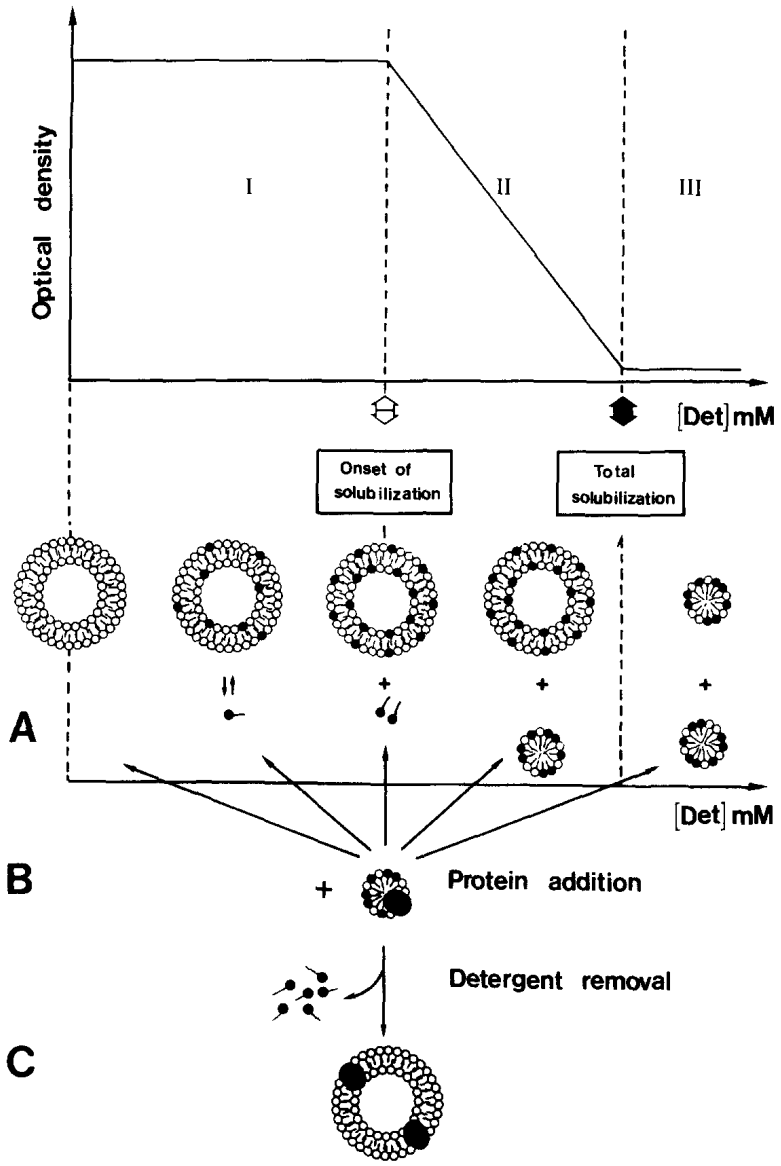

Figure 1.12: Schematic representation of Rigaud et al.'s strategy for membrane protein reconstitution. A) Stepwise solubilization of preformed liposomes. The three stages I, II, III and their corresponding change in optical density are shown in the upper panel. B) The protein is added at each step of the lamellar to micellar transition. C) Detergent removal drives the reconstitution and formation of proteovesicles. Figure from Rigaud et al. [110].

reconstitution of a membrane protein can be found [110,25].The detergent removal is a critical step and the applied technique strongly depends on the selected detergent. One can distinguish between high cmc detergents, which form small micelles (like n-Octyl-β-D-Glucopyranoside), and low cmc detergents, which form large micelles (like n-Dodecyl-β-D-Maltopyranoside)[26]. In case of high cmc detergents, gel chromatography, dialysis and hydrophobic adsorption can be applied, whereas dialysis is the most commonly used. During dialysis the detergent is diluted to concentration values below the cmc, resulting in the disintegration of the micelles to individual detergent monomers[26].

1.3.3 *Insertion of membrane proteins into the membrane of polymer vesicles*

INSERTION OF MEMBRANE PROTEINS into membranes is a more delicate task, and successful reconstitution usually takes years to be developed, especially in the case of sensitive membrane proteins, which rapidly denature in any environment that is slightly different from the biological one[26]. First reconstitution trials are usually performed in lipid membranes because being significantly thinner (3-5 nm thickness), they are closer to the natural cellular membrane environment. Procedures to reconstitute a membrane protein have been in development for the last two decades and underlying mechanisms have been investigated[25]. The most common method for reconstitution of membrane proteins in lipid membranes relies on the use of detergents, which serve both as a stabilizer for the water-insoluble membrane proteins, and as a mediator during their insertion into the membrane[111,112,113]. Then, removal of the detergent by dialysis or addition of biobeads leads to re-formation of closed liposomes with the membrane protein incorporated. Procedures with respect to the lipids used, detergents, detergent removal, etc. usually have to be developed for each individual membrane protein[25,26]. When polymersomes are designed to serve as reaction compartments, such as in the development of nanoreactors, nanodevices and artificial organelles, the permeability of their membrane is a crucial property. This should allow transport of reactants through (substrates and products) in order to fulfil the *in situ* reaction. There are various approaches to obtain polymersomes with permeable membranes: *i)* use of polymer forming porous membranes[114], *ii)* use of polymer forming membranes with permeability to specific ions, such as oxygen species[115], *iii)* chemical treatment of membranes to induce pore formation[116], and *iv)* insertion of pores or membrane proteins[60,62,77]. The approach involves insertion of transmembrane proteins and pores, as in cell membranes[75,76,26]. Successful insertion of the small pore forming peptide gramicidin in polymer membranes based on PMOXA-*b*-PDMS-*b*-PMOXA enables diffusion of protons, Na^+ and K^+ ions through it, whilst preserving the polymersome architecture[62]. These examples indicate that it is possible to functionally insert small biopores in thick polymer membranes, with thickness up to 6 times larger than the biomolecule if the membrane has appropriate properties. The most obvious difference between lipid membranes and those formed by self-assembly of copolymers is the latter's higher molecular weight, which is usually in the range of two to five times greater[29], and leads to much thicker membranes (Table 1.1). Therefore the properties of synthetic membranes and their interactions with detergent molecules are different. A bilayer based on diblock copolymers cannot relieve the tension induced by detergent integration in a flip-flop mechanism that is common with lipids[117]. Different stages of interaction between synthetic self-assembled supramolecular structures and de-

tergents correspond to a co-existence of polymersomes and detergent micelles, whilst further increases of detergent concentrations induce membrane dissolution, as the most likely mechanism to relieve the surface tension[117]. Therefore, the procedures for membrane protein reconstitution in lipid membranes may not be appropriate for synthetic membranes, or at least not easily adapted. Moreover, there is still a shortage of extensive data on the interactions of different types of block copolymer (*e.g.* diblock, triblock) and different block compositions with detergent classes. The increased hydrophobic mismatch between the hydrophobic block of the copolymer and the membrane protein represents an additional problem, since the hydrophobic domains of membrane proteins are adapted to their lipid environments, and depending of the protein, are around 2-4 nm in size[24]. However, it has been shown that various membrane proteins can be successfully inserted into polymer membranes, if the polymer chains are sufficiently flexible to adjust the hydrophobic domain of the membrane near the protein to the size of the protein[59,34,28,54].

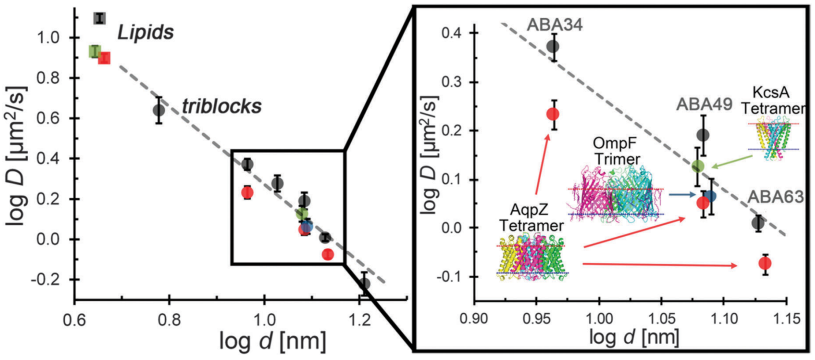

Figure 1.13: Dependence of the diffusion coefficient D to the membrane thickness d. The power law dependence (dashed line) highlights the decrease of increasing molecular weight of the membrane building blocks and thus increasing membrane thickness. Depending on their thickness and thus rigidity, the diffusion coefficient can be close to phospholipid membranes. The membrane proteins AqpZ, OmpF and KcsA where tested in triblock copolymer membranes of different thickness and their lateral diffusion was measured. Compared to lipid membranes, their mobility in the membranedecreased due to the increased membrane thickness. From Palivan et al.[1].

Adjustment of the thickness of synthetic membranes to the protein size is limited to a certain thickness as has been demonstrated by insertion of gramicidin (2 nm size) in PMOXA-*b*-PDMS-*b*-PMOXA membranes up to, but not greater than, 13.2 nm thickness[62]. Membrane thickness and copolymer flexibility are key factors for successful membrane protein insertion[62]. Very recently, the lateral movement of various membrane proteins within GUV membranes of a library of PMOXA-*b*-PDMS-*b*-PMOXA triblock copolymers was found to be similar to their diffusion in lipid bilayers but at a timescale, which is an order of magnitude slower[54]. When membrane proteins have to be inserted in thick synthetic membranes, and also preserve their functionality, the membrane thickness combined with its flexibility represents a crucial molecular parameter. The first successful reconstitution of a membrane protein was that of the highly stable porin, outer membrane protein F (OmpF) into PMOXA-*b*-PDMS-*b*-PMOXA triblock copolymer membranes[28]. During the formation of vesicles OmpF was inserted into the membrane and allowed diffusion of molecules up to 600 Da into the inner cavity. Similarly, the alpha-helical model protein bacteriorhodopsin (BR) has been reconstituted in PEtOz-*b*-PDMS-*b*-PEtOz polymersomes during the self-assembly

process[77,118]. These examples are based on integration of the membrane protein during assembly of the synthetic membrane assembly, but a different approach has been used for the reconstitution of a very sensitive membrane protein, complex I, into polymersome membranes: the protein was inserted into preformed polymersomes by destabilization of the membrane with small amounts of detergent Triton X-100 followed by removal of detergent[61]. This approach allowed protein insertion with a desired orientation, and serving for electron transport from the environment of the polymersomes inside the membrane. Indeed, the final orientation of a protein in a membrane can be crucial for its functionality, as for example when electrochemical gradients are formed. In order to orient a protein, one can exploit structural features such as its shape[119] or large hydrophilic domains[61,118]. For other proteins, as for example proteorhodopsin (PR), insertion can be guided by charges on the membrane surface[120]. In this respect, polymers with charged head groups may be used to guide protein reconstitution in polymersomes. An alternative way to guide proteins into membranes was shown by the use of asymmetric block copolymers (ABC type) together with the membrane protein aquaporin (AqpZ). By using two different hydrophilic blocks, the formed membrane induced a preferential orientation of the protein[121]. These examples demonstrate the possibility of tailoring block copolymers for controlling the orientation of membrane proteins, and helping to achieve functional reconstitution. However, investigations of the requirements for polymer membranes and their properties that allow membrane protein reconstitution is still at an early stage of research, and systematic studies on libraries of various copolymer types have not been performed.

1.4 *Design of experiments*

Statistical design of experiments (DoE) is a powerful approach to optimize processes. In general, this approach involves all stages during the selection of the experiments when testing a hypotheses. That includes the choice of the experimental subjects, measurements and measuring instruments[123]. The simplest and traditional method used by researchers and engineers is the one-factor- at-a-time (OFAT or OVAT) strategy. This method selects a starting point, called base line set of levels, for each factor and then varies one factor at a time over its range. This approach requires high amount of resources (experiments, time, material) and fails to detect any possible interactions between the factors due to the underlying assumption of independent factors[123,124]. In 1926, the British statistician R. A. Fisher proposed an innovative methodology for designing experiments, called factorial design. This strategy can detect interactions between the factors, by varying them all together at the same time. The objective of this design is to identify the interdependency between changes in system outputs (responses) and system inputs factors[124,125,126]. In Figure

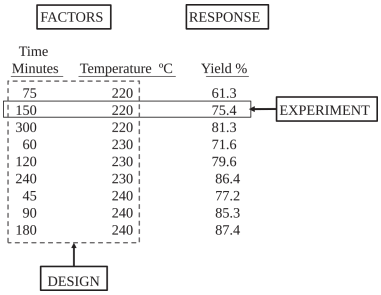

Figure 1.14: Example of an experimental design. From Lawson and Erjavec [122].

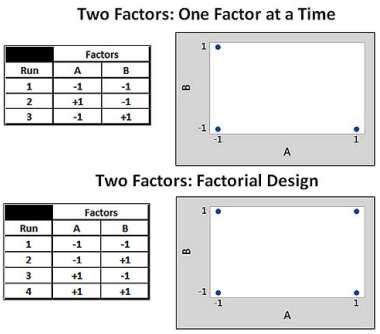

Figure 1.15: Schematic presentation of an OFAT experiment with two factors and three runs and two factor factorial design with the same factors. Factor settings are presented in the left table and their corresponding points in parameter space on the right. *From https://www.qualitydigest.com/inside/quality-insider-article/understanding-design-experiments.html.*

1.15, the OFAT approach is visualized in the upper row, whereas the lower row shows the corresponding factorial design. Notice that due to lack of (1, 1) combination, no information about possible interactions can be generated.[124]. Over the last years, this systematic approach started to be used by life science researchers. One of the more complex designs is the response surface methodology (RSM). This methodology was published by G. Box and coworkers in 1951[127]. RSM is a collection of mathematical and statistical techniques which technique aims to optimize the responses which are influenced by several variables. When applying RSM as an optimization technique some steps need to be followed[128,129,130].

Present ⇓ Goal ⇓

0% **Knowledge** 100%

Objective:	Preliminary Exploration	Screening Factors	Effect Estimation	Optimization	Mechanistic Modeling
No. of Factors		5 - 20	3 - 6	2 - 4	1 - 5
Model:	Variance Components	Linear	Linear + Interactions	Linear + Interactions + Quadratics	Mechanistic Model
Purpose:	Identify Sources of Variability	Identify Important Factors	Estimate Factor Effects + Interactions	Fit Empirical Model Interpolate	Estimate Parameters of Theory Extrapolate
Designs:	Nested Designs	Fractional Factorials	Two-level Factorials	RSM	Special Purpose

Figure 1.16: The process of knowledge gained over the course of experimentation. From Lawson and Erjavec[122].

Screening analysis Selection of independent factors with major effects on the system through screening studies and the delimitation of the experimental region. This is based on the study and the experience of the researcher.

Choice of the experimental design RSM approximates a complex unknown function with a low-order polynomial, commonly a first-order or a second-order model[130].

$$y = \beta_0 \sum_{i=1}^{k} \beta_i X_i + \epsilon \tag{1.1}$$

$$y = \beta_0 \sum_{i=1}^{k} \beta_i X_i + \sum_{i=1}^{k} \sum_{j>i}^{k} \beta_{ij} X_i X_j + \sum_{i=1}^{k} \beta_{ii} X_i^2 + \epsilon \tag{1.2}$$

with $y = Response, x = Factors, \beta = Coefficient$

A first-order model (Equation (1.1)) is used if the response can be defined by a linear function of independent variables. On the other hand, if there is a curvature in the response surface, then the second-order model should be used (Equation (1.2)). In this model,

the first sum represents all linear terms, the second all quadratic terms and the last sum the interaction terms.

The method of least square This technique generates a mathematic–statistical treatment of the obtained experimental data through the fit of the polynomial function previously chosen and the estimation of the polynomial parameters ($\beta_0, \beta_i, \beta_{ij}, ...$). Least squares means that the overall solution minimizes the sum of the squares of the errors made in the results of every single equation[131].

Evaluation of the model Select the necessary optimal design measurements in order to compare the estimation and prediction of the design. The design allows to understand the topography of the response surface (local maximum, local minimum, ridge lines) and finding the region where the optimal response occurs[128,129,130].

1.5 Examples of the application for synthetic biology

Reaction compartments POLYMERSOMES CONTAINING ACTIVE COMPOUNDS (proteins, enzymes, mimics) have been developed to serve as nanoreactors[60,28,132,133], or as artificial organelles inside cells[6,7,118]. For example, nanoreactors containing an enzyme were able to produce antibiotics *on demand* both in solution and when immobilized on surfaces[69,134]. The catalytically active species are usually one or more enzymes, or mimics, which are encapsulated during the vesicle formation process. For example, HRP[7] and laccase[115] were shown to catalyse substrate conversion in the interior of polymersomes. Encapsulation of enzymes provides the advantage of working in a protected environment and avoids degradation by proteases or the influence of factors such as pH or ion concentrations. However, the greater the protection provided by the polymer membrane, the lower the exchange to the exterior, e.g. diffusion of substrates and products into and out of the polymersomes. In order to circumvent this hindrance, either permeable membranes are used, or they are permeabilised by various methods. The polymer membrane itself is either permeable towards the substrate in general due to its composition[114,115,118] or permeability can be triggered by an external stimulus such as pH. Poly(N-vinyl-pyrrolidone)-*block*-poly(dimethylsiloxane)-*block*-poly(N-vinylpyrrolidone) (PNVP-*b*-PDMS-*b*-PNVP) based polymersomes are permeable towards reactive oxygen species (ROS), and allow their diffusion through the membrane[115]. Using PEG for the hydrophilic block, and a statistical mixture of a pH-sensitive poly(diethylaminoethyl methacrylate) (PDEAEM) and a photo-cross-linkable poly(3,4-dimethyl maleic imido butyl methacrylate) (PDMIBM) for the hydrophobic block, triggerable polymersomes were formed. Crosslinking of the PDMIBM blocks allows the structure of polymersomes to be preserved, and membrane permeability increased[116]. The drawback of these approaches is their non-specificity. Moreover, when a strong pH change (e.g.

from 6 to 8)[116] is required, it can strongly influence or completely inhibit enzymatic activity. A possible approach is the encapsulation of desired enzymes together with the reconstitution of a membrane protein, which facilitates the transport of the substrate[6,134,133,135]. In this case, substrate transport can be highly specific depending on the employed membrane proteins. However, fabrication of these systems gets more difficult as their complexity increases. Appropriate conditions must be chosen to ensure preservation of enzymatic activity during encapsulation, and at the same time to allow reconstitution of the membrane protein. So far, this has only been realized with model proteins, such as OmpF[6,136,134,133,135,137], FhuA[138] and biopores[62]. Using more than one enzyme to facilitate cascade reactions in confined spaces increases the complexity of the systems[116,139]. Cascades can be created by encapsulating one enzyme in a polymersome, which provides the substrate for one outside (or vice versa), co-encapsulation of both enzymes or encapsulation in separate polymersomes[114,116]. Similar to co-encapsulation of two different enzymes, a three step cascade reaction has been realized in a single polymersome[139]. A more biological approach for immobilization of a protein on the membrane was developed by fusing the amphiphilic Cecropin A peptide to enhanced green fluorescent protein (EGFP) where Cecropin A serves as an anchor in the polymer membrane[140]. Cellular processes make great use of spatial separation for control of biochemical reactions. Various nanoreactors have been produced with biomolecules encapsulated/entrapped inside[6,7,77,28,118,141,142]. PNVP-*b*-PDMS-*b*-PNVP triblock copolymers were used to encapsulate laccase from Trametes versicolor. The substrate 2,2'-azino-bis(3-ethylbenzothiazoline-6-sulphonic acid) (ABTS) was co-encapsulated and served to allow *in situ* reaction. This process produced ROS, which diffused through the membrane, and oxidized ABTS in the vicinity of the polymersomes[115]. In order to detoxify the well-known ROS, peroxynitrites, and simultaneously function for oxygen storage, a nanoreactor has been designed based on encapsulation of hemoglobin (Hb)[137]. In another example of a nanoreactor, an artificial metalloenzyme located in the inner cavity of polymersomes, permeabilised by the reconstitution of OmpF, was able to fulfil *in situ* its bioactivity[133]. The enzyme -gal preserved its activity inside PICsomes, which allowed the diffusion of the substrates and products through their membrane[86,143]. Polymersomes have been used to build cascade reaction systems. For example, PS-*b*-PIAT compartments allow diffusion of small molecules, and have been used to encapsulate two enzymes, GOx and HRP[114]. The peroxide generated from GOx was then utilized by HRP for conversion of ABTS. A three-enzyme cascade reaction is also possible, by using the combination of CalB, GOx and HRP located in different regions of the polymersome[139]. Although these examples are still model systems, they demonstrate the feasibility of creating nanoreactors and the ability to conduct cascade reactions. Furthermore, recent examples have demonstrated the use of this concept for distinct applications. ROS are generated in cells as a result of stress and lead to cell death if

they reach critical concentrations[6,136]. In order to protect cells from ROS, two enzymes SOD and LPO/catalase were encapsulated in a PMOXA-*b*-PDMS-*b*-PMOXA polymersome, with membranes permeabilised by the reconstitution of OmpF to mimic a natural peroxisome; the two enzymes acted in tandem to detoxify superoxide radicals and related H_2O_2[136,144]. A completely different type of nanoreactor was used to generate ROS *on demand* for use in photodynamic therapy. The photosensitizer Rose Bengal-bovine serum albumin (RB-BSA) encapsulated inside polymersomes with oxygen permeable membranes produced ROS in a light-responsive manner. The nanoreactor acted like a Trojan horse as it was taken up by HeLa cells with no cell toxicity on its own. However, upon irradiation at a wavelength of 543 nm, it produced ROS, which then led to cell death[6]. Nanoreactors have also been used for local antibiotic production to combat bacterial infections in implants. The encapsulated enzyme, penicillin acylase, was able to produce antibiotics under physiological conditions and to inhibit bacterial growth for up to 7 days[69,134].

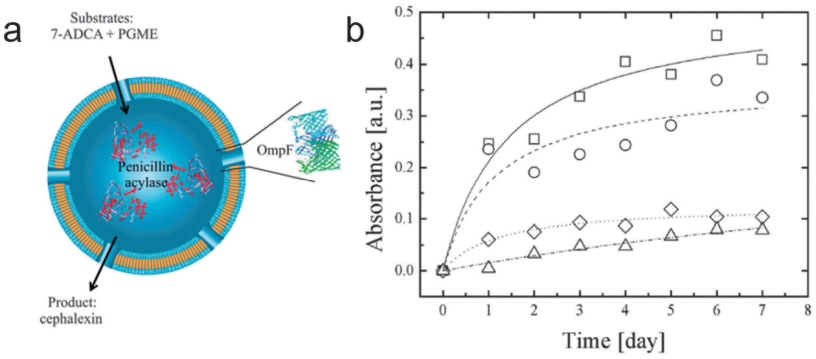

Figure 1.17: Penicillin acylase nanoreactor, which catalyzes the conversion of its substrates into cephalexin (left). The reaction curves (right) show the catalytic activity of the encapsulated penicillin acylase over 1 week. From Palivan et al. [1].

However, the design of nanoreactors has been limited by the availability and compatibility of building blocks, especially regarding membrane proteins; mainly OmpF has been used, and this permits passive transport of molecules[6,7,14,28,133,137,141,145]. Further studies on the development of membrane protein reconstitution might produce a higher specificity in terms of substrate/product selectivity, and the use of active transporters. The development of membranes with incorporated aquaporin appears to have reached a sufficient quality level for application[34,35,146,147,148]. Aquaporins are alpha-helical transmembrane pore proteins which allow the selective diffusion of water molecules through the membrane. These functionalized membranes have potential applications in water desalination, and comparative measurements have shown, that this type of membrane can outperform classical reverse osmosis (RO) membranes by a factor of approximately 750 times[34]. Recently, other members of the aquaporin family have been successfully reconstituted in membranes[148] and a framework has been proposed for quality assurance of reported methods and results[35].

Synthetic biology & multicompartment systems The bottom-up approach in the field of synthetic biology aims to recreate cellular processes, starting from simplified compartmentalization and ultimately leading to an artificial cell in the future[43,23]. Within this perspective, cascade reactions in separate reaction compartments can be seen as a first step in mimicking cellular processes. The definition of a living entity contains not only reproduction but also the capability to form and maintain its own metabolism. On a cellular level this requires the formation of electrochemical gradients, which are used to power various processes. Among the first examples is the creation of an artificial organelle, which uses BR to form a proton gradient that is utilized by a co-reconstituted ATP-synthase. The resulting polymersomes were able to mimic one of the fundamental energy generating processes and provide ATP upon continued illumination[77,118]. The bacterial respiratory enzyme complex NADH:ubiquinone oxidoreductase (complex I) translocates protons by a series of redox reactions from NADH to ubiquinone, and thus helps to generate and maintain the proton motive force. This principle was re-created in PMOXA-*b*-PDMS-*b*-PMOXA polymersomes, having complex I reconstituted in their membrane, whereas the protein maintained its activity in the synthetic environment[61]. Normally polymersomes for medical applications have sizes in the nanometer range and thus the visualization of these systems is barely manageable. So far, only electron microscopy can visualize these structures at a reasonable resolution, but it does not allow live-imaging of processes taking place. GUVs composed of either lipids or block polymers are advantageous for investigation via optical microscopy due to their size in the range of 10 – 50 μm[3,37,23,149,150,151,152]. By labelling of the polymers or lipids with fluorescent dyes, the formation of hybrid membranes could be observed which showed depending on the building blocks and their composition homogenous distribution of the lipids and polymers or domain formation[93]. Their cell-like size allows the investigation of their physical membrane properties via techniques like micropipette aspiration[37,149]. Moreover this allows the detection of inserted pores[62,150] and incorporation of lipids in the membrane by measuring the change of membrane elasticity[46,150]. A fundamental process in cellular activity and reproduction is the expression of proteins. GUVs can be used to encapsulate the expression machinery required to produce the protein MreB, a bacterial actin-like protein that is part of the cytoskeleton which defines the shape of a microorganism[151]. Successful expression of the fluorescent fusion protein MreB-RFP was visualized by confocal microscopy. Polymer stromatocytes can be loaded with platinum nanoparticles which function as a catalytic nanomotor, and the catalytic decomposition of hydrogen peroxide enables directed movement of the stromatocytes[153]. Furthermore, it has been demonstrated that polymersomes can possess an uptake mechanism that is similar to cell membranes[154]. The cascade reactions described in the previous section show the concept of compartmentalized reactions, which are used in nature. An elegant approach has now

been used to create multicompartments that are required for more complex systems[155,152]. By encapsulating PS-*b*-PIAT nanoreactors in PB-*b*-PEO polymersomes a fully active multicompartment system has been introduced[3,43]. However, all of the above mentioned examples are still model systems and are extremely simplified compared to nature. They only recreate certain functionalities, such as gradient generation[61,77,118], or protein synthesis in a confined environment[151] for the study of the underlying mechanisms. However, the goal of making these applicable to specific requirements has still not been achieved; nor has it yet been possible to recreate the high complexity required to mimic a cell.

2
Motivation: The molecular hoover

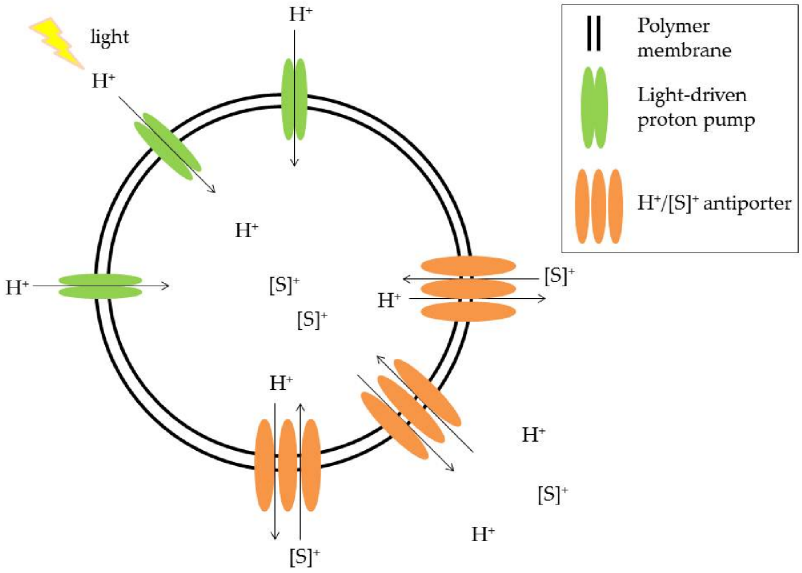

Figure 2.1: Schematic view of the molecular Hoover. Light induces the transport of H^+ into the inner cavity, building up a gradient. The H^+ / $[S]^+$ antiporter uses the gradient to transport the substrate $[S]^+$ into the cavity in exchange for a proton.

The vision for this work is the creation of a nanometer-sized molecular hoover. This nanoscale device is capable of specific molecular transport into its inner cavity and triggered release. As an example of the bottom up approach of synthetic biology it is assembled from *i)* a robust membrane in which *ii)* light-driven proton pumps generate energy (see section 1.2.2, p. 32) and *iii)* transporters provide the transport functionality. Open questions concerning the mechanisms of membrane protein reconstitution remain and provide a demanding challenge for researchers, even though numerous examples of devices acting as nanoreactors have emerged over the years in literature (see section 1.5, p. 41). As most transport processes are vectorial in their nature, the orientation of a transmembrane transporter is crucial for the functionality of an assembled system. How can we achieve unidirectional insertion of membrane protein? Taking PR as a model protein this work investigates the underlying pathways, which can lead to the desired formation of a proton gradient. As proposed in literature, PR's final orientation can be influenced by the correct choice

of detergent or by polarization of the membrane. Which pathway is dominant and under which conditions? With the knowledge obtained about the important parameters influencing the reconstitution, is it possible to use polymeric membranes as a host for the protein? And if yes, what adjustments to the reconstitution process need to be made, taking into account that having a protein far from its natural environment is a delicate task? As mentioned in section 1.1, p. 22, lipid based and polymer based membranes can be largely different. Having both membrane systems available allows a comparative study between them. Are proteopolymersomes able perform on the same level as proteoliposomes? The complexity of these systems demands a thorough and detailed characterization of their physical and chemical properties. Using design of experiments, the experimental work could be planned from the beginning to allow a detailed, efficient and targeted exploration. Apart from the explanatory assessment can optimal working conditions be derived? Statistical models offer the opportunity of mathematical optimization, finding the best suited factor combinations. Building up system like the molecular hoover described above requires the creative application of scientific principles of physics, chemistry and biology: *engineering*. Being guided by these principles allowed the creation of a theoretical and practical scaffold for a custom-made, functional nano-device, which is based on the desired robust polymer membrane and is powered by illumination.

3
Materials and methods

3.1 Chapter 4

3.1.1 Materials

All chemicals used in this project were provided by Sigma-Aldrich (Switzerland) if not stated otherwise. β-D-1-thiogalactopyranoside (IPTG) was prepared as 1M aqueous stock and stored at -20 °C. Lipids were supplied by Avanti Polar Lipids (USA) as a powder and solubilized in chloroform and stored at -20 °C. The detergent n-Octyl-β-D-Glucopyranoside (OG) was provided by Affymetrix.

3.1.2 Cultivation of Escherichia coli BL21 pLysS and expression of proteorhodopsin

Expression of PR was done as described in previous works[106]. *E. coli* BL21 pLysS culture containing the pZUDF plasmid[1] with the PR coding sequence was grown in LB-Miller medium at 37 °C and 180 rpm in 2L Erlenmeyer flasks. The sterile medium was inoculated with 1 % (v/v) of an over-night grown culture. During the incubation, growth was observed via measurement of the optical density (λ = 600 nm). The expression of PR was triggered by the addition of 0.1 mM IPTG and 5 μM all-*trans*-retinal when the culture reached an optical density of 1. Then, the cells were incubated for additional 3 h, harvested by centrifugation (3-18K, Sigma) at 4000 x g for 20 min and the supernatant removed. The pellets were collected and suspended in 20 mM TrisHCl, 100 mM NaCl, pH 7.4, and stored at -20 °C until preparation of the membrane.

[1] Kindly supplied by Prof. D. Fotiadis, University of Bern.

3.1.3 Membrane preparation

The frozen cells were thawed and subsequently lysed by using a french press (EmulsiFlex, Avestin), operated at 1500 bar. The resulting lysate was first centrifuged (3-18K, Sigma) at 4000 x g for 20 min in order to remove cell debris and then at 150000 x g for 1 hour (Optima XE-90, Beckman Coulter) to isolate the membrane. The pellet was

homogenized, washed with 20 mM TrisHCl, 100 mM NaCl, 10 % (w/v) glycerol, pH 7.4 two times, aliquoted to 1 mL and stored at -80 °C until further use.

3.1.4 *Proteorhodopsin purification*

The crude membrane fraction was solubilized in 7 ml of buffer (20 mM TrisHCl, 300 mM, NaCl, 10 % (w/v) Glycerol, pH 7.5, 3 % (w/v) OG and 0.5 mM TCEP) and protected overnight from light at room temperature. The next day, 1 mL Ni-NTA Resin (Quiagen) was washed 3 times with the buffer mentioned before and added to 7 mL extra of buffer with 30 mM of Imidazole and the 7 mL of previously solubilized protein, resulting in 15 mL final volume. The suspension was incubated 3 h on a roller shaker to ensure complete binding to the resin. After the incubation, the suspension was transferred into spin-columns (Promega) and the flow through collected. The resin was washed with 20 mM TrisHCl, 300 mM NaCl, 30 mM Imidazole, 10 % (m/v) glycerol and pH 7.5 containing 1 % OG and 1 mM TCEP and again the flow-through collected. In order to remove the remaining washing buffer, the spin column was centrifuged at 200 x g for 1 minute. Subsequently, the end of the column, that contains the resin with the protein, was cut, 450 μL of 20 mM TrisHCl buffer, pH 7.6, 150 mM NaCl, 10 % (w/v) glycerol, 400 mM imidazole, 1% OG, 0.01 % NaN_3 and 0.5 mM TCEP was added to elute the protein, properly sealed with parafilm and incubated for 1 h on a roller shaker at room temperature and protected from light. Finally, to elute the protein, the tube was placed in a 2 mL eppendorf and centrifuged in a bench-top centrifuge (miniSpin, Eppendorf) for 1 minute at maximum speed. The proteorhodopsin was stored at 4 °C and protected from light. The protein concentration was determined by measuring the absorbance at 525 nm (ϵ_{mol} = 45000 $M^{-1} \cdot cm^{-1}$)[106]. The typical protein yields were in the range of 1-1.5 mg/mL.

3.1.5 *Response surface modeling*

In order to find the optimal conditions of the reconstitution of PR in positively charged liposomes, a RSM design was created by using a custom design in the statistical software JMP® Pro 11.0.0 (64-bit) from SAS institute. The important input factors of the reconstitution conditions with associated ranges and appropriate response parameters were defined. Six variables as continuous factors were selected.

1. Lipid membrane composition
   (a) Neutrally charged, 100 % DOPC
   (b) Positively charged, 100 % DOTAP
2. pH during dialysis

3. Lipid to protein ratio
4. Salt concentration
5. Detergent concentration
6. Valinomycin concentration

RSM design requires adding single interactions (X1; X2), second-order interactions (X1*X2) and squared terms ($X1^2$; $X2^2$) for analysis, allowing to fit curved surfaces, which resulted in 27 runs in total. As the RSM was made under the custom design features of JMP® Pro 11.0.0, six extra degrees of freedom (runs) were added as default to minimize the model error, resulting in a total of 34 experiments, including the intercept.

3.1.6 Liposome preparation

The lipids used in this project were 18:1 (Δ9-Cis) 1,2-Dioleoyl-sn-glycero-3-phosphocholine (DOPC) and 18:1 1,2-dioleoyl-3-trimethylammonium-propane (DOTAP) (Avanti Polar Lipids, Alabaster, AL). Based on the response surface experimental design (see Table 3.1), the membrane composition limits were defined as:

- Low limit: Neutrally charged (100 % DOPC)
- Centre point: Partially positively charged (DOPC:DOTAP, 50:50 mol%)
- High limit: Positively charged (100 % DOTAP)

The liposomes were prepared by using the film rehydration technique. A certain volume of the lipid stock solution in chloroform was dried in vacuum and hydrated with 1 mL of 20 mM HEPES buffer (pH is based on the conditions of the RSM model,see Table 3.1), 150 mM KCl and 20 μM Pyranine, resulting in a final concentration of 3 mg/mL of liposomes. The suspension was allowed to stir at room temperature for at least 2 h. To ensure large unilamellar vesicles (LUVs) formation as the major population, the sample was extruded through a polycarbonate membrane (Nucleopore, Whatman) with a diameter of 200 nm.

3.1.7 Reconstituion of proteorhodopsin

The reconstitution of PR was carried out via a detergent-mediated pathway[25,26]. The OG concentration limits for the RSM model were selected to create a detergent concentration range where the point of detergent-saturated liposomes can be found (see section 1.3.2). The liposomes suspension was treated with OG by adding a certain volume of an aqueous stock solution of OG 10 % (w/v) and 1 mM of TCEP and gently stirred for 30 min. Afterwards, PR solubilized in OG was

Sample	Charge	pH	LPR (w/w)	OG [%, w/v]	KCl [mM]	Valinomycin [nM]
1	0.00	7	13	0.50	300	0
2	1.00	6	13	1.00	0	500
3	1.00	7	29	1.50	0	0
4	1.00	8	45	1.50	150	0
5	0.00	6	29	1.00	150	250
6	1.00	6	45	0.50	0	250
7	0.00	7	45	0.50	0	500
8	1.00	8	13	0.50	300	250
9	0.00	8	29	0.50	150	250
10	0.50	7	13	1.00	0	250
11	1.00	8	29	1.50	300	500
12	1.00	8	45	1.00	0	500
13	0.00	8	29	1.50	0	500
14	1.00	6	45	1.00	300	500
15	0.00	7	45	1.50	300	250
16	1.00	7	29	0.50	150	500
17	0.50	8	29	1.00	300	0
18	0.50	7	29	1.00	150	250
19	0.50	8	13	1.50	150	0
20	0.00	8	45	1.00	0	0
21	0.00	6	45	0.50	300	0
22	0.50	8	45	0.50	150	250
23	0.50	7	29	1.00	150	250
24	1.00	6	13	1.50	300	0
25	0.00	7	13	1.50	300	500
26	1.00	7	45	0.50	300	0
27	0.50	6	45	1.00	150	0
28	0.00	6	13	1.50	0	0
29	1.00	8	29	0.50	0	0
30	0.50	6	29	0.50	300	500
31	0.50	6	45	1.50	0	500
32	0.50	6	13	0.50	150	0
33	0.00	8	13	0.50	0	500
34	0.00	8	45	1.00	300	500

Table 3.1: Experimental design for the investigation of the governing factors for the reconstitution of PR

added to the liposomes to reach the lipid protein ratio (LPR) and the final OG concentration defined in Table 3.1. LPR limit descriptions are found below:

- Low limit: 13 w_{lipid}/w_{PR} or 460 mol_{lipid}/mol_{LPR}
- Centre point: 29 w_{lipid}/w_{PR} or 1100 mol_{lipid}/mol_{LPR}
- High limit: 45 w_{lipid}/w_{PR} or 1500 mol_{lipid}/mol_{LPR}

The lipid/detergent/protein suspension was stirred for 20 min and transferred into a visking dialysis tubing (Carl Roth GmbH Co. KG) with a cutoff of 14 kDa, previously washed with distilled water. The tubing was placed into a 1 L detergent-free buffer solution of 20 mM HEPES, with the pH and KCl concentration as defined in Table 3.1. The dialysis assembly was stirred over night to achieve the complete removal of the detergent. Subsequently, excess of pyranine was removed and the liposomes were purified by eluting them through a PD-10 size exclusion chromatography column (GE Healthcare), equilibrated with 20 mM HEPES, 150 mM KCl, pH 7.5.

3.1.8 Proton pumping activity assay

To investigate the functionality of PR in the proteoliposomes previously prepared, the internal pH was monitored via fluorescence spectroscopy. The fluorescence measurements were carried out in a similar way as the method published by Tunuguntla and coworkers[156] with PR and by Rigaud and coworkers[157] with BR. The proteoliposome solutions were diluted to 0.6 mg/mL lipid concentration in 20 mM HEPES buffer, pH 7.5, and 150 mM KCl. The sample was placed in the fluorimeter measuring chamber and allowed to equilibrate in the dark for 30 min with stirring. The intravesicular pH was monitored by using the pH-sensitive fluorescent dye pyranine. After the 30 min the sample was illuminated with a 120 W xenon lamp (Osram), utilizing a 530 nm $\pm$ 10 nm bandpass filter (FB530, Thorlabs). Excitation of the pyranine was carried out at 460 nm and the emission recorded at 510 nm (both 5 nm slit width) over time. The temperature was controlled and set within 19.5-20.5°C. Valinomycin was added to prevent the formation of back-pressure gradient[110,158]. The concentration of this ionophore was defined in Table 3.1.

3.1.9 Dynamic light scattering

Dynamic light scattering was used to determine the vesicles' size distribution on a Malvern Zetasizer Nano instrument at 25°C and equipped with a He-Ne laser (λ = 633 nm, measured at 173°). In all cases, the final lipid concentration was 0.3 mg/mL in 20 mM HEPES buffer pH 7.5 and a cumulant fit was used.

3.1.10 *ζ-potential measurements*

To measure the surface potential of the proteoliposomes a Malvern Zetasizer Nano instrument at 25°C was used and equipped with a He-Ne laser (λ = 633 nm). In all cases, the final lipid concentration was 0.3 mg/mL in 20 mM HEPES buffer pH 6[156,159].

3.2 *Chapter 5*

3.2.1 *Materials*

All chemicals were provided by Sigma-Aldrich (Switzerland) if not stated otherwise. Experiments were carried out in triplicates and their standard deviation used to estimate the error if not stated otherwise. Lipids were supplied by Avanti Polar Lipids (USA) and were supplied as a powder, solubilized in chloroform and stored at -20°C. The used detergents were supplied by Affymetrix (USA).

3.2.2 *Cultivation of Escherichia coli*

The cultivation of *E. coli* and expression and purification of PR-GFP was done essentially as described before[160,161]. *E. coli* carrying the PR-GFP containing pLEMO plasmid[1] was grown in LB-Miller medium at 30 °C and 180 rpm. An over-night culture was grown in the presence of 100 g/mL ampicillin. The sterile medium was inoculated with 1 % (v/v) of the over-night culture and 100 g/mL ampicillin and 34 g/mL chloramphenicol was added. The optical density (λ = 600 nm) was measured during growth and the expression triggered at a density of 0.8 – 1 via the addition of 0.1 mM β-D-1-thiogalactopyranoside (IPTG) and 5 μM all-trans-retinal. Subsequently, cells were incubated for additional 3 h, harvested by centrifugation (3-18K, Sigma) at 4000 x g for 20 min and the supernatant removed. As a last step, the pellets were collected and suspended in 20 mM TrisHCl, 100 mM NaCl, pH 7.4 and stored at -20°C until preparation of the membrane.

[1] Kindly supplied by Prof. D. Müller, ETH Zürich.

3.2.3 *Proteorhodopsin purification*

The isolation of PR out of its native membrane was carried out by using His-tag chromatography. The crude membrane fraction was solubilized in 7 mL buffer (20 mM TrisHCl, pH 7.4, 300 mM NaCl, 10 % (w/v) Glycerol) and 2.5 % Cymal-5. The solution was protected from light and placed on an orbital shaker at room temperature overnight. On the next day, 1 mL Ni-NTA resin (Quiagen) was washed 3 times with the solubilization buffer and added to another 7 mL buffer with 30 mM imidazole resulting in a total volume of 15 mL.

Subsequently, the suspension was placed in a an orbital shaker for 3 hours to ensure complete binding to the resin. The suspension was transfered into spin-columns (Promega) and the flow-through was collected. 20 mM TrisHCl, pH 7.4, 300 mM NaCl, 30 mM imidazole, 10 % (m/v) glycerol containing 0.4 % Cymal-5 were used to wash the resin and the flow-through was collected again. In order to remove residual washing buffer, the spin- column was centrifuged with 200xg for 1 minute. The end of the column containing the resin was cut off and the column sealed with parafilm. 450 μL of 20 mM KP_i buffer, pH 7.4, 150 mM NaCl, 10 % (w/v) glycerol, 400 mM imidazole and 0.4 % Cymal-5 were added to elute the protein. It was incubated for 1 hour on an orbital shaker at room temperature protected from light. The tube was placed in a 2 mL reaction tube and centrifuged in a bench-top centrifuge for 1 minute at maximum speed. A spin-filter (30 kDa cut-off) was used with 20 mM KP_i buffer, pH 7.4, 150 mM NaCl, 10(w/v) glycerol and 0.4 % Cymal-5 to increase the protein concentration and remove the residual imidazole. 1 μL of 1 mM TCEP was added after purification and the concentration determined by measuring the absorbance at 280 nm (ϵ = 96510 L $\cdot$ mol^1 $\cdot$ cm^1). Typical concentrations were around 10 to 20 mg/mL. The purified PR-GFP was stored at 4 °C and used within 3 days.

3.2.4 *Vesicle preparation and reconstitution of PR-GFP*

The vesicles were formed using a variation of the film rehydration method[160,34]. A certain volume of the DOPC (in chloroform) or $PMOXA_{17}$-$PDMS_{65}$-$PMOXA_{17}$ (in ethanol) solution was transferred into 1.25 mL flat bottom flasks and dried under high vacuum for 90 minutes. The resulting film was rehydrated with an aqueous buffer which always contained 20 mM potassium phosphate buffer, 150 mM potassium chloride and OG. The pH values and OG concentrations were adjusted accordingly to the experimental plan (see Table 5.1, 5.2 and 5.3, p. 74). The final volume was 500 μL and the membrane concentration 4 mg/mL. If the vesicles were used for proton translocation measurements, 100 μM of pyranine was added. The solutions were stirred overnight at room temperature and protected from light. Subsequently, the vesicle preparation were homogenized by extrusion (11x times) through a polycarbonate membrane (200 nm, Nucleopore, Whatman). Now the necessary volume of PR-GFP was added according to the desired LPR/PPR (see Table 5.1, 5.2 and 5.3, p. 74) and the protein-vesicle suspension stirred for 30 – 60 minutes. The dilution during the addition of PR-GFP to the reconstitution buffer lowers the concentration of CYMAL-5 by factor of 20 below the cmc (0.12 %) and thus, the impact of residual Cymal-5 was considered negligible[156]. Afterwards the samples were transferred into dialysis tubes (15 kDa cut-off, Visking) and dialysed against 20 mM KPi and 150 mM KCl for 48 hours. The pH was the same as the sample pH value. Furthermore, approximately 100 mg of SM-2 biobeads (Bio-Rad) were

added to ensure a constant dialysis gradient[162]. After the dialysis was complete, the samples were again extruded with a 200 nm membrane to ensure a homogeneous solution, remove any formed aggregates and purified by eluting them through a G-25 MiniTrap size exclusion chromatography column (GE Healthcare), equilibrated with 20 mM potassium phosphate buffer, 150 mM KCl, pH 7.2. The final volume was 1 mL and the membrane concentration 2 mg/mL.

3.2.5 *Dynamic light scattering*

The samples were measured in a Zetaziser Nano (Malvern) at 25 °C. A HeNe laser (λ=633 nm, measured at 173°) was uses as a light source. The samples were not diluted and allowed to equilibrate for 120 seconds. A cumulant fit was used for analysis.

3.2.6 *Fluorescence correlation spectroscopy*

The FCS measurements were performed as already described[163]. Briefly, an inverted microscope (Axiovert 200 M, Zeiss), equipped with a laser scanning microscopy module LSM 510 (Zeiss) and a ConfoCor2 (Zeiss) module was used. A 488 nm HeNe laser was focused into the 5 μL sample using a 488 nm dichroic mirror and a 40x water immersion objective. The emission beam was guided through a 70 μm pinhole and detected. The autocorrelation curve was fitted by using the equation

$$G_{3D}(\tau) = \frac{1}{N} \cdot \frac{1}{1+\tau/\tau_D} \cdot \frac{1}{1+\tau/S^2 \cdot \tau_D} \tag{3.1}$$

with τ_D being the diffusion time, equivalent to the decay time of the autocorrelation curve. The equation

$$D = \frac{\omega_0^2}{4\tau_D} \tag{3.2}$$

with D being the diffusion coefficient was used to calibrate ω, the radius of the confocal volume, by using the known flourescent dye oregon green 488[164]. Finally, the Stokes-Einstein equation

$$D = \frac{k_B T}{6\pi\eta r} \tag{3.3}$$

with T being the temperature (298 K), k_B the Boltzmann constant and η the viscosity was used to calculate the hydrodynamic radius r. Measurements were performed in 10 second intervals and 30 repetitions. The number of PR-GFP molecules was determined by estimating the molecular brightness of a single PR-GFP molecule in 20 mM potassium phosphate buffer, 150 mM KCl, pH 7.2 and 0.4 % Cymal-5 which resulted in 2.4 $\pm$ 0.19 counts per molecule (cpm). Dividing the vesicles' molecular brightness by PRGFP's one results in an estimate of the number of PR-GFP molecules per vesicle.

3.2.7 *Proton pumping assay*

To detect PR-GFP's ability to transport protons across a membrane when put under illumination we followed the well-established pyranine assay[157,165]. The measurements were carried out in a fluorescence spectrometer (LS55, Perkin Elmer), illuminating the sample with an 100 W xenon lamp (Intralux 4100, Volpi), utilizing a fibre guide to place the beam directly over the sample. The wave length was adjusted to 530 ± 10 nm by using a band-pass filter (Thorlabs). The samples were measured undiluted and in the dark for 30 minutes in order to equilibrate them. Afterwards the measurement was carried out under illumination, whereby the illumination was cycled between 50 seconds on and 10 seconds off. The fluorescence measurement was done during the off cycle to avoid interference. After the illumination measurement, the sample was measured for another 30 minutes in the dark to observe the re-equilibration of the fluorescence signal. The temperature was controlled at 20 ± 1 °C. The measurement data from the first 30 minutes in the dark was used for a linear fit whose slope was used as a correction factor for the measurement in order to remove potential artifacts from pH drift. The fluorescence intensity data was normalized by using ΔF_{460} / F_{460}. In order to calculate the gradients' amplitude in pH units, we used a calibration curve (see 5.2.3, p. 3.2.7).

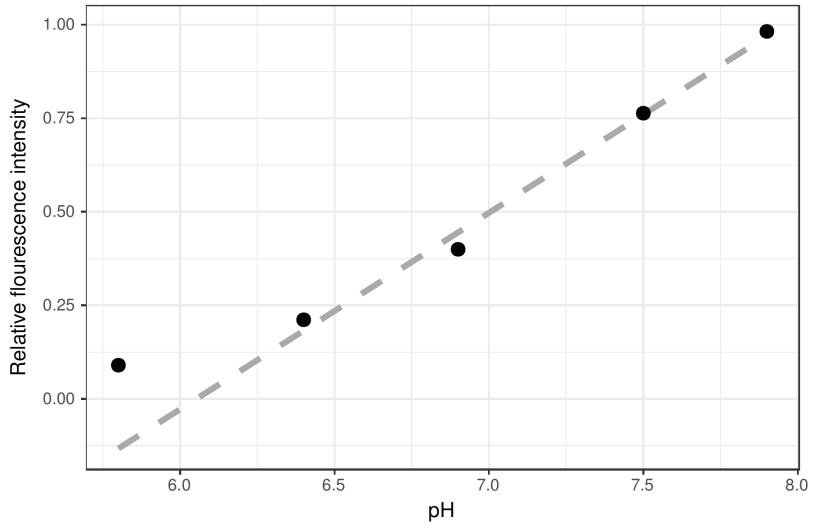

Figure 3.1: Calibration curve used to calculate the ΔpH values from the flourescence intensity. The change of pyranine's flourescence intensity is linear between 6.25 and 8 and thus this regime was chosen for linear regression. The resulting equation was $rel.F_{460} = -3.18 + 0.53 \cdot pH$ (R^2 = 0.98). Thus, $= \frac{rel.F_{460}}{0.53}$.

3.2.8 *Experimental design and data assessment*

The design proposed by Jones and Nachtsheim called definitive screening design was followed which allows a one-step screening and optimization process[166,167]. All experimental designs were created using the DoE module of the software JMP (SAS). The factors were

chosen to be the pH value, the lipid-to-protein or polymer-to-protein ratio (LPR or PPR) and the OG concentration in % (w/v). Their high, middle and low settings can be found in the Tables 5.1 - 5.3, p. 74. All designs were repeated three times in total to assess the variance. The data assessment was done by using the software R (Version 3.4). The model equations were derived by using a stepwise forward regression variant which enforces effect heredity, thus higher order effects are only included together with their corresponding linear effect[168]. All possible models were fitted and the one with the highest adjusted R2 was chosen. Blocking variables were used to take the possible batch-to-batch variation into account. The equations in section 5.2.5, p. 95, were used for the optimization.

4
Reconstitution of proteorhodopsin can be mediated via two distinct pathways

The correct insertion of a membrane protein into cellular membrane mimetic systems is crucial for the study of the function and structure of these molecules. This chapter focuses on the investigation of the underlying mechanisms of the reconstitution of proteorhodopsin and how various factors influence the resulting proteovesicles. Design of experiments will be applied as a framework to set up the experimental plan. Six factors will be investigated, the polarization of the membrane, the pH value during reconstitution, the lipid to protein ratio, the salt concentration in the buffer, the amount of detergent used and the effect of the addition of the ionophore valinomycin. Their effect on the responses vesicle size, vesicle population homogeneity, ζ-potential and proton pumping will be studied with the use of a second order polynomial model. It revealed two pathways which can mediate an oriented reconstitution of proteorhodopsin, one by the detergent OG and another by the use of charges on the membrane. Having a low detergent concentration around 0.5 % OG will induce a pathway which is nearly independent of the charge present on the membrane. The charge becomes the dominant mediator in high detergent regimes around 1.5 % OG and orients PR.

This study is in preparation for submission at *Physical Chemistry Chemical Physics*. Reconstitution of proteorhodopsin can be mediated via two distinct pathways.

4.1 Introduction

Membrane proteins perform vital functions in the cell, being it cellular communication, transport of substrates in and out of the cells, adhesion and movement or generating electrochemical gradients necessary for metabolic processes[25,95]. About one quarter of the genome of various organisms encodes membrane proteins.Membrane proteins represent the vast majority of clinical drug targets and are a in the focus of pharmaceutical and biotechnological research[75]. This explains the increasing interest of science and industry in their structure and function. Membrane proteins can be difficult to study in their native environment due to the complexity of their native membranes and interferences with other membrane constituents[110]. Therefore, it is necessary to incorporate them into liposomes in order to elucidate both functional and structural aspects[110]. Detergent-mediated reconstitution of membrane proteins has become the de

facto standard process. The amphiphilic detergent molecules allow a gentle extraction of the proteins out of their natural membrane environment and due to their interaction with phospholipids mediate the proteins' insertion. The first step to reach this goal is the production of the membrane protein. Since the prokaryotic membrane proteins cannot be found in high abundance naturally, thus the main production platform is *Escherichia coli*. In contrast to BR, it is possible to overexpress PR in *E. coli* making it also a good advantage for protein engineering[100].The next step is to isolate the protein from the cellular membrane which requires the use of detergent to solubilize the membrane. Detergents are amphiphilic molecules and tend to form micelles in aqueous solution above a critical concentration called critical micelle concentration (cmc). Membrane proteins are protected from agglomeration when they are inside of micelles. This agglomeration happens due to interactions with other membrane protein subunits. Nevertheless, the ionic detergents like sodium dodecyl sulfate (SDS) can induce to protein denaturation. That is why the non-ionic detergents are applied, n-Octyl-β-D-Glucopyranoside (OG), n-Decyl-β-D-Maltopyranoside (DM), n-Dodecyl-β-D-Maltopyranoside (DDM) and Triton X-100 being the ones most frequently used[25,75,26]. There are four basic strategies concerning the reconstitution of proteins into liposomes which have been used over the decades (see section 1.3.1, p. 34). Those are mechanical means, freeze-thawing, organic solvents and detergents. Most of these methods lead to the degradation and denaturation of many membrane proteins[25]. At the same time, many techniques to prepare pure liposomes are difficult to apply to proteoliposomes reconstitution because most membrane proteins are purified through the use of detergents, which interfere with the process of vesicle formation[25]. For this reason, the most successful and frequently used strategy for proteoliposomes preparation is the detergent-mediated technique (see section 1.3.2, p. 35). Here, the protein is first solubilized with lipids and the appropriate detergent in order to form a solution of lipid-protein-detergent and lipid-detergent micelles. Next, the detergent is removed resulting in the bilayer vesicle formation with inserted protein[110]. In 1995, Rigaud et al.[110] published a strategy to reconstitute membrane proteins by a stepwise solubilization of preformed liposomes. This technique allows experimental monitoring of the mechanism by which the protein interacts with lipids. The final results evidence that the reconstitution of proteins into liposomes can be described as a three stage process: In the stage I, the monomeric detergent molecules saturate the liposome membrane but the structure of the vesicle remains intact. A structural transition occurs in stage II, as the detergent- saturated liposomes start to dissolve into binary detergent-phospholipid micelles. In stage III, the transition is completed and only micelles are present. At the end of this process, the detergent is removed as the mirror image of the solubilization process[25]. The detergent removal is a critical step and the applied technique strongly depends on the selected detergent (see section 1.3.2. p. 35). One can distinguish between high

cmc detergents, which form small micelles (like OG), and low cmc detergents, which form large micelles (like DDM). In case of high cmc detergents, gel chromatography, dialysis and hydrophobic adsorption can be applied. The dialysis method is the most commonly used for high cmc detergent removal. During dialysis the detergent is diluted to concentration values below the cmc, resulting in the disintegration of the micelles to individual detergent monomers[26]. Having been used in successfully in former studies[160,161], this method is selected for the purpose of this project. As described in the previous section, PR reconstitution process depends on a number of factors, such as the used buffer, detergent, amount of protein. Despite several attempts, successful reconstitution of PR have been rarely reported[156,106,107]. Thus, it is necessary to create a more comprehensive strategy. Statistical design of experiments (DoE) is a powerful approach to optimize processes. In general, this approach involves all stages during the selection of the experiments when testing a hypotheses. That includes the choice of the experimental subjects, measurements and measuring instruments[123]. The simplest and traditional method used by researchers and engineers is the one-factor-at-a-time (OFAT) strategy. This method selects a starting point, called base line set of levels, for each factor and then varies one factor at a time over its range. This approach requires high amount of resources (experiments, time, material), and is not highly precise because it fails to detect any possible interactions between the factors[123,128]. In 1926, the British statistician R. A. Fisher proposed an innovative methodology for designing experiments, called factorial design. This strategy can detect interactions between the factors, by varying them all together at the same time. The objective of this design is to identify the interdependency between changes in system outputs (responses) and system inputs factors[124,125,126]. Within this work we employ design of experiments to investigate the reconstitution of PR into liposomes. The focus will be on the influence of membrane composition (ratio of neutrally charged DOPC to positively charged DOTAP), pH value, KCl concentration, OG concentration, LPR and valinomycin concentration. The formation of the proton gradient is the main function of PR and will be used to determine the success of a reconstitution. It has been described in literature that PR is able to orient itself during reconstitution with the use of a polarized membrane[156,120]. However, it remains unclear if this mechanism is independent of the type of detergent used and if not, which of the two factors is dominating the resulting orientation in proteoliposomes. The resulting data will be used to identify underlying mechanisms which govern the insertion of PR into the membrane under the various conditions. The two potential pathways, detergent mediated and charge mediated, will be of special interest.

4.2 *Results and discussion*

THE GOAL WITHIN THIS project was to gather knowledge about the way PR inserts itself into the membrane. Two different mechanisms have been proposed but up to now it remains unclear if and which one is dominant. Design of experiments was used to set up the experimental conditions to investigate the influence of the factors pH, LPR, detergent concentration, KCl concentration and the positive membrane charge. Valinomycin's influence on the gradient formation was investigated by addition during the proton translocation assay. The measured responses were the size via DLS, the polydispersity index, zeta potential and maximum ΔpH after 15 minutes of illumination as well as the ΔpH measured 15 minutes after the illumination. The ΔpH after the measurement was used to identify artifacts or "fuzzy" measurements (*e.g.* drifting fluorescence values). Because this work focuses on the activity of PR after reconstitution, the two ΔpH responses were considered as the primary ones, whereas the size, PdI and zeta potential were considered secondary.

4.2.1 *Observations and characterization*

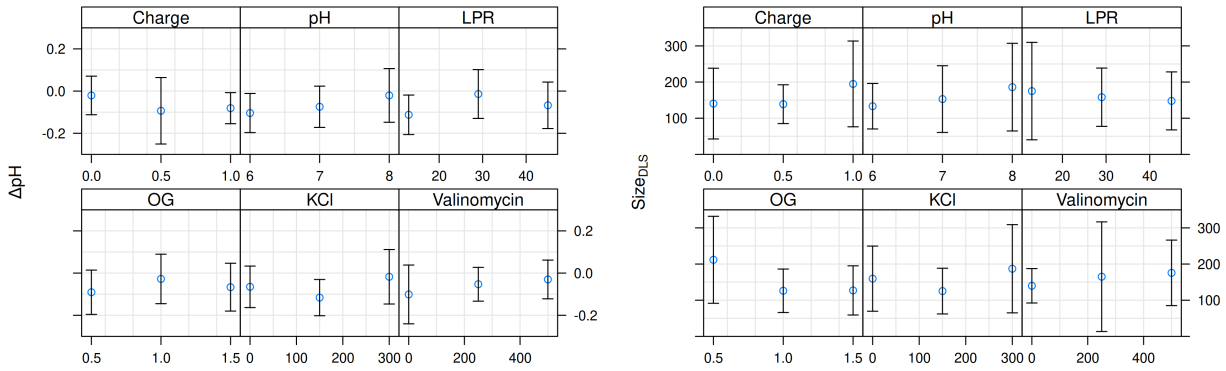

Figure 4.1: The mean response of the formed pH gradient (left) and the sizes measured via DLS. The data is grouped by the factors which were varied throughout the experiments. The error bars represent the corresponding standard deviation.

INVESTIGATING THE FORMED GRADIENT after 15 minutes of illumination as a primary response shows that most of the factors seem to have a local maximum of minimum setting (see Figure 4.1, left), indicated by the lowest or highest measured response value. Only the response of increasing valinomycin concentrations and the pH values seem to follow a linear increase, as an increase in their value or concentration leads to decrease of the formed gradient. The OG concentration, LPR and KCl concentration on the other hand have a clear parabolic shape, with the local minimum or maximum measured at the central value. Similar observations can be made in case of the membrane charge, although the trend is not as obvious. Increasing the positive charge on the membrane from a neutrally charged 100 % DOPC to 50 %

DOPC / 50 % $DOTAP^+$ leads from an observed amplitude of -0.02 ± 0.09 pH units to -0.08 ± 0.07. A contrary observation can be made in case of an increase of used detergent during reconstitution. The highest observed pH gradient of -0.09 ± 0.11 pH units is found at 0.5 % OG whereas an increase to 1.0 % decreases the amplitude to -0.03 ± 0.12 pH units. The size of the formed proteoliposomes is follows trends observed in former studies. On average, the size decreases as the detergent concentration increases (see Figure 4.1, right). 212 ± 120 nm are observed on average when 0.5 % of OG are used which decreases down to 126 ± 60 nm (0.5 % OG) and 127 ± 68 nm. The ζ-potential's behavior towards an increasing positively charged membrane composition follows a similar logical trend (see Figure 4.2, left). DOPC proteoliposomes exhibit 2.1 ± 6.1 mV, whereas a composition of 50 % DOPC / 50 % DOTAP results in 20.1 ± 12.2 mV. A further increase to a 100 % DOTAP membrane does not lead to a further increase in ζ-potential, 9.7 ± 17.2 mV are measured.

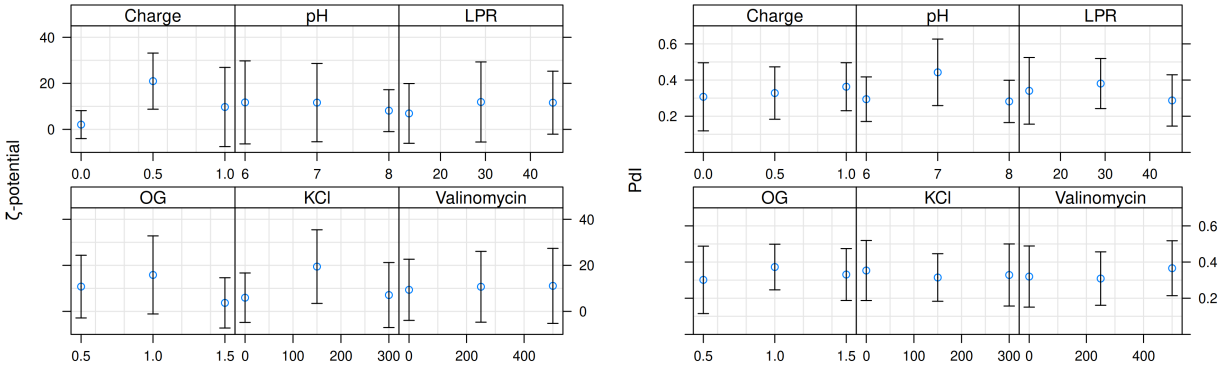

Figure 4.2: The mean response of the measured ζ-potential (left) and the PdI. The data is grouped by the factors which were varied throughout the experiments. The error bars represent the corresponding standard deviation.

4.2.2 *Identifying important factors*

To estimate the importance of a factor towards a certain response its influence was determined via the following steps: The response values were scaled to [0, 1] and a simple linear model of the form was fitted. The slope is used to determine the influence of a certain factor on a response and summarized in Figure 4.3. This simplification is useful to gain first knowledge and gives already a good overview of each factors effect. The amplitude of the pH gradient after illumination and after relaxation in the dark is influenced in a similar way. Increasing the charge of the membrane increases the amplitude whereas an increase of the other factors lead to a decrease. Adding valinomycin has surprisingly a negative impact on the amplitude of the proton gradient. Removing the potential back-pressure effect caused by other ions in the system should lead to faster and higher formation of the proton gradient. Increasing the LPR and thus decreasing the protein concentration leads to slightly smaller vesicles,

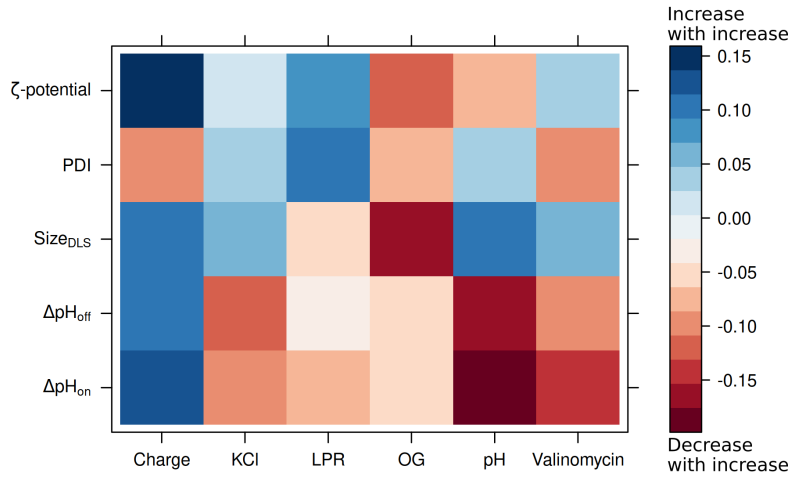

Figure 4.3: The color describes the direction of the observed change: blue colors correspond to an increase of the measured response (e.g. size) if the factor value is increased as well, whereas red colors correspond to a decrease of the measured response if the factor value is increased. Values are adjusted such that an increase of the measured response represents the actual measurement (e.g. a lower PDI is desirable). Note that this is a simplification and disregards any interactions between the various factors.

on the other hand to a lower amplitude of the pH gradient, as less pumps can be present in the membrane. The size of the formed proteovesicles is positively influenced by the presence of charged lipids as well as higher pH values. Contrary, increasing the concentration of the used detergent OG has a negative impact, as an increase in the detergent concentration leads to the dissolution of the preformed vesicles into binary or tertiary micelles. More heterogeneous vesicle populations are observed when using more charged lipids and higher OG concentrations whereas a a high LPR decreases the PDI. As expected, the ζ-potential correlates nicely with the number of charges present in the membrane but does not increase when more PR is used during reconstitution. This analysis gives a good overview about the linear effects present. The potential interactions between factors and quadratic effects will be analyzed in the next section with the help of a response surface model.

4.2.3 *Response surface modeling*

Fitting the response surface to the data allows a more detailed analysis of the data. A second-degree polynomial model was fitted to the data and stepwise forward regression applied to trim unnecessary model terms. This procedure generates models which describe the data well and have a good prediction power. Due to the method obeying the effect heredity, introduced bias is lower as in conventional stepwise regressions[168]. Not all factors have an equal effect on each response, thus within the first step the most influential ones were identified (see Figure 4.4). In terms of statistical significance, KCl plays the most important role for the formation of the proton gradient. Its quadratic and linear effect are highly significant. Furthermore, the quadratic term of the detergent concentration is significant as well as its interaction with terms with valinomycin and the LPR.

Looking at the complementary models describing the size, PDI and ζ-potential of the proteoliposomes, no term is significant in all models (see Figure 4.5 and Table 4.1, p. 67). The relaxation of the proton gradient shows similar significant terms as its formation, the pH value has a significant quadratic effect. It should be noted that the ζ-potential model shows only the KCl^2 and the OG*Valinomycin terms as significant. However, the model's overall fit to the data is also the worst (adj. R^2 = 0.58).

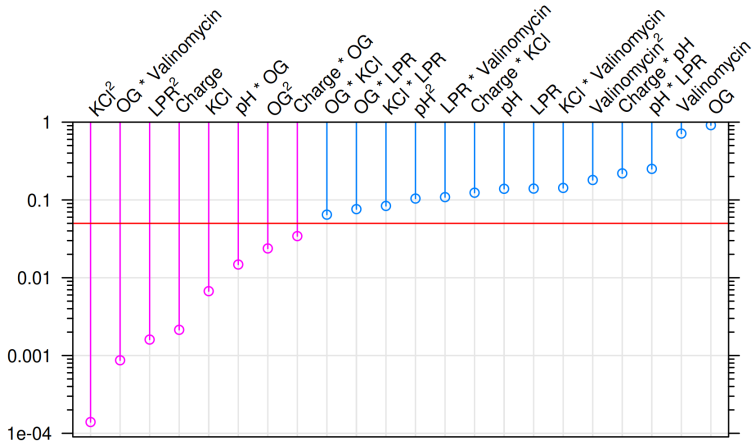

Figure 4.4: Factors sorted by the significance on the formed pH gradient. The red line indicates the significance level α = 0.05

In order to visualize the behavior of the system it is helpful to look at the response surface. In Figure 4.6 the three significant interactions are shown. OG * Valinomycin (Figure 4.6, a)) has a parabolic shape which means that minimum and maximum gradient amplitude are found in the extremes of the graph. A high ΔpH is found at either 1.5 % OG and 500 nM valinomycin or 0.5 % OG and 0 nM valinomycin. Intermediate combination have a lower ΔpH value. The quadratic effect of the OG concentration and the linear effect of the lipid membrane composition are observable in Figure 4.6, b). Maximum ΔpH values can be found at the combination of 100 % DOTAP and 1.5 % OG. Figure 4.6, c) presents the interaction of the quadratic effects of the factors pH value and OG concentration. Again, maximum proton gradient amplitudes are expected to be found in the extremes of the surface.

4.2.4 *Effect of the salt concentration*

THE MOST SIGNIFICANT EFFECT detected for the model is the quadratic effect of KCl (see Figure 4.4). Its parabolic shape (see Figure 4.7) clearly shows only a very narrow range around 150 mM KCl where the functional reconstitution of PR is possible. Protein aggregation was observed after dialysis either when there was no KCl in the buffer or when the buffer was prepared with the maximum KCl con-

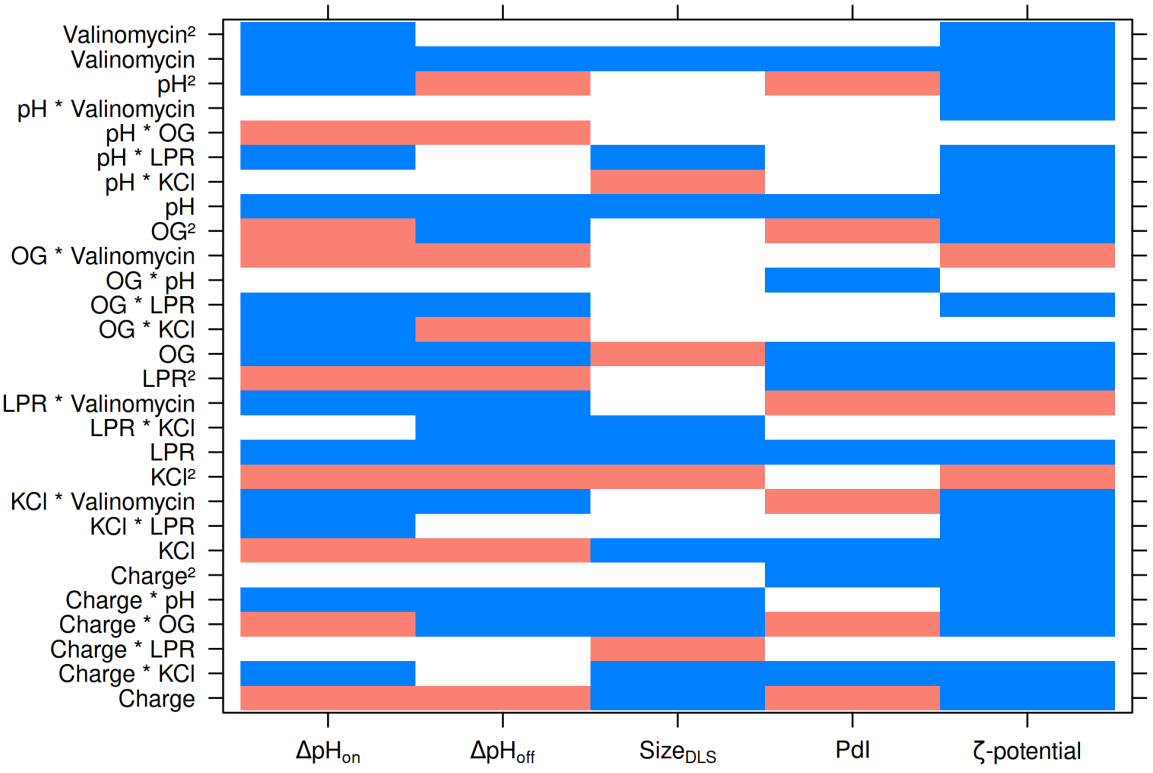

Figure 4.5: Overview of the statistical significance of all factors towards the measured responses. A blue color indicates no statistical significance, whereas a red color indicates statistical significance. $\alpha = 0.05$.

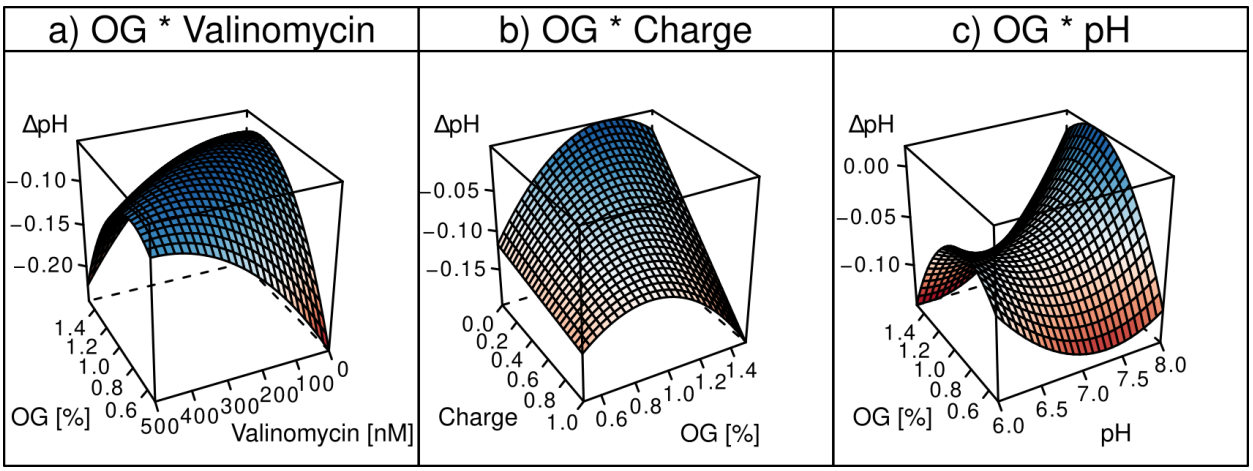

Figure 4.6: Visualization of the response surfaces for selected interactions. Shown are the three significant interaction terms (see Figure 4.4). The color indicates low (blue) to high (red) amplitudes of the measured pH gradient.

	ΔpH_{on}			ΔpH_{off}			$Size_{DLS}$			ζ-potential			PdI		
	B	std. Error	p	B	std. Error	p	B	std. Error	p	B	std. Error	p	B	std. Error	p
Intercept	-0.06	0.03	0.085	-0.10	0.04	**0.033**	119.56	21.85	**<0.001**	25.05	5.07	**<0.001**	0.52	0.05	**<0.001**
Charge	-0.05	0.01	**0.002**	-0.06	0.02	**0.003**	27.16	13.98	0.067		4.55	2.08	0.053	0.04	0.02
0.048															
pH	0.02	0.01	0.139	0.03	0.02	0.101	26.90	13.93	0.069	-0.02	2.10	0.993	-0.01	0.02	0.798
LPR	0.02	0.01	0.140	0.01	0.02	0.695	-17.13	14.20	0.243	1.50	2.14	0.498	-0.02	0.02	0.240
OG	0.00	0.01	0.915	0.01	0.02	0.781	-53.26	14.37	**0.001**	-3.09	2.14	0.179	0.01	0.02	0.562
KCl	0.04	0.01	**0.007**	0.06	0.02	**0.005**	6.53	13.88	0.643	-0.85	2.05	0.688	-0.01	0.02	0.446
Val	0.01	0.01	0.713	0.00	0.02	0.990	15.37	14.18	0.292	1.01	2.13	0.646	0.01	0.02	0.747
Charge:pH	0.02	0.02	0.220	0.03	0.02	0.268	22.47	17.26	0.208	-3.50	2.54	0.198			
Charge:LPR							-36.93	16.82	**0.041**						
Charge:OG	-0.04	0.02	**0.034**	-0.05	0.02	0.052	21.80	16.20	0.194	-4.57	2.56	0.105	0.06	0.02	**0.014**
Charge:KCl	0.02	0.01	0.124				29.14	15.20	0.070	2.32	2.28	0.335	0.03	0.02	0.201
pH:LPR	0.02	0.02	0.251				-21.01	16.88	0.228	-3.51	2.57	0.202			
pH:OG	0.05	0.02	**0.015**	0.05	0.02	**0.050**									
pH:KCl							46.79	17.00	**0.013**	-4.19	2.52	0.128			
pH:Val										-2.04	2.53	0.437			
LPR:KCl				-0.03	0.02	0.240	-26.94	15.86	0.106						
LPR:Val	-0.03	0.02	0.109	-0.04	0.02	0.109				7.49	2.49	**0.013**	0.08	0.02	**0.002**
OG:pH													0.03	0.02	0.249
OG:LPR	0.03	0.02	0.076	0.03	0.02	0.199				3.64	2.56	0.185			
OG:KCl	0.03	0.02	0.065	0.06	0.02	**0.018**									
OG:Val	-0.07	0.02	**<0.001**	-0.09	0.02	**0.002**				6.36	2.68	**0.039**			
KCl:LPR	-0.03	0.02	0.084							4.47	2.43	0.096			
KCl:Val	-0.02	0.02	0.143	-0.03	0.02	0.223				4.30	2.39	0.102	-0.07	0.02	**0.004**
Charge²										-7.14	4.45	0.140	0.07	0.04	0.085
pH²	0.04	0.02	0.104	0.08	0.03	**0.021**				-6.02	3.78	0.143	-0.17	0.04	**<0.001**
LPR²	-0.10	0.02	**0.002**	-0.12	0.03	**0.005**				4.02	3.92	0.330	-0.08	0.04	0.052
OG²	-0.06	0.02	**0.024**	-0.06	0.03	0.080				-5.07	3.96	0.229	-0.09	0.04	**0.017**
KCl²	0.15	0.03	**<0.001**	0.16	0.04	**<0.001**	55.27	25.88	**0.046**	-16.59	4.60	**0.005**			
Val²	-0.04	0.03	0.180							8.94	4.42	0.070			
Observations	34			34			34			34			34		
R^2/adj. R^2	0.906/0.718			0.838/0.619			0.732/0.535			0.873/0.581			0.811/0.654		
F-statistics	4.825***			3.818***			3.710***			2.986***			5.160***		

Table 4.1: Model coefficients of the response surface model describing the characteristics of the formed PRGFP proteopolymersomes. Bold text highlights statistical significance ($\alpha = 0.05$).

centration (300 mM). This phenomenon can be explained by *i)* the effect of the ion concentration on protein structures and *ii)* by protein-protein interactions, which both affect the solubility of proteins[169]. As PR is an asymmetrically charged protein which contains differently charged surface residues, the presence of KCl in the buffer increase repulsive electrostatic forces between PR's extra-membrane residues and thus, decrease the protein-protein attractive force. Furthermore, high concentrations of KCl will salt out the protein as described in the Hofmeister series[170,171]. The presence of high amounts of KCl in the buffer solution decreases the hydrogen bonds interactions with PR peptides and makes the protein insoluble, increasing the likelihood of aggregation[169,172]. In the absence of KCl, the buffer allows the internal interaction of the basic residues with the acid residues of PR. This internal interaction can expose the hydrophobic core and finally aggregates PR.

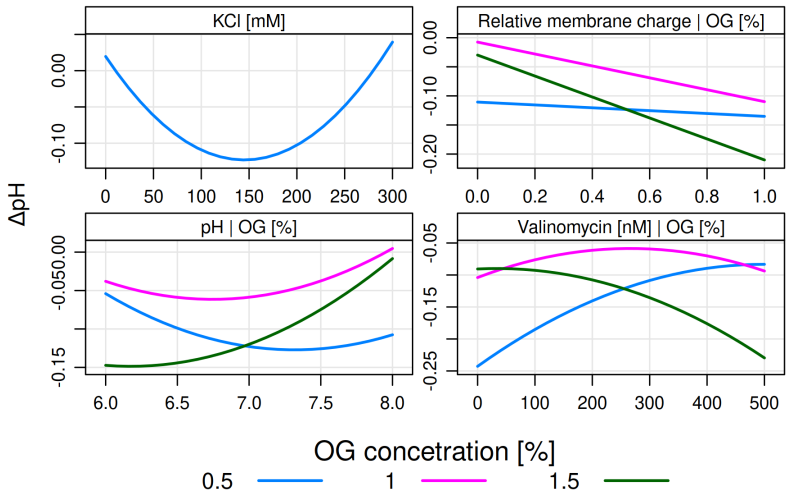

Figure 4.7: Interaction plots of the model's significant interaction terms. All plots shown have the ΔpH value on their y-axis, whereas their x-axis is stated in the panel titles. Where applicable, results are grouped by the OG concentration, indicated in the panel titles and by the color.

4.2.5 *Effect of the membrane polarization and detergent concentration*

STUDIES FOCUSING ON BR have concluded that its final orientation after reconstitution was more unidirectional when performed into detergent-saturated liposomes. OG facilitates the direct insertion of BR through its most hydrophobic domain (N-terminus) leaving the most hydrophilic domain outside of the liposome (BR contains five COOH groups)[95]. PR has a different amino acid sequence but the resulting tertiary structure is highly similar to BR and similar results when using OG as a detergent have been described[160]. Additionally, it was shown that PR can be guided by the polarization of the membrane[156]. Indeed, our results show that both mechanisms are possible for the insertion of PR, however they require different conditions. The model analysis shows significant interactions between OG and the

membrane charge (see Figure 4.4) which is visualized in Figure 4.7. It can be seen that the influence of the membrane charge is dependent on the OG concentration and two regimes can be identified. *i)* Within the low detergent regime, the resulting ΔpH is largely not influenced by the membrane charge and nearly identical values around 0.10 pH units are measured. PR is expected to insert itself into detergent saturated liposomes. *ii)* Within the high detergent regime however, the resulting proton gradient is heavily affected by the membrane charge. Using a combination of neutral 100 % DOPC liposomes together with 1.5 % OG results no measurable activity, which changes to approximately 0.20 pH units when 100 % DOTAP liposomes are used. Here, the detergent-lipid mixture contains a large amount of lipid-detergent-protein micelles. In this moment the negative side of PR interacts with the positively charged lipids, generating a strong electrostatic binding during the detergent removal. These results provide strong indication that the OG mediated pathway is dominant under the tested conditions.

4.2.6 Effect of the pH value

The interaction of the pH value with the detergent concentration (see figure 4.7) is related to the two reconstitution mechanisms explained above. At pH 6 the two extramembrane domains of PR are oppositely charged which allows the interaction with the positively charged lipid membrane. As stated above, this requires an OG concentration of 1.5 % for full effect. The low functionality of PR in samples at pH 7 is due to the isoelectric point of the extra-membrane amino acids of PR (pI). At this pH PR's extramembrane domains are slightly negatively charge. Hence, the unidirectionality of PR cannot be achieved.

4.2.7 Effect of the addition of valinomycin

Similar to the effects discussed before, the effect of valinomycin is strongly dependent of concentration of OG used during reconstitution. A large ΔpH can be achieved when using 0.5 % of OG and no valinomycin whereas at 1.5 % OG the addition of 500 nM valinomycin leads to the formation of a similar proton gradient. These results suggest that the detergent mediated pathway leads to a high unidirectionality of reconstituted PR. On the other hand it appears that when PR is reconstituted by detergent removal after lipid-detergent-protein micelles formation, random orientation of PR cannot be avoided, decreasing the proton pumping functionality of PR. Such low proton pumping activity can be overcome by the addition of valinomycin (500 nM) which then prevents the formation of an inhibitory back pressure effect with a compensatory K^+ movement through the membrane.

4.3 Conclusion

From the results of this work we can conclude that *i)* PR can be reconstituted via two pathways into liposomes in which the detergent OG or the membrane charge is the mediator for the final orientation. *ii)* The detergent OG seems to be the dominant pathway and does not need high protein concentration to yield functional proteoliposomes. *iii)* The addition of valinomycin was only beneficial when used in samples which resulted from a high detergent / high charge composition. The good unidirectionality in samples from low detergent compositions made decoupling of the proton gradient unnecessary. Furthermore, approaching this study by using design of experiments allowed the investigation of the underlying mechanics with ease and detail. Further similar studies will shed more light on the interplay of detergent, membrane proteins and membrane building blocks and how to assemble them into functional units.

5
Optimized reconstitution of membrane proteins into synthetic membranes

Herein this chapter, a detailed analysis of the formation of proteoliposomes and proteopolymersomes and the requirements for a successful reconstitution of the membrane protein proteorhodopsin is presented. Light-driven proton pumps such as proteorhodopsin have been proposed as an energy source in the field of synthetic biology. The energy is required to power biochemical reactions within artificially created reation compartments like proto- or nanocells, which are based on either lipid or polymer membranes. The insertion of membrane proteins into these membranes is delicate and quantitative studies comparing these two systems are needed. To this end, we applied design of experiments to provide a mathematical framework for the reconstitution process. Mathematical optimization identified suitable reconstitution conditions for lipid and polymer membranes and the obtained data fitted well to the predictions. Altogether, our approach provides experimental and modeling evidence for different reconstitution mechanisms depending on the membrane type which resulted in a surprisingly similar performance.

This study will be published in *Nature Communications Chemistry*. **Roland Goers**, Johannes Thoma, Noah Ritzmann, Alfredo Di Silvestro, Claudio Alter, Gesine Gunkel-Grabole, Dimitrios Fotiadis, Daniel Müller and Wolfgang Meier. Optimized reconstitution of membrane proteins into synthetic membranes

5.1 Introduction

Methodologies from biology and engineering are combined in the bottom-up approach in synthetic biology[173,23], which aims at building a biological system with a desired functionality from the bottom by using dedicated building blocks. An example of such a system is the design and construction of artificial proto-cells, cell-like objects exhibiting fundamental functionalities[23]. Despite the low complexity of proto-cells, their design and implementation requires in-depth knowledge about cellular machineries and their assembly. This knowledge could ultimately lead to the development of synthetic systems not found in nature, which can be utilized for example in the industrial production of biotechnological goods or pharmaceuticals[23,1]. An important biomedical application of such synthetic systems is mimicking metabolic processes, which are fundamental in the cellular environment and every living organism[1,134,174]. Energy generation and transport processes are crucial for the proper function of a cell. Within cells, reactions often occur inside specialized compartments,

where membrane proteins mediate the transport of substrates and products[43]. The membrane protein can form a pore and allow passive diffusion up to a specific size. Larger and more complex molecules or gated processes, which only allow passage upon a certain criterion (*e.g.* voltage or molecular recognition), usually require a source of energy. Building artificial proto-cells requires reconstitution of membrane proteins into the compartment's membrane in order to facilitate exchange of metabolites. Different approaches and techniques have evolved over the decades to reconstitute membrane proteins into lipid membranes. The research resulted in an applicable framework for detergent mediated reconstitutions into liposomes which is still used in variations today[25,26]. For reconstitutions into polymer membranes, which structurally resemble lipid membranes but are composed of amphiphilic polymers and are therefore more robust and also thicker[1], no such framework exists making the reconstitution of functional proteins more challenging.

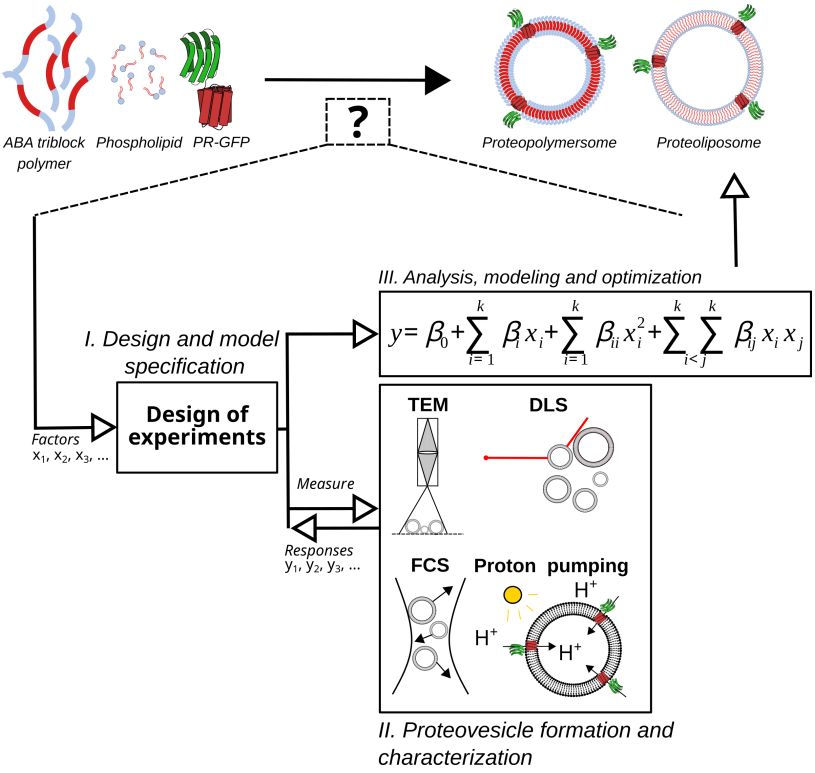

Figure 5.1: Schematic visualization of the concept. The assembly of phospholipids or triblock copolymers together with membrane proteins is an induced self-assembly process and the resulting structure depends on the starting conditions. A priori knowledge about the factors (*e.g.* buffer conditions, protein concentration, membrane concentration) is usually lacking and optimal results cannot be achieved. Having two different membrane building blocks further increases complexity. **I.** By using DoE and defining influential factors along with characteristic responses one can devise an experimental plan to investigate the system's behavior in resource-efficient way. **II.** Here, the effect of the factors pH value, detergent concentration and membrane-to-protein ratio on the proteovesicles' characteristics size, homogeneity and functionality was investigated. **III.** The results were used to fit a model for detailed analysis of the process and subsequent optimization, which allowed to find optimal assembly conditions to yield the desired functional proteoliposomes and proteopolymersomes.

Only brief guidelines have been proposed and the potentially very different interactions between polymers, detergents and proteins compared to lipid-based systems have not been studied in detail[117], underlining the need for a detailed comparative study and formulation of a comprehensive framework[35]. Two highly important requirements need to be fulfilled to apply this concept in engineering: reproducibility and predictability. So far, the proposed approaches fail to satisfy at least one of these requirements. Design of experiments (DoE) is a method, which has emerged in the 1930s[128]. The underlying idea is to devise an experimental plan that samples a given parameter space

optimally and thus keeps the number of experimental runs low and uses them efficiently. In contrast to the common one-factor-at-a-time method (OFAT or OVAT), which keeps factors constant and varies only one, DoE can identify interactions and requires fewer runs with the same precision in estimating the factors' effects. Subsequently, the whole parameter space is interpolated via linear model regression. The derived model can in turn be optimized to find experimental conditions that yield a predicted response. Within the past two decades, block copolymers have emerged as a synthetic alternative to natural phospholipids as membrane building blocks[1,27,28]. These polymers assemble into similar structures as phospholipids, because they are composed of a hydrophobic and one (AB-type, diblock) or two (ABA-type, triblock) hydrophilic blocks. Hence, similar to lipids block copolymers can self- assemble to form spherical particles, worm-like structures, hollow vesicles and planar membrane sheets[29,175]. In contrast to lipids, polymers can be adjusted to meet specific needs: the membrane thickness, rigidity and permeability can be controlled by tuning the block length and the hydrophilic to hydrophobic block ratio[1,29]. Beside poly(butadiene)-*block*-poly(ethylene oxide) (PB-PEO) diblock copolymers, poly(2-methyloxazoline)-*block*-poly-(dimethysiloxane) (PMOXA-PDMS) diblock or poly(2-methyloxazoline)-*block*-poly-(dimethysiloxane)-*block*-poly(2-methyloxazoline) (PMOXA-PDMS-PMOXA) triblock copolymers are commonly used for self-assembly involving proteins or other biomolecules. Their low glass transition temperature and resulting flexibility as well as lateral diffusion properties make them good candidates for the reconstitution of membrane proteins[1]. The combination of PDMS-PMOXA polymer membranes and the efficiency and selectivity of biological components such as enzymes and membrane proteins combines the "best of both worlds" and can be exploited towards building synthetic nanoscale devices[1]. Such molecular factories can be envisioned performing enzymatic production or degradation of specific compounds (antibiotics, etc.) or take over a desired functionality[176]. Examples described in the past decade were facilitated by the progress of structural biology and the derived methods for membrane protein reconstitution[177,178,179,180,181,165]. Yet, in case of polymer systems progress has been slower due to their lower prominence and commercial availability compared to phospholipids. Thus far, mainly robust membrane proteins have been used for reconstitution in polymer membranes and the goal to combine biological with synthetic parts from chemistry has only partly been achieved[1]. More sophisticated systems require the presence of an energy source such as the generation and upkeep of proton gradients in addition to the reconstitution in the synthetic membrane. Bacteriorhodopsin (BR) and proteorhodopsin (PR) are well-known for their ability to form proton gradients upon illumination[105,110,100]. BR has been extensively studied over the years, from solving its crystal structure to using it as a light-triggered conductor[181]. PR has a similar structure to BR but is more accessible to genetic engineering and can be easily ex-

pressed in *Escherichia coli*. Examples from possible modifications are the adjustment of its absorption wavelength, integration of a chemical on/off-switch and the attachment of a hydrophilic protein to guide the orientation during insertion into the membrane, which is crucial for its functionality[103,160,161]. In this work, we employ DoE to optimize reconstitution of a proteorhodopsin-green fluorescent protein fusion protein (PR-GFP) into liposomes and polymersomes. GFP guides the orientation during the insertion process into preformed vesicles due to its hydrophilic nature, which does not allow passage through the hydrophobic inner part of the membrane[161]. Additionally, GFP's fluorescence enables detection of the protein in the resulting assemblies. 1,2-dioleoyl-sn-glycero-3- phosphocholine (DOPC) and $PMOXA_{17}$-$PDMS_{65}$-$PMOXA_{17}$ (ABA) were used as phospholipid or block copolymer building blocks[1,182], whereby DOPC served as a benchmark and allowed a direct comparison of the two membrane systems. The proteovesicle formation under varying pH values, detergent (n-octyl-β-D-glucopyranoside, OG) and PR-GFP concentrations was investigated in a first step to identify factor combinations that yield uniform vesicles containing PR-GFP. Subsequently, the PR-GFP's function was assessed. Based on the obtained data, the reconstitution was optimized for DOPC liposomes and ABA polymersomes to yield fully functional proteovesicles.

5.2 *Results & Discussion*

WITHIN THIS PROJECT A definitive screening design (DSD) as proposed recently by Jones and Nachtsheim[166,167] was used, which focuses on efficiency and reduces the number of experimental trials. In contrast to the classical sequential approach (screening, effect estimation, optimization), it is possible to apply a one-step screening and optimization to the process of interest. Additionally, the factors' significance was estimated via stepwise regression and only significant factors were kept in the model equations[167]. The factors lipid/polymer-to-protein ratio (LPR or PPR, w/w), detergent concentration (OG) and pH value were determined to be critical for a functional reconstitution of PR-GFP[25,26]. The size of the formed vesicles was determined via dynamic light scattering (DLS) and fluorescent correlation spectroscopy (FCS) and was used as one response. As FCS only detects objects associated with PR-GFP, we could potentially detect different vesicle populations. The polydispersity index (PdI), obtained from cumulant analysis, was utilized as a measure for homogeneity. In order to measure PR-GFP's proton pumping capability, we encapsulated the pH- responsive fluorescent dye pyranine and calculated the pH change over time during illumination via the change of fluorescence intensity[165]. The screening was split in two steps and the corresponding experimental plans for each run can be found in Table 5.1, 5.2 and 5.3. Assuming that the formation of a proton gradient should work best with PR-GFP reconstituted in

Sample #	pH	LPR/PPR (w/v) / $c_{PR-GFP}[mg/mL]$	OG [%](w/v)
1	7	80 / 0.05	1.25
2	8	80 / 0.05	2.00
3	7	135 / 0.03	2.00
4	6	135 / 0.03	1.25
5	8	135 / 0.03	0.50
6	6	25 / 0.16	2.00
7	7	25 / 0.16	0.50
8	6	80 / 0.05	0.50
9	8	25 / 0.16	1.25

Table 5.1: Experimental plan of the used definitive screening design. The plan was used for the first screening experiments for both membrane types. Each experiment was done in triplicates.

Sample #	pH	LPR (w/v) / $c_{PR-GFP}[mg/mL]$	OG [%](w/v)
1	7	75 / 0.05	2.00
2	6	75 / 0.05	1.38
3	8	50 / 0.08	2.00
4	8	25 / 0.16	1.38
5	7	25 / 0.16	0.75
6	6	50 / 0.08	0.75
7	7	50 / 0.08	1.38
8	8	75 / 0.05	0.75
9	6	25 / 0.16	2.00

Table 5.2: Experimental plan of the second screening design. The plan was used for the DOPC proteoliposomes. Each experiment was done in triplicates.

Sample #	pH	PPR (w/v) / $c_{PR-GFP}[mg/mL]$	OG [%](w/v)
1	6.50	125 / 0.03	1.13
2	8	70 / 0.06	1.13
3	8	97.5 / 0.04	1.75
4	6.50	97.5 / 0.04	0.50
5	8	125 / 0.03	0.50
6	7.25	70 / 0.06	0.50
7	7.25	97.5 / 0.04	1.13
8	7.25	125 / 0.03	1.75
9	6.50	70 / 0.06	1.75

Table 5.3: Experimental plan of the second screening design. The plan was used for the ABA proteopolymersomes. Each experiment was done in triplicates.

large unilamellar vesicles, we investigated the vesicle formation via film rehydration in the presence of PR-GFP for DOPC and ABA [25,183]. These results defined a parameter region, which fulfilled the predetermined criteria for size and homogeneity. In a second experimental run, this region of interest was investigated in more detail and the proton pumping activity was measured. Combining both data sets for the regression, a second-degree polynomial model as described in section 1.4, equation 1.2, p. 40 was derived for each response. The multi-response optimization was carried out with the help of corresponding desirability functions [184]. We carried out an optimization towards maximum size, homogeneity and proton pumping activity.

5.2.1 *Formation of DOPC and ABA proteovesicles*

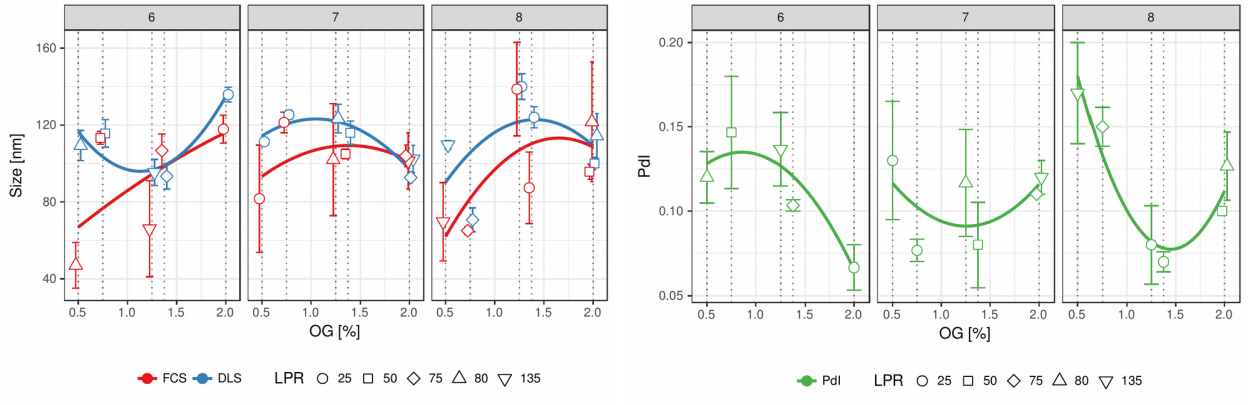

Figure 5.2: The interaction plots show the behavior of formed proteoliposomes towards changing reconstitution conditions. The data is grouped by pH value, different LPR values are indicated by the data point's symbol and the used OG concentrations are presented on the x-axis. The lines show a potential trendline and serve as a guide to the eye only. Error bars represent the standard error of the mean, n = 3. The underlying data can be found in Table 5.4, p. 77 and Table 5.5, p. 78. The DLS data is plotted in Figure 5.5, p. 81 and Figure 5.6, p. 82. FCS data is plotted in Figure 5.7, p. 83 and Figure 5.8, p. 84. TEM images can be found in Figure 5.9, p. 85.

In the first round of experiments, the OG concentration was varied between 0.5 and 2 % and a clear tendency towards bigger sizes at detergent concentrations above 1 % is observed in case of the proteoliposomes (Figure 5.2, left). The observed sizes are well below the pore size of the last extrusion step (200 nm, see section 3.2.4, p. 55 . This effect is pronounced at pH 6 and pH 8 as well as low LPR values. However, at pH 6 and LPR 80 / 0.05 mg/mL PR-GFP, the measured sizes diverge clearly (Figure 5.2, left). The objects detected by FCS are in the range of 45 nm whereas DLS detects objects around 110 nm. A similar difference is seen at pH 6, LPR 135 / 0.03 mg/mL PR-GFP as well as at pH 7, LPR 25 / 0.16 mg/mL PR-GFP and 80 / 0.05 mg/mL PR-GFP, albeit not as pronounced as at lower pH values. This indicates the presence of two populations and a tendency of PR-GFP to partition into smaller sized structures. Imaging the sample via transmission electron microscopy (TEM) confirmed the presence of two populations (Figure 5.9). Estimating the median number of PR-GFP per proteoliposome via FCS provides further evidence (see Figure 5.11, p. 86). At pH 6, LPR 80 and 0.5 % OG, only a median value of 18 PRG-FP molecules (first quartile (Q1): 2/third quartile (Q3): 30) is detected whereas at pH 7, LPR 80 and

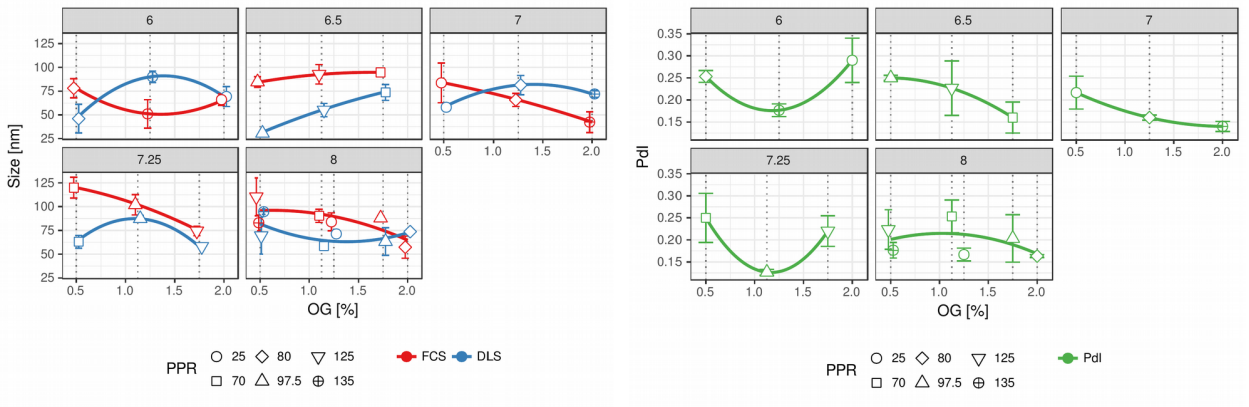

Figure 5.3: Similar to the proteoliposomes' interaction plot (Figure 5.2), he data is grouped by pH value and different PPR values are indicated by the data point's symbol. The used OG concentrations are presented on the x-axis. The lines show a potential trend-line and serve as a guide to the eye only. Error bars represent the standard error of the mean, n = 3. The underlying data can be found in Table 5.6, p. 79 and Table 5.7, p. 80. The DLS data is plotted in Figure 5.5, p. 81 and Figure 5.6, p. 82. FCS data is plotted in Figure 5.7, p. 83 and Figure 5.8, p. 84. TEM images can be found in Figure 5.10, p. 85

1.25 % OG 32 PR-GFP molecules (Q1: 20/Q3: 54) are detected. The proteopolymersomes' formation at various conditions is different from the liposomes (Figure 5.3, left). First of all, the observed sizes are smaller, ranging from 30 to 100 nm. Second, we observed that the sizes determined by FCS and DLS disagree stronger compared to the liposomes (Figure 5.3, left).

At pH 6, 1.25 % OG and PPR 135 / 0.03 mg/mL PR-GFP, FCS reports sizes of 51 ± 26 nm on average whereas DLS estimates 90 ± 11 nm. Similar to the observations made with the proteoliposomes, the results indicate two vesicle populations and the partitioning of PR-GFP into the smaller population. TEM shows an increase of small spherical objects as seen in Figure 5.10. It should be noted that the preparation method used in this work always lead to the formation of small micelle-like objects. However, in contrast to the proteoliposomes, the phenomenon is pronounced at medium to high detergent concentration (1.25 % and 2 % OG) and nearly disappears at pH 8, as can be seen at pH 8, PPR 25 and 1.25 % OG. The number of PR-GFP molecules increases to 31 (Q1: 21/Q3: 59), which is a threefold increase compared to the 11 PR- GFP molecules (Q1: 2/Q3: 46) detected at pH 6, 1.25 % OG and PPR 135 / 0.03 mg/mL PR-GFP (see Figure 5.12, p. 87). The PdI value was used as an indicator for the homogeneity of the vesicle populations. At low LPR values, acidic and basic conditions, the proteoliposomes are more homogeneous (Figure 5.2, right). At neutral pH no clear trend can be observed. Contrary to the liposomes, the pH has a strong influence on the PdI of the proteopolymersomes (Figure 5.3, right). At pH 6, values range from 0.17 to 0.33 whereas at pH 8, it only slightly deviates around 0.17. The measurements from the second round of experiments (see Table 5.2) fit within the trends observed in the first round experiments (compare Figure 5.2 with Table 5.4 and 5.5 as well as Figure 5.3 with Tables 5.6 and 5.7). The data for the size and the PdI were combined with the first set of experiments to increase the accuracy of the model (see Tables 5.4, 5.5, 5.6, 5.7).

Moreover, we used the models derived from the first set of experiments to predict the outcome of the second one and to validate our

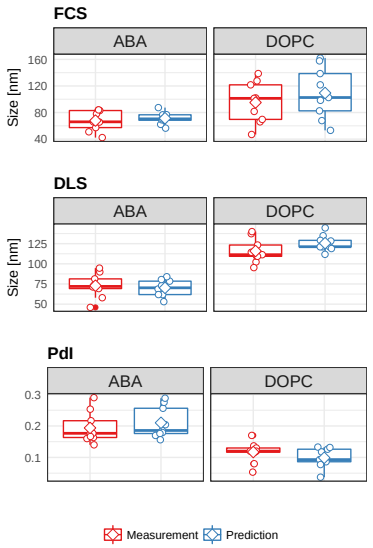

Figure 5.4: Comparison of a) FCS, b) DLS and c) PdI measurement and predicted data via boxplots. Underlying data is presented as white points, whereas the diamonds show the mean. The center line of the box represents the median, the box limits the 25th and 75th percentiles, and the whiskers extend to the largest value no further than 1.5 * IQR. Here, data beyond the whiskers are considered outliers. T-tests indicate that the predicted and the measured values are not significantly different for the proteoliposomes (p-values for FCS: 0.3989, DLS: 0.1243 and PdI: 0.2515) or proteopolymersomes (p-values for FCS: 0.5618, DLS: 0.6584 and PdI: 0.4939).

approach. The size of PRGFP-containing liposomes increases with higher amounts of OG at pH 6 and pH 8, whereas at pH 7 the size remains stable (see Figure 5.2). A low LPR benefits the formation of larger proteoliposomes. The trend that increasing pH values are beneficial for the formation of larger proteopolymersomes is further supported by additional data, including new pH values fitting into the new experimental boundaries (see Figure 5.3). The largest proteopolymersomes containing PRGFP are obtained at a pH range from 7.25 to 8. Similarly, the new data points of the PdI measurement fit as anticipated (see Figure 5.2 and 5.3). A low LPR is beneficial for a low PdI when reconstituting PR-GFP into DOPC lipsomes. Across all measured pH values, the lowest PdI was obtained when a LPR of 25 / 0.16 mg/mL PR-GFP was used. Contrary to the proteoliposomes, the pH value has a bigger influence on the PdI of the proteopolymersomes, with the lowest values being present at pH > 7 (see Figure 5.3). The upcoming analysis of the model fitted to the data will offer some explanations for the observed phenomena.

Table 5.4: Summarized tabular results of the first DSD run for DOPC proteoliposomes.

pH	LPR	OG [%] (w, v)	FCS [nm]	DLS [nm]	PdI	Block
7	80	1.25	120	127	0.08	1
8	80	2.00	125	127	0.09	1
7	135	2.00	116	92	0.14	1
6	135	1.25	99	82	0.12	1
8	135	0.50	92	114	0.20	1
6	25	2.00	139	146	0.04	1
7	25	0.50	113	112	0.09	1
6	80	0.50	53	103	0.15	1
8	25	1.25	147	151	0.08	1
7	80	1.25	141	134	0.18	2
8	80	2.00	174	125	0.16	2
7	135	2.00	116	116	0.11	2
6	135	1.25	82	104	0.18	2
8	135	0.50	88	109	0.20	2
6	25	2.00	134	141	0.05	2
7	25	0.50	106	114	0.20	2
6	80	0.50	64	125	0.11	2
8	25	1.25	176	128	0.12	2
7	80	1.25	45	109	0.09	3
8	80	2.00	66	91	0.13	3
7	135	2.00	72	99	0.11	3
6	135	1.25	17	100	0.11	3
8	135	0.50	29	106	0.11	3
6	25	2.00	110	125	0.07	3
7	25	0.50	26	108	0.10	3
6	80	0.50	24	100	0.10	3
8	25	1.25	93	141	0.04	3

pH	LPR	OG [%] (w,v)	FCS [nm]	DLS [nm]	PdI	ΔF_{460} [%]	Block
7	75	2.00	115	94	0.11	-4.61	1
7	75	2.00	101	97	0.11	-5.08	1
7	75	2.00	96	87	0.11	-4.47	1
6	75	1.38	121	104	0.10	-4.34	1
6	75	1.38	108	81	0.10	-3.38	1
6	75	1.38	91	95	0.11	-4.07	1
8	50	2.00	88	105	0.10	-6.76	1
8	50	2.00	101	101	0.10	-3.97	1
8	50	2.00	98	94	0.10	-3.46	1
8	25	1.38	64	115	0.08	-1.95	2
8	25	1.38	74	134	0.06	-2.51	2
8	25	1.38	124	123	0.07	-4.91	2
7	25	0.75	132	124	0.07	-1.52	2
7	25	0.75	116	122	0.09	-7.53	2
7	25	0.75	116	130	0.07	-8.29	2
6	50	0.75	110	126	0.08	-5.16	2
6	50	0.75	120	102	0.18	-4.48	2
6	50	0.75	110	119	0.18	-4.81	2
7	50	1.38	110	105	0.13	-6.83	3
7	50	1.38	102	126	0.06	-5.15	3
7	50	1.38	103	117	0.05	-4.00	3
8	75	0.75	61	83	0.13	-2.59	3
8	75	0.75	67	63	0.15	-4.47	3
8	75	0.75	67	66	0.17	-3.30	3
6	25	2.00	94	126	0.13	-4.40	3
6	25	2.00	126	132	0.06	-4.61	3
6	25	2.00	104	145	0.05	-4.61	3

Table 5.5: Summarized tabular results of the second DSD run for DOPC proteoliposomes. Note that the proton gradient amplitude has not been converted to pH units.

pH	PPR	OG [%] (w, v)	FCS [nm]	DLS [nm]	PdI	Block
7	80	1.25	70	98	0.15	1
8	80	2.00	34	71	0.16	1
7	135	2.00	34	65	0.16	1
6	135	1.25	35	94	0.15	1
8	135	0.50	87	97	0.15	1
6	25	2.00	59	90	0.35	1
7	25	0.50	125	62	0.29	1
6	80	0.50	69	76	0.24	1
8	25	1.25	102	73	0.19	1
7	80	1.25	52	83	0.16	2
8	80	2.00	70	73	0.17	2
7	135	2.00	29	76	0.12	2
6	135	1.25	37	98	0.18	2
8	135	0.50	95	89	0.21	2
6	25	2.00	61	56	0.33	2
7	25	0.50	68	57	0.17	2
6	80	0.50	67	29	0.28	2
8	25	1.25	80	75	0.14	2
7	80	1.25	75	63	0.17	3
8	80	2.00	68	77	0.16	3
7	135	2.00	64	75	0.14	3
6	135	1.25	81	78	0.20	3
8	135	0.50	67	98	0.17	3
6	25	2.00	78	62	0.19	3
7	25	0.50	58	55	0.19	3
6	80	0.50	98	33	0.24	3
8	25	1.25	70	66	0.17	3

Table 5.6: Summarized tabular results of the first DSD run for ABA proteopolymersomes.

pH	PPR	OG [%] (w,v)	FCS [nm]	DLS [nm]	PdI	ΔF_{460} [%]	Block
6.50	125.00	1.12	85	62	0.16	-5.52	1
6.50	125.00	1.12	80	62	0.17	-1.00	1
6.50	125.00	1.12	113	41	0.35	-1.70	1
8.00	70.00	1.12	94	53	0.30	-2.94	1
8.00	70.00	1.12	77	57	0.28	-4.77	1
8.00	70.00	1.12	100	65	0.18	-0.64	1
8.00	97.50	1.75	85	35	0.31	-1.02	1
8.00	97.50	1.75	86	72	0.16	-4.29	1
8.00	97.50	1.75	93	83	0.14	-1.21	1
6.50	97.50	0.50	95	33	0.25	-0.58	2
6.50	97.50	0.50	83	28	0.26	-5.98	2
6.50	97.50	0.50	76	31	0.24	0.37	2
8.00	125.00	0.50	83	32	0.31	-0.98	2
8.00	125.00	0.50	99	97	0.16	-6.30	2
8.00	125.00	0.50	149	79	0.20	-6.30	2
7.25	70.00	0.50	141	64	0.29	-3.37	2
7.25	70.00	0.50	115	51	0.32	-6.78	2
7.25	70.00	0.50	104	74	0.14	-1.80	2
7.25	97.50	1.12	121	84	0.14	-5.30	3
7.25	97.50	1.12	101	94	0.12	-4.16	3
7.25	97.50	1.12	84	84	0.12	-4.00	3
7.25	125.00	1.75	83	55	0.28	-4.36	3
7.25	125.00	1.75	66	61	0.16	-2.02	3
7.25	125.00	1.75	74	58	0.22	-2.89	3
6.50	70.00	1.75	95	82	0.13	0.95	3
6.50	70.00	1.75	95	82	0.12	-3.99	3
6.50	70.00	1.75	94	57	0.23	-1.52	3

Table 5.7: Summarized tabular results of the second DSD run for ABA proteopolymersomes. Note that the proton gradient amplitude has not been converted to pH units.

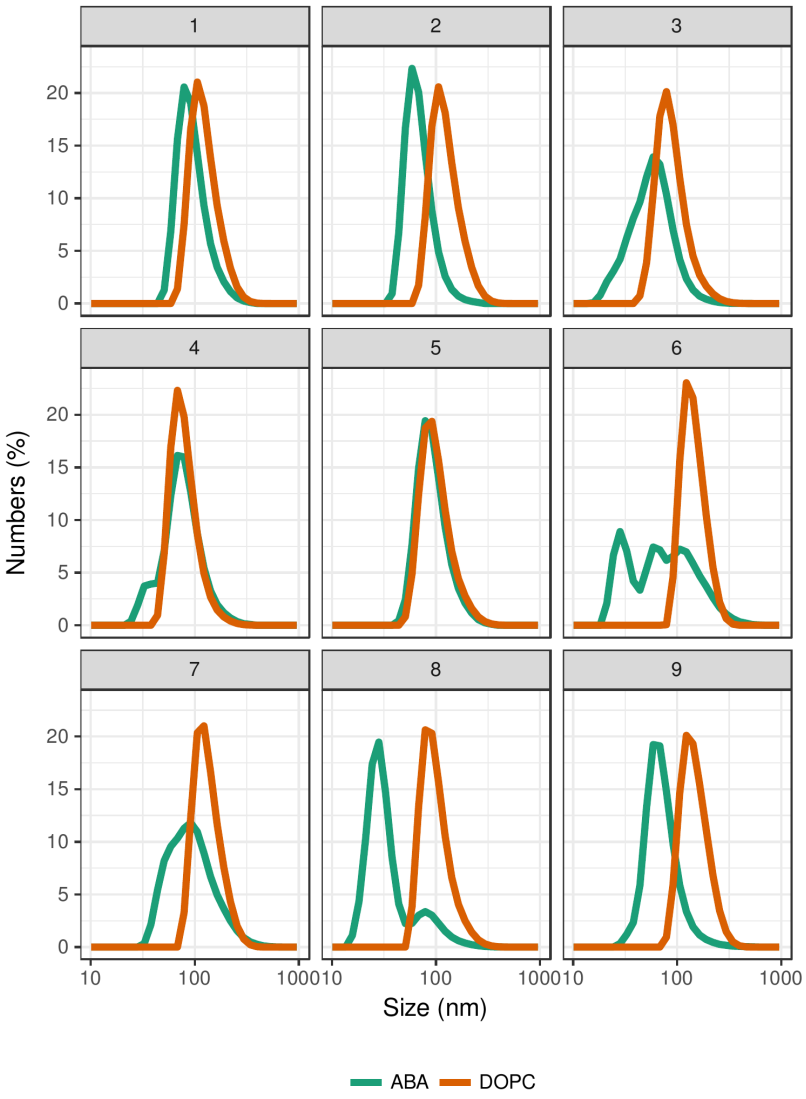

Figure 5.5: Numbers distributions of the formed proteovesicles of the first DSD. The DOPC and ABA vesicles are shown side by side and are sorted by their corresponding sample number (see Table 5.1).

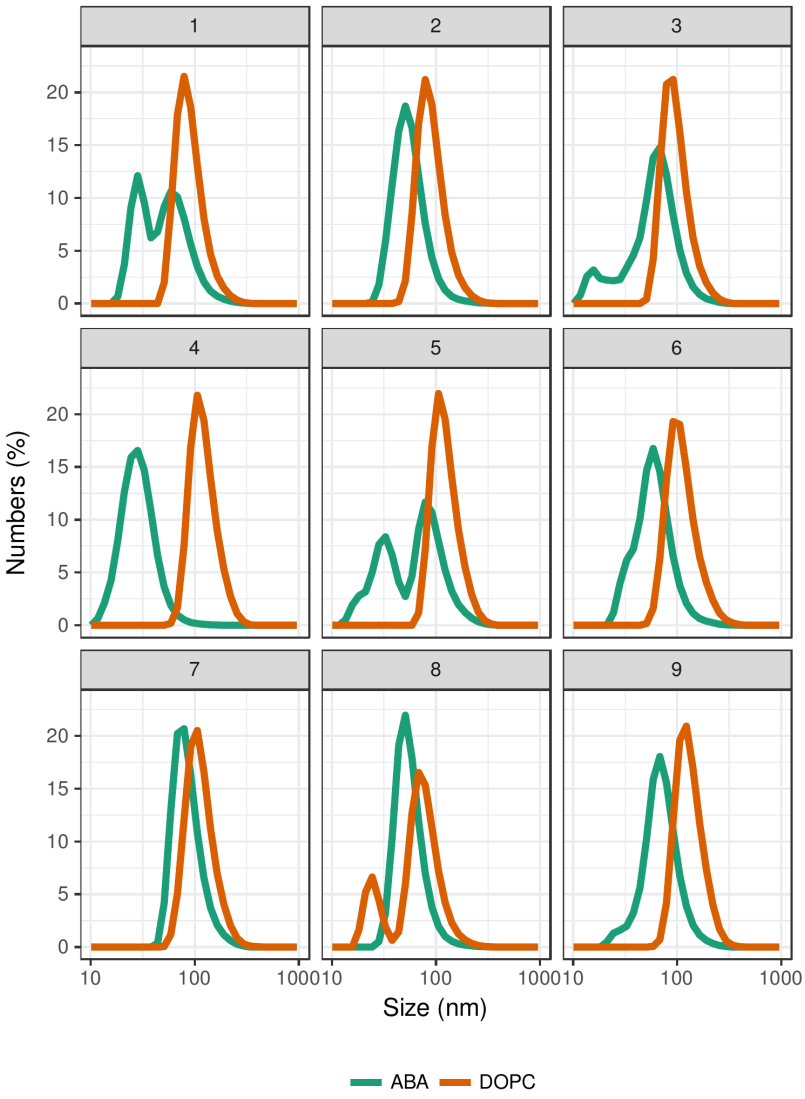

Figure 5.6: Numbers distributions of the formed proteovesicles of the second DSD. The DOPC and ABA vesicles are shown side by side and are sorted by their corresponding sample number. Please note that the conditions for each sample differ in the second DSD (see Table 5.2 and 5.3).

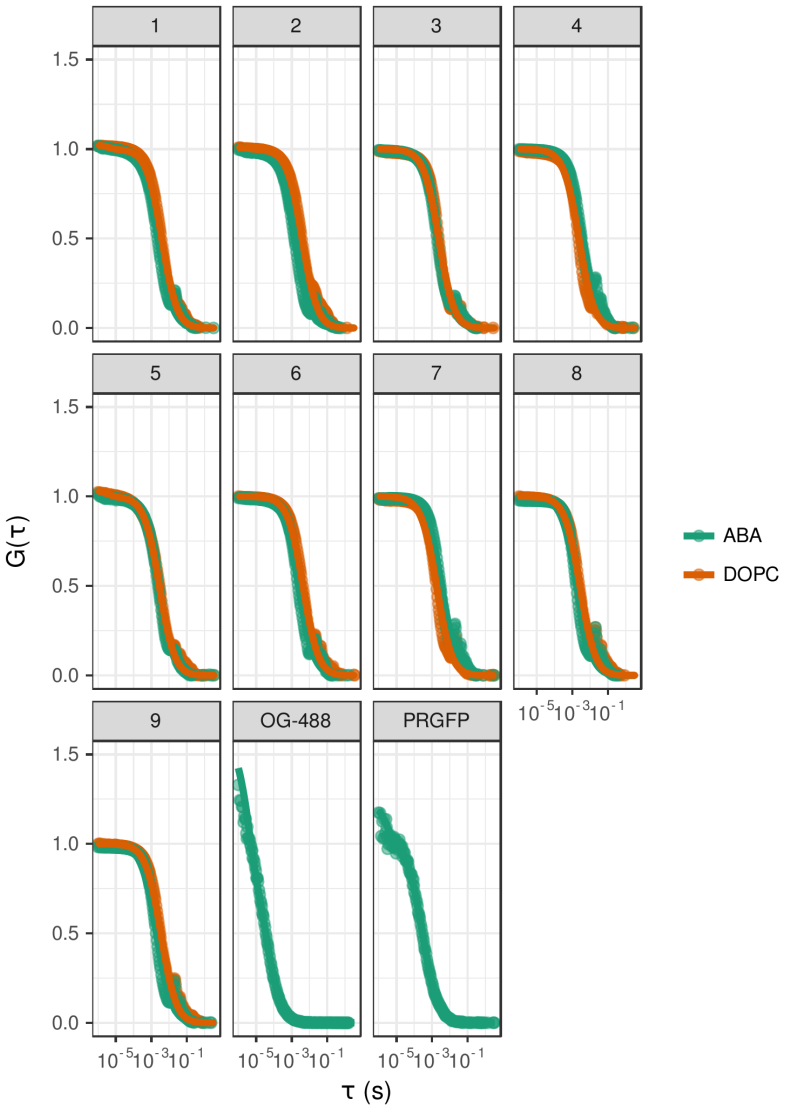

Figure 5.7: FCS correlation curves of the formed proteovesicles of the first DSD. The DOPC and ABA vesicles are shown side by side and are sorted by their corresponding sample number (see Table 5.1). Oregon green 488 and PR-GFP in reconstitution buffer (see section 3.2.6) are shown for comparison.

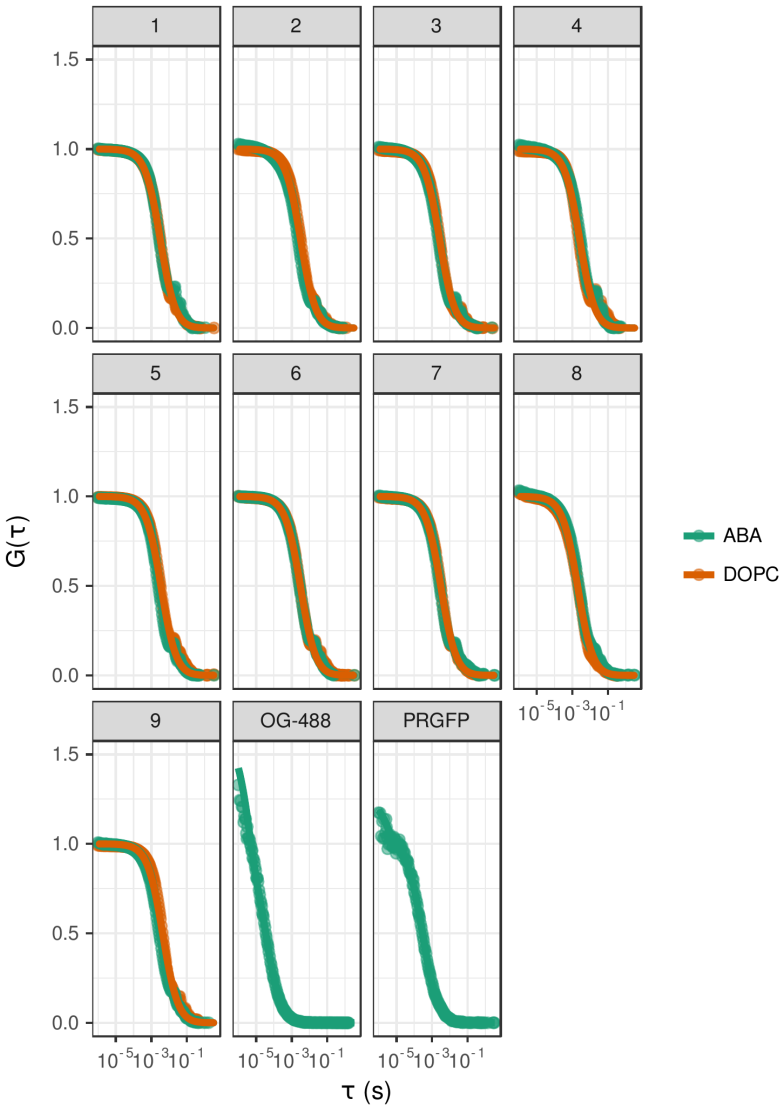

Figure 5.8: FCS correlation curves of the formed proteovesicles of the second DSD. The DOPC and ABA vesicles are shown side by side and are sorted by their corresponding sample number. Please note that the conditions for each sample differ in the second DSD (see table 5.2 and 5.3). Oregon green 488 and PR-GFP in reconstitution buffer (see section 3.2.6) are shown for comparison.

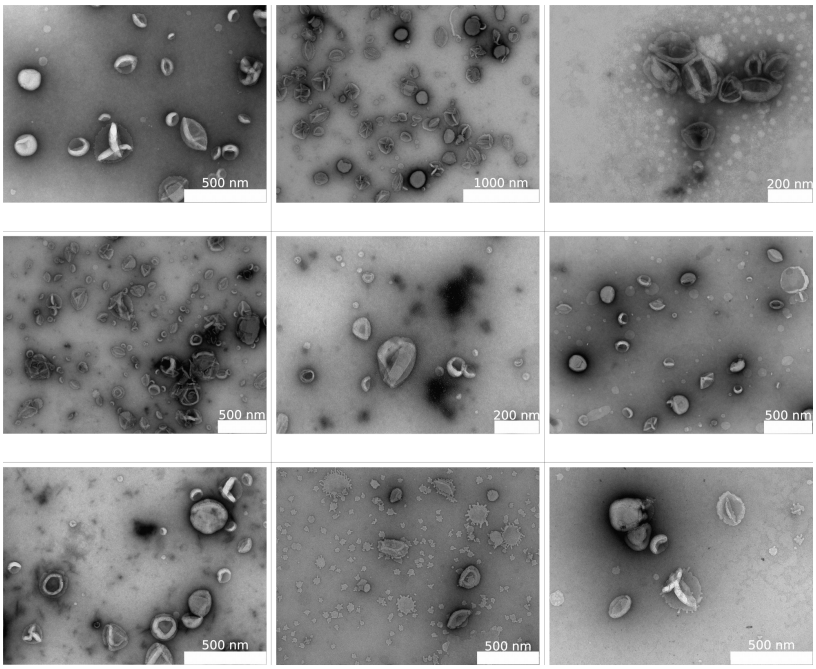

Figure 5.9: Transmission electron micrographs of the objects formed by DOPC and PR-GFP after the first DSD. Shown are representative pictures of the sample 1-9, from left to right (see Table 5.1).

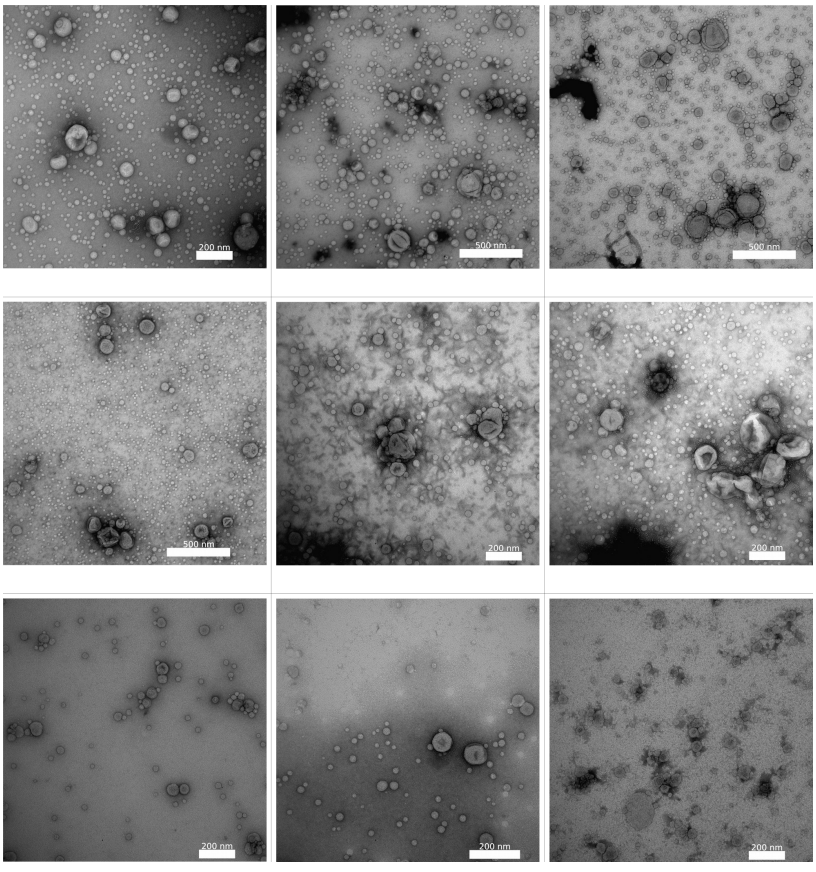

Figure 5.10: Transmission electron micrographs of the objects formed by PMOXA-PDMS-PMOXA and PR-GFP after the first DSD. Shown are representative pictures of the sample 1-9, from left to right (see Table 5.1).

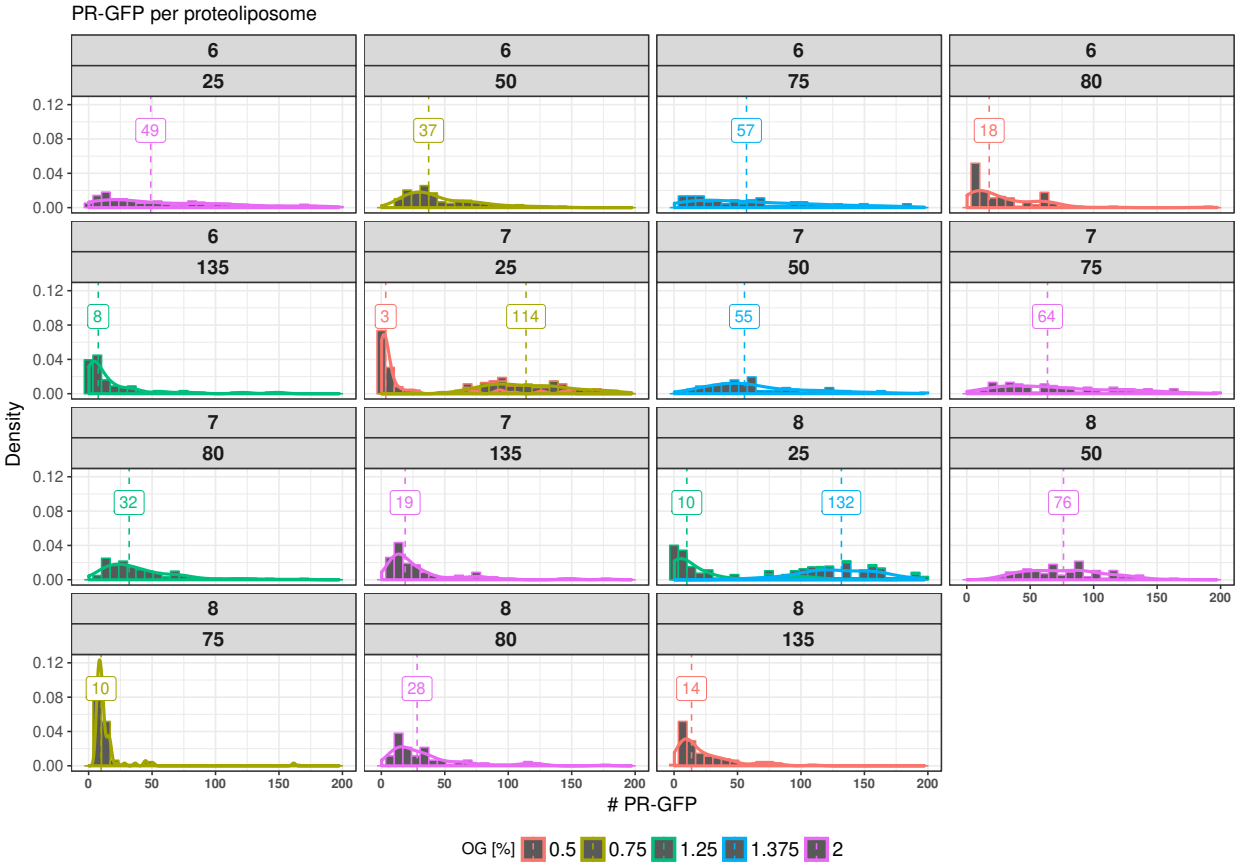

Figure 5.11: The distribution of the number of PR-GFP per proteoliposome determined via FCS. The data is grouped by pH (upper line) and LPR (lower line). The color indicates the OG concentration. Shown are only vesicles with up to 200 PR-GFP molecules. The histogram is overlain by the corresponding density function which shows the theoretical distribution based on the data. The median of the distribution is given in the text label.

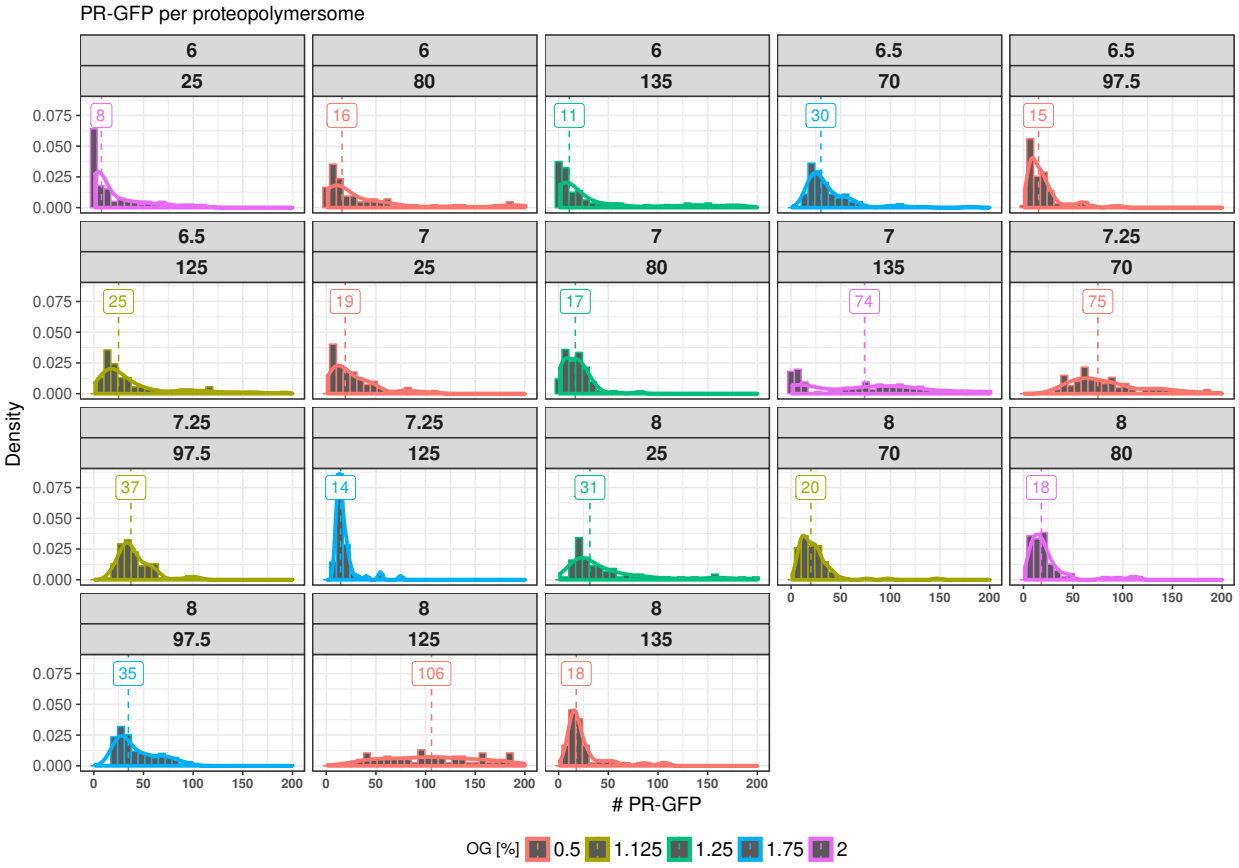

Figure 5.12: The distribution of the number of PR-GFP per proteoliposome determined via FCS. The data is grouped by pH (upper line) and LPR (lower line). The color indicates the OG concentration. Shown are only vesicles with up to 200 PR-GFP molecules. The histogram is overlain by the corresponding density function which shows the theoretical distribution based on the data. The median of the distribution is given in the text label.

5.2.2 *Model analysis*

A SECOND-DEGREE POLYNOMIAL model (see Equation 1.2, p. 40) was fitted to the two data sets via forward stepwise regression (see section 3.2.8, p. 57), allowing a deeper analysis of the behavior of the two membrane systems (see Figure 5.13). From a modeling perspective it should be noted that the variance is higher in case of the polymersomes and cannot be explained well by the model (compare Table 5.9, p. 89 and Table 5.10, p. 90). The formation of proteopolymersomes under the tested conditions results in a higher variety of sizes that cannot be explained purely by batch-to-batch variations as the designated blocking variables in the model are mostly insignificant (blocking variables represent any non-controllable environmental condition which can have an influence on the experiment). Our approach to select a sub-region of the parameter space which yields well-formed vesicles (illustrated in Figure 3) allowed us to verify predictions based on the models obtained in the first DSD.

Comparing the overall means of the responses to the predictions (Figure 5.4, p. 76) results in no statistical significant difference. Looking at the two membrane systems it can be concluded that the formation of proteoliposomes and proteopolymersomes is different. Only one combination, namely pH 8, LPR 135 / 0.03 mg/mL and 0.5 % OG, resulted in nearly identical results for lipid and polymer assemblies (compare Figure 5.5, p. 81 and Figure 5.7, p. 83). The only significant factor shared among all models for both membrane types is the LPR or PPR (see Table 5.9, p. 89 and Table 5.10, p. 90). This is rather surprising as previous studies suggested that the detergent concentration would be the most influential factor during the protein reconstitution [25,26]. Indeed, the size of the LPR/PPR coefficient is comparable to or higher than OG's (see Table 5.9, p. 89 and Table 5.10, p. 90). PR-GFP concentration (see Tables 5.1–5.3, p. 74) plays an important role in all three responses, FCS, DLS and PdI, for both membrane types and appears in linear and interaction terms. Additionally, the detergent concentration appears to have the highest influence on the proteoliposome formation whereas the pH value alone does not. It is only significant for the description of the FCS data. The pH value naturally has an effect on proteins, which is reflected by highly significant interaction term pH*LPR (see Table 5.9, p. 89). In case of the proteopolymersomes, the pH value has considerable more influence on the homogeneity of the vesicle population. This trend is verified further in the second DSD (see Table 5.10, p. 90) and supports the assumption that polymer membranes are different from lipid membranes when used for protein reconstitution. It should be assumed that the pH affects the polymer self-assembly or the pH value affects PR-GFP, which then in turn interacts with the polymer assembly. It was stated in literature that detergents do not interact in the same way with polymersomes as with liposomes [117]. The detergent micelles coexist with the vesicles up to a threshold limit and a further increase

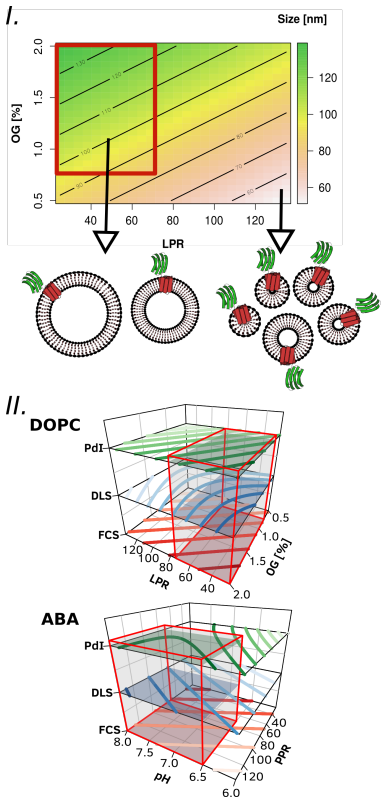

Figure 5.13: **I.** The contour plot visualizes the proteolipsomes size, modeled from the first round of experiments depending on the LPR and OG concentration, whereas the pH value is fixed at 7. The color gradient indicates different sizes and shows a trend towards a region within the design space which yields homogeneous, large proteoliposomes (highlighted by the red box). **II.** This region of interest applies to all three responses as shown in the stacked contour plots for both membrane types. Red boxes encompass the subregions of the design space which was subsequently screened for proteovesicles with functioning PR-GFP.

	DOPC	ABA
pH	6-8	6.5-8
OG [%, w,v]	0.75-2	0.5-1.75
c_{PR-GFP} [mg/mL]	0.16-0.05	0.06-0.03
LPR / PPR	25-75	70-135

Table 5.8: The factor limits derived for the second definitive screening design. These limits create the boundaries for a sub-region of the parameter space that yields large uniform proteovesicles.

leads to dissolution of the polymer membranes[117]. This observation is supported by the data and results from this study and the role of the pH should move into the focus of research. The effect of the detergent concentration on the reconstitution of PR-GFP is interesting. As described in literature, the formation of proteoliposomes and successful reconstitution of membrane proteins into them is highly dependent on the type and amount of used detergent[26]. This is again reflected by the obtained model which includes LPR*OG interaction terms for the FCS' description. This mirrors the requirement of the correct amount of detergent necessary to destabilize the liposome membrane and allows transfer of the protein during detergent removal into it. However, this term is completely absent in case of the proteopolymersomes' models. Generally, OG terms are only significant in two (FCS and DLS) of three cases (see Table 5.10, p. 90).

	FCS			DLS			PdI		
	B	std. Error	p	B	std. Error	p	B	std. Error	p
Intercept	130.75	8.78	**<0.001**	123.88	5.86	**<0.001**	0.11	0.01	**<0.001**
Block									
Block 2	8.56	8.46	0.318	4.67	5.10	0.366	0.04	0.02	**0.023**
Block 3	-58.00	8.46	**<0.001**	-8.33	5.10	0.110	-0.01	0.02	0.343
Block 4	-15.45	10.59	0.152	-22.95	6.42	**<0.001**	0.01	0.02	0.636
Block 5	-28.45	10.57	**0.010**	-12.34	6.44	0.063	0.01	0.02	0.472
Block 6	-37.03	10.14	**<0.001**	-18.82	6.11	**0.004**	0.01	0.02	0.438
pH	10.58	3.66	**0.006**	0.99	2.25	0.663			
LPR	-17.26	4.15	**<0.001**	-14.07	2.51	**<0.001**	0.03	0.01	**<0.001**
OG	22.69	3.90	**<0.001**	5.10	2.42	**0.041**	-0.02	0.01	**0.004**
pH:LPR	39.34	9.32	**<0.001**	16.44	5.82	**0.007**			
pH:OG	11.18	8.55	0.199	15.29	5.17	**0.005**			
LPR:OG	14.64	5.35	**0.009**	-13.03	4.59	**0.007**			
LPR^2	14.46	10.19	0.164	18.37	6.15	**0.005**	-0.01	0.01	0.228
OG^2	-43.25	10.06	**<0.001**	-19.71	6.13	**0.003**	0.02	0.01	0.093
pH^2				-8.82	4.45	0.054			
Observations	54			54			54		
R^2/adj. R^2	0.792/0.724			0.776/0.695			0.533/0.438		
F-statistics	11.687***			9.627***			5.590***		

Table 5.9: Model coefficients of the response surface model describing the characteristics of the formed PRGFP proteoliposomes of the combined data set. Bold text highlights statistical significance (α = 0.05).

5.2.3 *Proton pumping*

The formation of a proton gradient should depend on the number of pumps present, their orientation and their structural integrity[185]. Thus, the highest proton-pumping activity is expected to be found within the derived region yielding homogeneous, large proteovesicles. The measurement was based on the encapsulation of the pH-sensitive molecular probe pyranine. Its change of fluorescence intensity was used to calculate the internal change of pH (see section 3.2.7)[165]. The

	FCS			DLS			PdI		
	B	std. Error	p	B	std. Error	p	B	std. Error	p
Intercept	71.15	8.15	**<0.001**	88.92	6.46	**<0.001**	0.16	0.03	**<0.001**
Block									
Block 2	-6.22	8.57	0.472	-10.00	7.21	0.172	-0.01	0.03	0.752
Block 3	4.89	8.57	0.571	-13.22	7.21	0.073	-0.02	0.03	0.409
Block 4	23.83	9.33	**0.014**	-31.44	8.10	**<0.001**	0.06	0.03	**0.047**
Block 5	22.10	10.48	**0.041**	-26.64	8.43	**0.003**	0.04	0.03	0.279
Block 6	27.65	9.63	**0.006**	-16.11	7.75	**0.044**	0.00	0.03	0.884
pH	4.33	3.53	0.226	6.70	2.96	**0.029**	-0.03	0.01	**0.018**
PPR	-8.95	3.97	**0.029**	6.89	3.22	**0.038**	-0.02	0.01	0.067
OG	-12.83	4.00	**0.003**	2.44	3.38	0.475	-0.01	0.01	0.527
pH:OG	-7.23	5.62	0.205	-12.01	3.76	**0.003**			
PPR²	-4.23	8.18	0.608						
OG²				-12.37	5.96	**0.044**	0.04	0.02	0.094
pH²							0.03	0.02	0.185
Observations	54			54			54		
R^2/adj. R^2	0.569/0.469			0.508/0.393			0.348/0.197		
F-statistics	5.684***			4.434***			2.300***		

Table 5.10: Model coefficients of the response surface model describing the characteristics of the formed PRGFP proteopolymersomes of the combined data set. Bold text highlights statistical significance (α = 0.05).

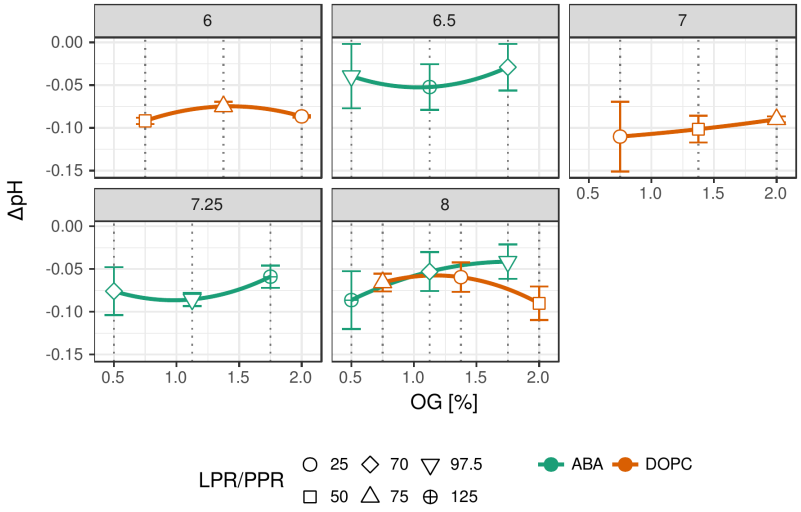

Figure 5.14: Interaction plots of the observed pH change in DOPC proteoliposomes and ABA proteopolymersomes grouped by pH values. Shown are the mean values of the corresponding measurements. Connecting lines represent a quadratic fit and serve as a guide to the eye. Error bars represent the standard error of the mean, n = 3.

highest decrease of 0.11 pH units was observed in proteoliposomes formed at pH 7 using 0.75 % of OG and a LPR of 25 / 0.16 mg/mL PR-GFP (see Figure 5.14 and 5.18, p. 92). However, also the variance was highest using these conditions. Proteoliposomes formed at pH 6 resulted in more reproducible gradients of 0.08 to 0.09 pH units. Overall, the highest gradients formed were observed using a low LPR of 25 / 0.16 mg/mL PR-GFP and non-basic pH (see Figure 5.18, p. 92, sample 5). The gradients formed within the proteopolymersomes were lower on average (see Figure 5.14 and 5.18, p. 92). A decrease of 0.04 pH units at pH 6.5, PPR 97.5 / 0.04 mg/mL PR-GFP and 0.5 % OG was the lowest observed (see Figure 5.18, p. 92, sample 9), whereas the combination of pH 8, PPR 125 / 0.03 mg/mL PR-GFP and 0.5 % OG resulted in a decrease of 0.09 pH units (see Figure 5.18, p. 92, sample 5 & 7).

In DOPC liposomes, the amplitude of the pH gradient is influenced by all three parameters during reconstitution (see Table 5.11, p. 93). The lower the LPR (i.e. the more pumps are present), or the lower the detergent concentration, the higher the activity (Figure 5.15, top). Furthermore, a near- neutral pH value in the range of 6.5 to 6.8 during reconstitution is beneficial for PR-GFP's activity. (Figure 5.15, top). Looking at the contour of LPR and OG one can see a clear gradient towards the low factor settings (LPR 25 – 40, 0.75 – 1.2 % OG, see Figure 5.17). A likely explanation is that in a low detergent regime, the vesicular structure remains largely intact, allowing a primarily oriented insertion of numerous proteins into the membrane[25]. In terms of pH, the opposite behavior is observed in polymersomes (Figure 5.15, bottom): A pH of 8 is suited best for a large gradient amplitude. Similar to the DOPC liposomes, the OG concentration is suitable in the lower range. However, the PPR moves towards a lower number of proteins available for insertion (Figure 5.15, top).

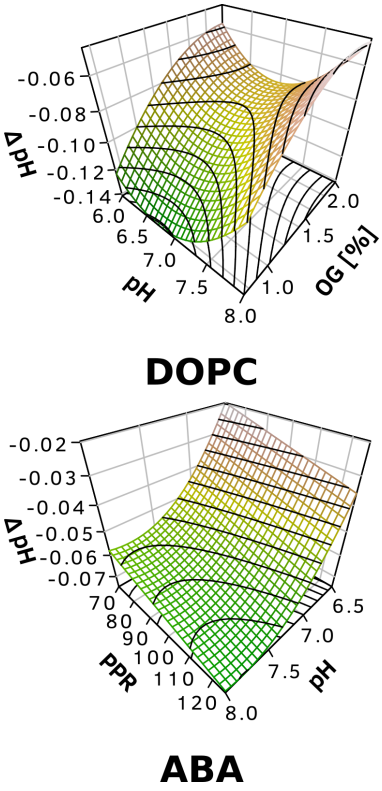

Figure 5.15: The modeled response surfaces of the pH gradient depending on the two most influential factors are shown. The preference of acidic pH values and low detergent concentrations for DOPC proteoliposomes becomes clearly visible (top). Contrary, the formed pH gradient becomes larger at basic pH values in case of the ABA proteopolymersomes as well as higher PPR values (bottom).

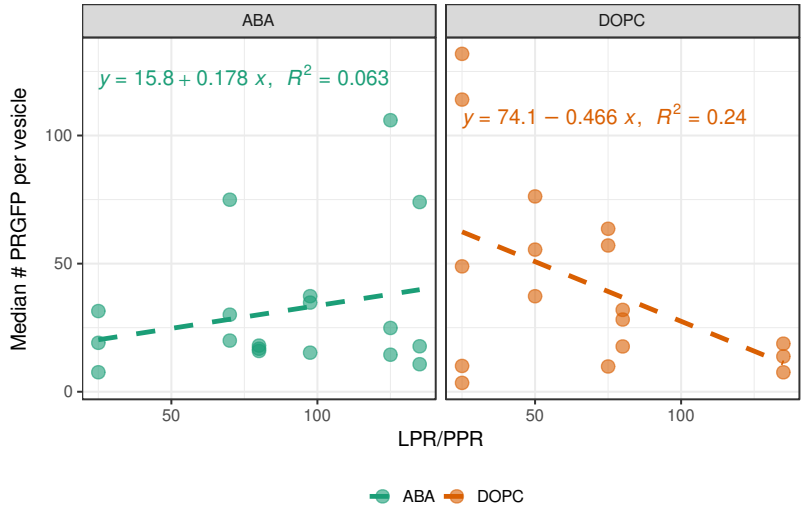

Figure 5.16: The median number of PR-GFP per vesicle plotted against the LPR or PPR. The plot is based on the data shown in figure 20 and 21 and no grouping has been applied to the data. The colors indicate the membrane type. Dashed lines indicate a linear trend which serves as a guide for the eye only.

Comparing the number of PR-GFP molecules detected by FCS after reconstitution with the starting LPR/PPR (see Figure 5.16) it

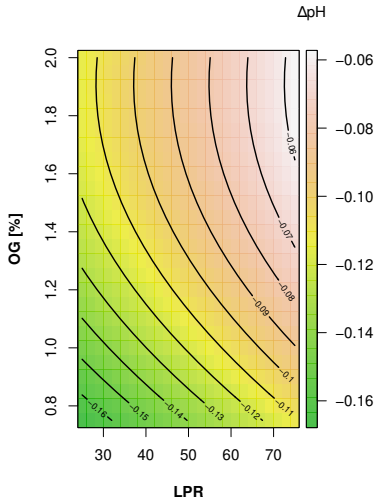

Figure 5.17: Contourplot of PR-GFP's activity in DOPC proteoliposomes. Shown are is the pH gradient formation dependent on the LPR and OG concentration.

is clearly visible that for proteoliposomes a decreasing LPR leads to more PR-GFP per vesicle. However, this seems not to be true for polymersomes, where the number of PR-GFP per vesicle remains largely constant and even an opposite trend can be observed. The similar amplitude of the proteopolymersomes' pH gradient (see Figure 5.18, p. 92, sample 5 & 7) with fewer pumps can be explained by a reduced back diffusion [1,185,158]. The permeability of protons through the PMOXA-PDMS-PMOXA membranes is lower and thus fewer pumps are necessary to achieve the same gradient. This underlines again the different mechanisms for lipid and polymer membranes resulting in a functional reconstitution, mainly the role of the detergent concentration and the pH.

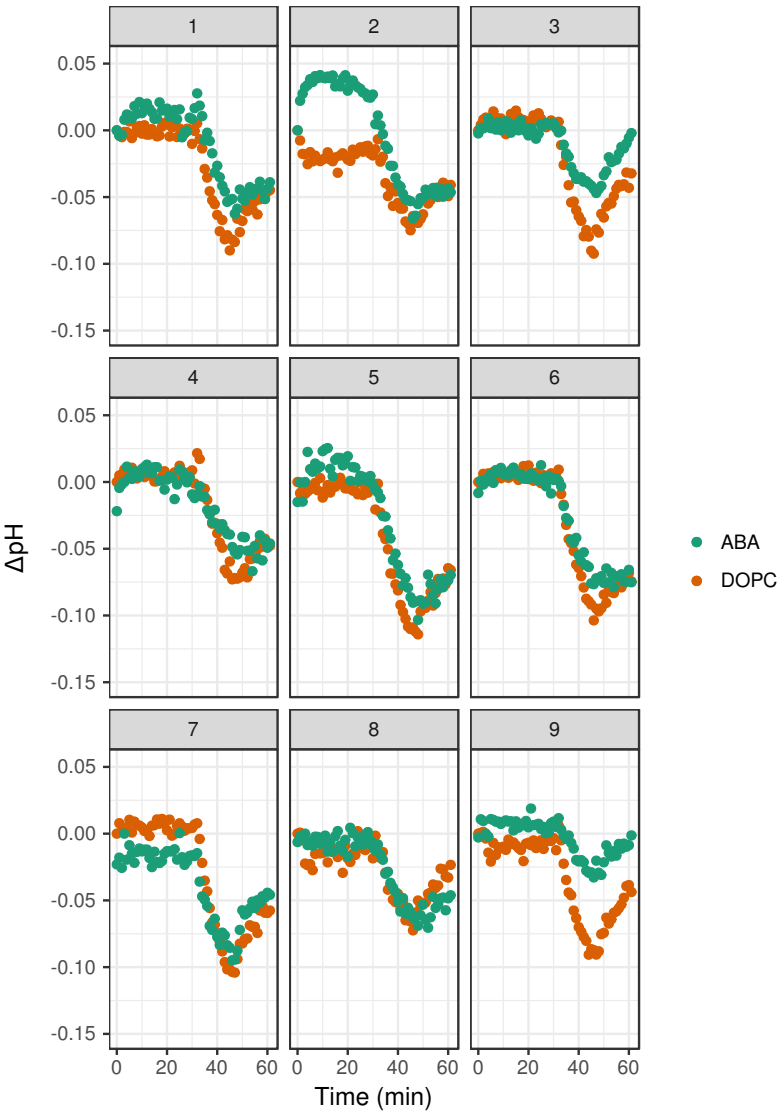

Figure 5.18: pH change inside ABA and DOPC proteovesicles calculated from the flourescence intensity change of pyranine. The DOPC and ABA vesicles are shown side by side and are sorted by their corresponding sample number. Please note that the conditions for each sample differ in the second DSD (see Table 5.2 and 5.3, p. 74).

	Activity		
	B	std. Error	p
Intercept	-5.23	0.46	**<0.001**
Block			
Block 2	3.27	1.15	**0.011**
Block 3	1.54	0.66	**0.031**
pH	0.63	0.17	**0.001**
LPR	3.26	0.99	**0.004**
OG	2.09	0.59	**0.002**
pH^2	1.73	0.32	**<0.001**
OG^2	-1.19	0.43	**0.014**
pH:OG	-0.37	0.34	0.294
Observations	27		
R^2/adj. R^2	0.811/0.728		
F-statistics	9.683***		

	Activity		
	B	std. Error	p
Intercept	-2.20	0.92	**0.028**
Block			
Block 2	0.55	0.92	0.557
Block 3	-0.78	1.16	0.510
pH	-1.67	0.45	**0.001**
PPR	-0.85	0.46	0.078
OG	1.10	0.86	0.215
pH:OG	1.70	0.77	**0.039**
pH^2	1.21	1.13	0.297
Observations	27		
R^2/adj. R^2	0.866/0.817		
F-statistics	17.610***		

Table 5.11: Model coefficients of the response surface model describing the observed change in pH in PRGFP proteoliposomes (left) and proteopolymersomes (right). Bold text highlights statistical significance (α = 0.05).

5.2.4 *Linear vs. linear mixed models*

Using blocking factors is very convenient to counter variations which are caused by different subjects or groups of subjects. For example, testing medication on different human test subjects usually requires looking at their response individually when they cannot form a homogeneous group. In biochemical experiments different batches of substrates like proteins, DNA, etc. can lead to strong variations between the experiments which are not caused by the experimenters manipulation. Within this work, the experiments were grouped in 3 runs of 9 experiments. Thus, each DSD was repeated three times and all samples within a block are prepared from the same starting materials. Even though blocking factors help in the analysis of the data, they can complicate making predictions from the derived models. If the effect of the blocking factor is significant and causes batch-to-batch variations and the blocking factor cannot be controled, then a linear mixed model needs to be employed. This model contains the fixed factors, here pH, OG concentration and LPR or PPR. A random factor, here called block, is added and takes the randomness into account. The problem arises when one is trying to assess the certainty of the predictions. Prediction intervals cannot be computed easily and it becomes necessary to estimate them via simulating several hundreds possible values. However, it is possible to assess the influence of the blocking factor via the intraclass-correlation coefficient (ICC). It is calculated by dividing the between-group-variance by the total variance. If the correlation is close to zero it means that the observations within groups is no more similar than from different groups. Thus, a linear mixed model is not necessary to employ. The Tables 5.12, 5.13 and 5.14 show the findings of using linear mixed models on the data.

	FCS			DLS			PdI		
	B	std. Error	p	B	std. Error	p	B	std. Error	p
Fixed Parts									
Intercept	108.71	11.44	**<0.001**	113.15	5.80	**<0.001**	0.12	0.01	**<0.001**
pH	10.44	3.63	**0.004**	1.19	2.22	0.594			
LPR	-16.88	4.10	**<0.001**	-13.31	2.46	**<0.001**	0.03	0.01	**<0.001**
OG	22.74	3.85	**<0.001**	4.56	2.39	0.056	-0.02	0.01	**<0.001**
pH:LPR	38.88	9.10	**<0.001**	17.67	5.54	**0.001**			
pH:OG	11.31	8.29	0.172	16.94	4.89	**<0.001**			
LPR:OG	14.51	5.33	**0.006**	-12.65	4.54	**0.005**			
LPR^2	14.49	9.77	0.138	21.35	5.65	**<0.001**	-0.01	0.01	0.182
OG^2	-42.60	9.83	**<0.001**	-20.48	5.86	**<0.001**	0.02	0.01	0.089
pH^2				-8.56	4.42	0.053			
Random Parts									
σ^2	321.286			117.082			0.001		
$\tau_{00,\,Block}$	581.947			90.940			0.000		
N_{Block}	6			6			6		
ICC_{Block}	0.644			0.437			0.150		
Observations	54			54			54		
R^2	0.791			0.771			0.516		

Table 5.12: Model coefficients of the linear mixed model describing the characteristics of the formed PRGFP proteoliposomes of the combined data set. The table is divided into fixed and random effects. Bold text highlights statistical significance (α = 0.05).

	FCS			DLS			PdI		
	B	std. Error	p	B	std. Error	p	B	std. Error	p
Fixed Parts									
Intercept	85.55	6.40	**<0.001**	72.36	5.67	**<0.001**	0.17	0.02	**<0.001**
pH	4.67	3.52	0.185	5.99	2.93	**0.041**	-0.03	0.01	**0.031**
PPR	-7.29	3.91	0.062	6.25	3.20	0.051	-0.02	0.01	0.099
OG	-12.84	3.83	**<0.001**	3.15	3.21	0.327	-0.01	0.01	0.330
pH:OG	-9.68	5.49	0.078	-12.22	3.73	**0.001**			
PPR^2	-10.05	7.76	0.195						
OG^2				-11.40	5.58	**0.041**	0.03	0.02	0.110
pH^2							0.03	0.02	0.154
Random Parts									
σ^2	332.796			233.281			0.004		
$\tau_{00,\,Block}$	131.634			101.562			0.001		
N_{Block}	6			6			6		
ICC_{Block}	0.283			0.303			0.145		
Observations	54			54			54		
R^2	0.556			0.499			0.324		

Table 5.13: Model coefficients of the linear mixed model describing the characteristics of the formed PRGFP proteopolymersomes of the combined data set. The table is divided into fixed and random effects. Bold text highlights statistical significance (α = 0.05).

	Activity		
	B	std. Error	p
Fixed Parts			
Intercept	-4.82	0.34	**<0.001**
pH	0.53	0.18	**0.002**
LPR	0.74	0.50	0.138
OG	0.53	0.25	**0.034**
pH:OG	-0.08	0.28	0.777
pH^2	1.71	0.33	**<0.001**
OG^2	-0.82	0.46	0.072
Random Parts			
σ^2	3.297		
$\tau_{00,\ Block}$	0.000		
N_{Block}	3		
ICC_{Block}	0.000		
Observations	27		
R^2	0.204		

	Activity		
	B	std. Error	p
Fixed Parts			
Intercept	-3.23	0.76	**<0.001**
pH	-1.67	1.07	0.118
PPR	-0.69	1.03	0.503
OG	0.58	0.67	0.388
pH:OG	0.72	1.01	0.475
pH^2	2.17	1.59	0.173
Random Parts			
σ^2	4.802		
$\tau_{00,\ Block}$	0.000		
N_{Block}	3		
ICC_{Block}	0.000		
Observations	27		
R^2	0.203		

Table 5.14: Model coefficients of the linear mixed model describing the observed change in pH in PRGFP proteoliposomes (left) and proteopolymersomes (right). The table is divided into fixed and random effects. Bold text highlights statistical significance (α = 0.05).

The ICCs of the proteoliposomes' FCS, DLS and PdI models are 0.644, 0.437 and 0.150 and for the proteopolymersomes 0.283, 0.303 and 0.145. This indicates a stronger clustering in the proteoliposomes' data. The models describing the pH gradient formation both have an ICC of zero. Overall, the ICC is low for all models except for the proteoliposomes' FCS data and thus it can be assumed that a linear mixed model is not necessary. Consequently, only the fixed part's coefficients were used and the predictions derived.

5.2.5 *Optimization*

For the optimization, the gradient formation, the proteovesicle size and PdI were used as a target to reach large and uniform vesicles. The model equations 5.1 - 5.8 were used for the optimization process, which was carried by the use of desirability functions[184].

Proteoliposomes

$$\begin{aligned} y_{FCS} = {} & 108.71 + 10.44 \cdot x_{pH} - 16.88 \cdot x_{LPR} + 22.74 \cdot x_{OG} \\ & + 38.88 \cdot x_{pH} \cdot x_{LPR} + 11.31 \cdot x_{pH} \cdot x_{OG} + 14.51 \cdot x_{LPR} \cdot x_{OG} \\ & + 14.49 \cdot x_{LPR}^2 - 42.60 \cdot x_{OG}^2 \end{aligned} \tag{5.1}$$

$$\begin{aligned} y_{DLS} = {} & 113.15 + 1.19 \cdot x_{pH} - 13.31 \cdot x_{LPR} + 4.56 \cdot x_{OG} \\ & + 17.67 \cdot x_{pH} \cdot x_{LPR} + 16.94 \cdot x_{pH} \cdot x_{OG} - 12.65 \cdot x_{LPR} \cdot x_{OG} \\ & - 8.56 \cdot x_{pH}^2 + 21.35 \cdot x_{LPR}^2 - 20.48 \cdot x_{OG}^2 \end{aligned} \tag{5.2}$$

$$y_{PdI} = 0.117 + 0.028 \cdot x_{LPR} - 0.021 \cdot x_{OG} - 0.014 \cdot x_{LPR}^2 + 0.017 \cdot x_{OG}^2 \quad (5.3)$$

$$y_{\Delta F460} = -4.82 + 0.53 \cdot x_{pH} + 0.75 \cdot x_{LPR} + 0.53 \cdot x_{OG} - 0.08 \cdot x_{pH} \cdot x_{OG} + 1.71 \cdot x_{pH}^2 - 0.83 \cdot x_{OG}^2 \quad (5.4)$$

Please note that the gradient is here calculated in relative flourescence units. This was done to streamline the computation process. Please refer to section 3.2.7 on how to calculate the ΔpH units.

Protepolymersomes

$$y_{FCS} = 85.56 + 4.67 \cdot x_{pH} - 7.29 \cdot x_{PPR} - 12.84 \cdot x_{OG} - 9.68 \cdot x_{pH} \cdot x_{OG} - 10.05 \cdot x_{PPR}^2 \quad (5.5)$$

$$y_{DLS} = 72.36 + 5.99 \cdot x_{pH} + 6.26 \cdot x_{PPR} + 3.15 \cdot x_{OG} - 12.22 \cdot x_{pH} \cdot x_{OG} - 11.40 \cdot x_{OG}^2 \quad (5.6)$$

$$y_{PdI} = 0.174 - 0.025 \cdot x_{pH} - 0.020 \cdot x_{PPR} - 0.012 \cdot x_{OG} + 0.028 \cdot x_{pH}^2 + 0.033 \cdot x_{OG}^2 \quad (5.7)$$

$$y_{\Delta F460} = -2.54 - 1.76 \cdot x_{pH} - 0.84 \cdot x_{PPR} + 0.39 \cdot x_{OG} + 1.96 \cdot x_{pH} \cdot x_{OG} + 1.59 \cdot x_{pH}^2 \quad (5.8)$$

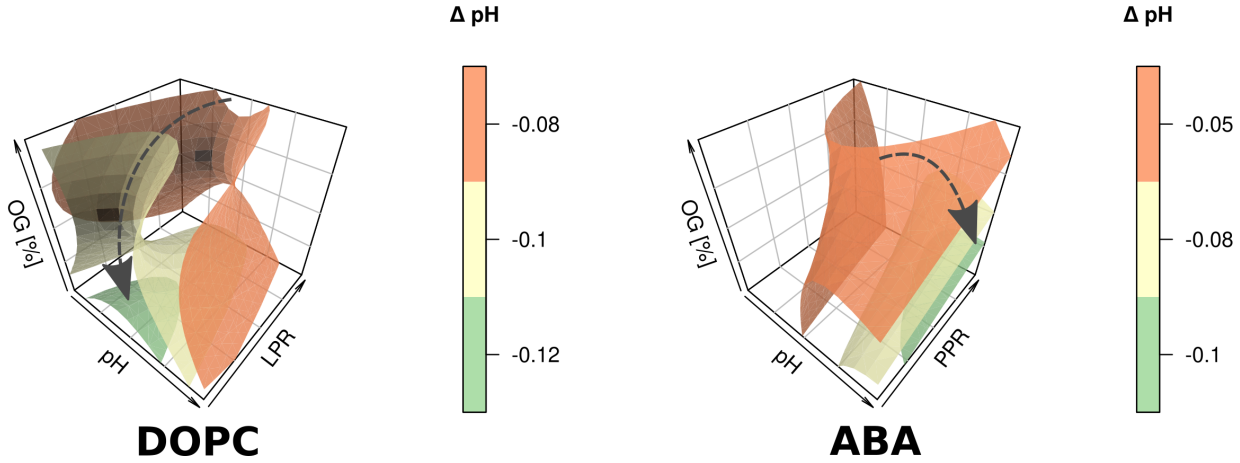

Figure 5.19: The optimization process can be illustrated via the use of isosurfaces. Here, the surfaces of the formed pH gradient are shown for DOPC (left) and ABA (right). Each isosurface corresponds to a certain ΔpH value and the factor combinations resulting in that value. The dashed arrow illustrates the convergence towards higher ΔpH values.

The optimization process is explained exemplarily for the proton gradient formation. The obtained models span the so-called response surface for all possible combinations of factors in the investigated parameter region for all 4 responses, namely the size determined via FCS and DLS, the corresponding PdI and the amplitude of the observed proton gradient. In order to find an optimal combination which maximizes size and gradient amplitude as well as minimizes

the PdI a global desirability function is used for optimization. The process of optimization is illustrated in Figure 5.19 for the gradient formation. Each isosurface represents the distribution of the gradient's given decrease depending on the factor combination. The different nature of the two membrane types becomes clear when comparing the trace of the convergence process between the proteoliposomes and the proteopolymersomes as illustrated by the arrows. As the amplitude of the gradient increases and thus the pH value inside the vesicles decrease, the factor combination resulting in this response narrows down. For a slight decrease of 0.09 pH units in proteoliposomes, approximately half of the parameter space is below the orange surface. This means, roughly half of all possible LPR, OG and pH combinations should result in a decrease of 0.09 pH units or higher. All tested pH values and protein concentrations are still included. Increasing the amplitude by just 0.02 pH units, the possible combinations become less and medium to high amounts of OG become cut-off, thus they do not achieve the required pH gradient. At the highest amplitude shown here, 0.12 pH units, the possible pH range is narrowed down to slightly acidic to neutral conditions, the OG concentration to minimal amounts and the LPR clearly converges towards the minimal amounts used. Contrary, the predicted activity of PR in polymersomes should be highest at pH 8. The potential pH range is smaller compared to the lipid system, starting at pH 6.5. PR's concentration and the amount of detergent used have again different behavior. Clearly they converge towards low amount of detergent and low PR concentration. In summary, the optimization process mirrors the observations made before and highlights the necessity to develop different factor combinations for lipid and polymer membranes for a successful functional PR-GFP reconstitution.

The optimal conditions and their anticipated responses are summarized in Table 5.15.

	Factor				Response			
	pH	LPR / PPR	c_{PR-GFP} [mg/mL]	OG [%]	$Size_{FCS}$	$Size_{DLS}$	PdI	ΔpH
DOPC	6	25	0.16	0.66	122	143	0.10	0.10
ABA	8	112	0.04	0.82	77	84	0.16	0.08

Table 5.15: Optimal factor settings and the predicted responses for DOPC and ABA proteovesicles. The optimization was based on the equations 5.1 - 5.8.

The optimization follows the observed trends discussed before: a slight acidic pH value of 6 in combination with a low LPR and medium-to-low amount of OG leads to the formation of highly homogeneous proteoliposomes which build up a proton gradient upon illumination. These results are very similar to the conditions determined experimentally earlier[160,161]. ABA triblock polymers follow a different route. The pH should be in the basic regime around 8 and the PPR at 112 / 0.04 mg/mL PR-GFP. A detergent concentration of 0.82 % (w/v) is found to be optimal, which is higher compared to the DOPC system and surprising taking the observed negative effects of

OG on the vesicle formation into account (see section 5.2.3).

5.2.6 *Verification*

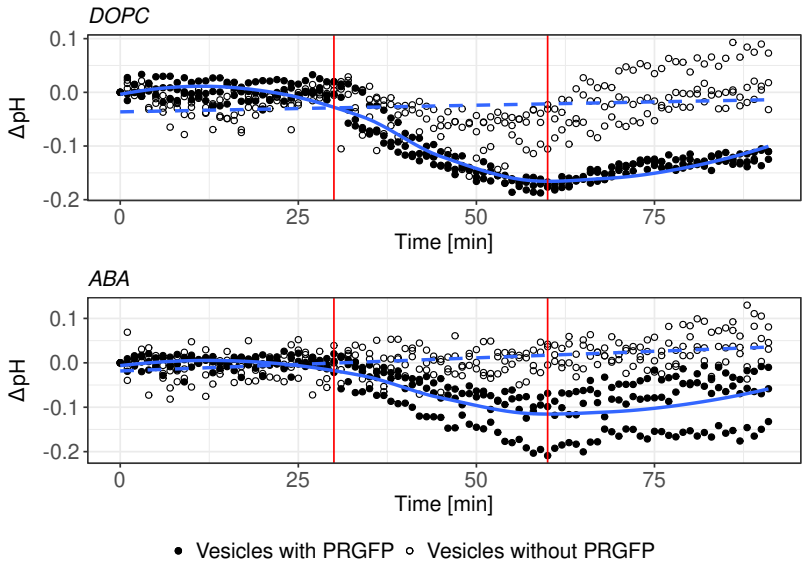

Figure 5.20: The proton transport kinetics for the reconstitutions carried out at derived optimal conditions and their corresponding controls. Shown are the measurements of three independent samples (with no summary statistics applied). The blue lines serve as a guide to the eye and the red lines indicate the illumination interval.

As a last step, the built up framework was put to a test. We used the derived optimal conditions to carry out the reconstitutions into DOPC and ABA membranes. Additionally, control reconstitutions were carried out under the same conditions but without PRGFP in order to confirm the measured response. In both cases, proteoliposomes and proteopolymersomes, the measured pH gradient was much higher than expected from the predictions (see Figure 5.20 and 5.21). In case of the proteoliposomes, 0.10 pH units were expected whereas the measurement resulted in 0.18 pH units (131 PR-GFP molecules (Q1: 110/Q3: 157)). Similarly, PRGFP's performance was higher in ABA membranes than expected, 0.12 pH units compared to the predicted 0.08 pH units (8 PR-GFP molecules (Q1: 7/Q3: 10)). It should be noted that the measured results are within the prediction interval, ranging from 0.04 till 0.19 pH units in case of the proteoliposomes and 0.03 till 0.17 pH units for the proteopolymersomes, even though the offset to the prediction is large. Vesicles not carrying PR-GFP have also shown a reaction towards illumination which was, however, either small (0.06 pH units, DOPC) or showing the opposite behavior (0.02 pH units, ABA). It should further be noted that looking at the kinetics in Figure 5.20 the dynamic of the control is different compared to the actual samples. Similar behavior observed in literature is likely attributed to the fluctuations in the fluorescence signal due to residual pyranine on the exterior vesicle membrane[118,186]. In terms of size, the difference between prediction, control and actual measurement are present, whereas the proteoliposomes are smaller than expected, but within the prediction interval. However, the controls fall out of that range.

Similar behavior is observed in case of the ABA proteopolymersomes, however their control FCS results are in good agreement with the predictions. For both membranes, the controls' PdI is much higher than expected and higher compared to PRGFP-containing vesicles.

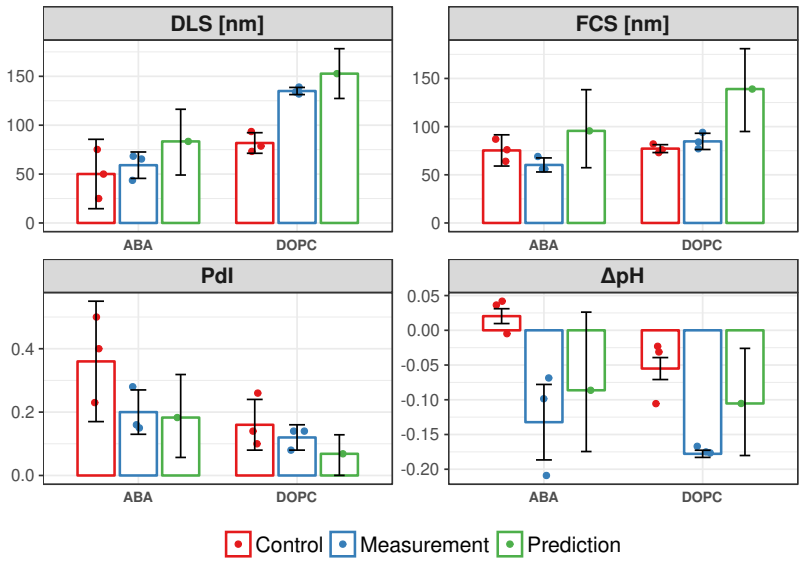

Figure 5.21: Comparison of the actual measurements, their controls and predictions for all four responses. Error bars represent the standard error of the mean, n = 3. In case of the predicted values, the bars represent the prediction interval containing 95 % of the outcomes. The underlying data is shown via dots which are jittered slightly to avoid overlapping. Liposomes and polymersomes prepared under the same conditions as the samples but without PR-GFP were used as controls.

5.2.7 *Conclusion*

Although membrane protein reconstitutions have been carried out for decades, examples for their application for the design of synthetic devices are rare and usually of model-like simplicity[1]. The inherent complexity of this approach provides a demanding challenge. With our study, we provide a possible framework to this field, showing an example of a thoroughly designed approach. Design of experiments has proven to be an excellent scaffold, which can be used as a guide to optimize relevant factors impacting the reconstitution conditions, which are crucial to the formation of a functional system. The easy accessibility of DoE allows detailed analysis and verified assumptions from literature and revealed new insights. Even though the models and results obtained via DoE are only valid for their specific case, the high coherence of this work supports the claim that the underlying method can be applied to further systems with other membrane proteins. Our results support the assumption that PMOXA-PDMS-PMOXA block copolymer membranes require very different conditions for the reconstitution of PR-GFP and potentially other alpha- helical membrane proteins. Even low OG concentrations can be disadvantageous for the vesicle integrity and the pH value during formation and reconstitution has a larger influence than expected. Only the lipid/polymer-to-protein ratio is a shared factor among the two membrane types but less PR-GFP seems to be incorporated into polymersomes. However, our data indicates a similar pH gradient am-

plitude in the proteopolymersomes. A future study could investigate this phenomenon. Most importantly, the potential optimization has been shown to yield functional proteovesicles composed of the lipid DOPC or an ABA block copolymer. The predictions were tested out for both systems and verified that DoE is an excellent approach to fulfill the above stated requirements of reproducibility and predictability. Thus, our framework allows access to two highly important characteristics of engineering: reproducibility and predictability. Our example shows the application of molecular engineering from protein design up to a mathematical model in order to achieve a functional product with the desired properties. Applying this methodology to further polymer (different block compositions, diblock copolymers) and lipid systems, as well as to other membrane proteins and detergent types, will potentially result in the identification of general mechanisms and important factors governing the assembly of proto-cells.

6
Conclusion & Outlook

Correlating the gained results to the topics and questions derived in section 2, p. 47, it can first be concluded that the reconstitution of PR into lipid membranes is possible via two distinct pathways. The detergent plays a pivotal role and it is the dominant mediator at a concentration around 0.5 %. The charge on the membrane surface only becomes the dominant mediator if OG is used at concentrations above 1 %. The salt concentration was identified as a 'binary switch'. Deviating from 150 mM leads to rapid loss of proteorhodopsin due to agglomeration, resulting in a non-observable function. The preferred pH value correlates to the reconstitution pathway. Slightly basic conditions lead to a higher observed activity when PR is reconstituted via the OG mediated pathway. In order to use the oppositely polarized extramembrane domains of PR, a pH value around 6 is necessary to use the available charges on the membrane. Valinomycin only had a beneficial effect on the proton gradient in samples which resulted from a high detergent and high charge composition. As a next step the use of polymer membranes as a host for PR was achieved. An extensive comparative study between DOPC as a benchmark and $PMOXA_{17}$-$PDMS_{65}$-$PMOXA_{17}$ was set up. The use of the PR-GFP fusion protein made the use of polarized membranes not necessary. The study identified distinct factor combinations under which proteopolymersomes and proteoliposomes assemble in a desired way. Whereas large, homogeneous proteoliposomes result from using around 1 % OG and take up large amounts of protein, proteopolymersomes are limited in the amount of PR taken up and form large structures only around 0.5 % OG. On average, the number of PR molecules present in proteopolymersomes is much smaller as FCS measurements revealed. Investigating the parameter space which yields the desired proteovesicles in terms of PR's proton pumping functionality showed further differences. In proteoliposomes the formed gradient mainly depends on the number of PR molecules present and the amount of detergent used. The combination low LPR, and thus high PR concentration, and low detergent concentration yielded a high activity. Proteopolymersomes benefit from a basic pH value and are easily disrupted at OG concentration above 1 % OG. Beside the differences of the assembly conditions, both systems were found to exhibit a

similar performance regarding the formation of a proton gradient. The lower number of available pumps in proteopolymersomes seems to get compensated by the lower diffusion through polymer membranes. The derived model equations could be used to find optimal reconstitution parameter settings which yield large, uniform and active proteovesicles. As observed before, the optimal settings were different. A low pH value, low LPR and low OG concentration was found for proteoliposomes whereas proteopolymersomes required a high pH, a approximately four times higher PPR and a slightly higher OG concentration. Verifying these optimal settings was successful and the predicted measurement results were in line with the actual measurements. Design of experiments proved to be a highly valuable framework for both projects and has the potential for being used in further studies.

More specifically, the created framework can be expanded with other membrane proteins, having different structures compared to the purely α-helical proteorhodopsin. As more complex membrane proteins usually require the use of milder detergents, other factors could be easily integrated into the experimental design and data assessment process. Due to the availability of mixture designs, it would also be possible to investigate the use and potential advantages of lipid-polymer-hybrid membrane systems. The lipid environment could provide a more natural host for the membrane protein and ease their reconstitution, whilst the polymers provide a robust and stable scaffold. These insights gained are not limited to vesiclar structures but could also easily applied to planar membranes. Planar membranes provide an easier platform for applications such as biosensing. Combining the aforementioned knowledge in a systematic way would lead to the realization of a library containing the necessary information about the interplay of various membrane systems, membrane proteins and their assembly. This would simplify the accomplishment of novel and complex systems such as the molecular hoover. The foundation for such a system have been established and an electro-chemical gradient can be established across lipid and polymer membranes. The conditions for the co-reconstitution with transport membrane proteins can be more conveniently predicted and achieved. Furthermore, this entire toolbox can be considerably useful for the establishment of highly developed systems acting as molecular factories.

Bibliography

[1] Cornelia G. Palivan, Roland Goers, Adrian Najer, Xiaoyan Zhang, Anja Car, and Wolfgang Meier. Bioinspired polymer vesicles and membranes for biological and medical applications. *Chemical Society Reviews*, 45(2):377–411, 2016. ISSN 0306-0012, 1460-4744. DOI: 10.1039/C5CS00569H.

[2] Clément Sanchez, Hervé Arribart, and Marie Madeleine Giraud Guille. Biomimetism and bioinspiration as tools for the design of innovative materials and systems. *Nature Materials*, 4(4):277–288, April 2005. ISSN 1476-1122, 1476-4660. DOI: 10.1038/nmat1339.

[3] Ruud J. R. W. Peters, Maïté Marguet, Sébastien Marais, Marco W. Fraaije, Jan C. M. vanHest, and Sébastien Lecommandoux. Cascade Reactions in Multicompartmentalized Polymersomes. *Angewandte Chemie International Edition*, 53(1):146–150, January 2014. ISSN 14337851. DOI: 10.1002/anie.201308141.

[4] Fei Wang, Pei Liu, Lin Sun, Cuncheng Li, Valery A. Petrenko, and Aihua Liu. Bio-mimetic Nanostructure Self-assembled from Au@Ag Heterogeneous Nanorods and Phage Fusion Proteins for Targeted Tumor Optical Detection and Photothermal Therapy. *Scientific Reports*, 4(1), May 2015. ISSN 2045-2322. DOI: 10.1038/srep06808.

[5] Patric Baumann, Pascal Tanner, Ozana Onaca, and Cornelia G. Palivan. Bio-Decorated Polymer Membranes: A New Approach in Diagnostics and Therapeutics. *Polymers*, 3(4):173–192, January 2011. ISSN 2073-4360. DOI: 10.3390/polym3010173.

[6] Patric Baumann, Vimalkumar Balasubramanian, Ozana Onaca-Fischer, Andrzej Sienkiewicz, and Cornelia G. Palivan. Light-responsive polymer nanoreactors: a source of reactive oxygen species on demand. *Nanoscale*, 5(1):217–224, 2013. ISSN 2040-3364, 2040-3372. DOI: 10.1039/C2NR32380J.

[7] Pascal Tanner, Stefan Egli, Vimalkumar Balasubramanian, Ozana Onaca, Cornelia G. Palivan, and Wolfgang Meier. Can polymeric vesicles that confine enzymatic reactions act as simplified organelles? *FEBS Letters*, 585(11):1699–1706, June 2011. ISSN 00145793. DOI: 10.1016/j.febslet.2011.05.003.

[8] Xiaoyan Zhang, Pascal Tanner, Alexandra Graff, Cornelia G. Palivan, and Wolfgang Meier. Mimicking the cell membrane with block copolymer membranes. *Journal of Polymer Science Part A: Polymer Chemistry*, 50(12):2293–2318, June 2012. ISSN 0887624X. DOI: 10.1002/pola.26000.

[9] M. Antonietti and S. Förster. Vesicles and Liposomes: A Self-Assembly Principle Beyond Lipids. *Advanced Materials*, 15(16): 1323–1333, August 2003. ISSN 0935-9648, 1521-4095. DOI: 10.1002/adma.200300010.

[10] David A. Christian, Aiwei Tian, Wouter G. Ellenbroek, Ilya Levental, Karthikan Rajagopal, Paul A. Janmey, Andrea J. Liu, Tobias Baumgart, and Dennis E. Discher. Spotted vesicles, striped micelles and Janus assemblies induced by ligand binding. *Nature Materials*, 8(10):843–849, October 2009. ISSN 1476-1122, 1476-4660. DOI: 10.1038/nmat2512.

[11] Gülay Bayramoğlu, Ayşegül Ü. Metin, Begum Altıntas, and M. Yakup Arıca. Reversible immobilization of glucose oxidase on polyaniline grafted polyacrylonitrile conductive composite membrane. *Bioresource Technology*, 101(18):6881–6887, September 2010. ISSN 09608524. DOI: 10.1016/j.biortech.2010.04.025.

[12] M. Fussenegger and J.E. Bailey. Molecular Regulation of Cell-Cycle Progression and Apoptosis in Mammalian Cells: Implications for Biotechnology. *Biotechnology Progress*, 14(6):807–833, December 1998. ISSN 8756-7938. DOI: 10.1021/bp9800891.

[13] A. Camilli. Bacterial Small-Molecule Signaling Pathways. *Science*, 311(5764):1113–1116, February 2006. ISSN 0036-8075, 1095-9203. DOI: 10.1126/science.1121357.

[14] Simona Mura, Julien Nicolas, and Patrick Couvreur. Stimuli-responsive nanocarriers for drug delivery. *Nature Materials*, 12 (11):991–1003, November 2013. ISSN 1476-1122, 1476-4660. DOI: 10.1038/nmat3776.

[15] Ashok Kumar, Akshay Srivastava, Igor Yu Galaev, and Bo Mattiasson. Smart polymers: Physical forms and bioengineering applications. *Progress in Polymer Science*, 32(10):1205–1237, October 2007. ISSN 00796700. DOI: 10.1016/j.progpolymsci.2007.05.003.

[16] Cornelia G. Palivan, Ozana Fischer-Onaca, Mihaela Delcea, Fabian Itel, and Wolfgang Meier. Protein–polymer nanoreactors for medical applications. *Chem. Soc. Rev.*, 41(7):2800–2823, 2012. ISSN 0306-0012, 1460-4744. DOI: 10.1039/C1CS15240H.

[17] Roberto J. Brea, Michael D. Hardy, and Neal K. Devaraj. Towards Self-Assembled Hybrid Artificial Cells: Novel Bottom-Up Approaches to Functional Synthetic Membranes. *Chemistry - A European Journal*, 21(36):12564–12570, September 2015. ISSN 09476539. DOI: 10.1002/chem.201501229.

[18] Stephen Mann. Self-assembly and transformation of hybrid nano-objects and nanostructures under equilibrium and non-equilibrium conditions. *Nature Materials*, 8(10):781–792, October 2009. ISSN 1476-1122, 1476-4660. DOI: 10.1038/nmat2496.

[19] Matthias C. Huber, Andreas Schreiber, Philipp von Olshausen, Balázs R. Varga, Oliver Kretz, Barbara Joch, Sabine Barnert, Rolf Schubert, Stefan Eimer, Péter Kele, and Stefan M. Schiller. Designer amphiphilic proteins as building blocks for the intracellular formation of organelle-like compartments. *Nature Materials*, 14(1):125–132, January 2015. ISSN 1476-1122, 1476-4660. DOI: 10.1038/nmat4118.

[20] Bruce Alberts. *Molecular biology of the cell*. Garland Science, Taylor and Francis Group, New York, NY, sixth edition edition, 2015. ISBN 978-0-8153-4432-2 978-0-8153-4464-3 978-0-8153-4524-4.

[21] Yuka Sakuma and Masayuki Imai. From Vesicles to Protocells: The Roles of Amphiphilic Molecules. *Life*, 5(1):651–675, March 2015. ISSN 2075-1729. DOI: 10.3390/life5010651.

[22] Jing Li, Xuling Wang, Ting Zhang, Chunling Wang, Zhenjun Huang, Xiang Luo, and Yihui Deng. A review on phospholipids and their main applications in drug delivery systems. *Asian Journal of Pharmaceutical Sciences*, 10(2):81–98, April 2015. ISSN 18180876. DOI: 10.1016/j.ajps.2014.09.004.

[23] Daniel A. Hammer and Neha P. Kamat. Towards an artificial cell. *FEBS Letters*, 586(18):2882–2890, August 2012. ISSN 00145793. DOI: 10.1016/j.febslet.2012.07.044.

[24] Jesper S. Hansen, Inés Plasencia, and Kamila Pszon-Bartosz. Strategies for Integrating Membrane Proteins in Biomembranes. In Claus Hélix-Nielsen, editor, *Biomimetic Membranes for Sensor and Separation Applications*, pages 251–271. Springer Netherlands, Dordrecht, 2011. ISBN 978-94-007-2183-8 978-94-007-2184-5. DOI: 10.1007/978-94-007-2184-512.

[25] Jean-Louis Rigaud and Daniel Lévy. Reconstitution of membrane proteins into liposomes. In *Methods in enzymology*, volume 372, pages 65–86. Elsevier, 2003.

[26] Annela M. Seddon, Paul Curnow, and Paula J. Booth. Membrane proteins, lipids and detergents: not just a soap opera. *Biochimica et Biophysica Acta (BBA) - Biomembranes*, 1666(1-2):105–117, November 2004. ISSN 00052736. DOI: 10.1016/j.bbamem.2004.04.011.

[27] Corinne Nardin, Thomas Hirt, Jörg Leukel, and Wolfgang Meier. Polymerized ABA Triblock Copolymer Vesicles. *Langmuir*, 16(3):1035–1041, February 2000. ISSN 0743-7463, 1520-5827. DOI: 10.1021/la990951u.

[28] Corinne Nardin, J. Widmer, M. Winterhalter, and W. Meier. Amphiphilic block copolymer nanocontainers as bioreactors. *The European Physical Journal E*, 4(4):403–410, 2001.

[29] J. F. Le Meins, O. Sandre, and S. Lecommandoux. Recent trends in the tuning of polymersomes' membrane properties. *The European Physical Journal E*, 34(2), February 2011. ISSN 1292-8941, 1292-895X. DOI: 10.1140/epje/i2011-11014-y.

[30] Feng Li, Sylvain Prévost, Ralf Schweins, Antonius T. M. Marcelis, Frans A. M. Leermakers, Martien A. Cohen Stuart, and Ernst J. R. Sudhölter. Small monodisperse unilamellar vesicles from binary copolymer mixtures. *Soft Matter*, 5(21):4169, 2009. ISSN 1744-683X, 1744-6848. DOI: 10.1039/b904522h.

[31] Qi Chen, Holger Schönherr, and G. Julius Vancso. Mechanical properties of block copolymer vesicle membranes by atomic force microscopy. *Soft Matter*, 5(24):4944, 2009. ISSN 1744-683X, 1744-6848. DOI: 10.1039/b903110c.

[32] James C.-M. Lee, Maria Santore, Frank S. Bates, and Dennis E. Discher. From Membranes to Melts, Rouse to Reptation: Diffusion in Polymersome versus Lipid Bilayers. *Macromolecules*, 35(2):323–326, January 2002. ISSN 0024-9297, 1520-5835. DOI: 10.1021/ma0112063.

[33] Fabian Itel, Mohamed Chami, Adrian Najer, Samuel Lörcher, Dalin Wu, Ionel A. Dinu, and Wolfgang Meier. Molecular Organization and Dynamics in Polymersome Membranes: A Lateral Diffusion Study. *Macromolecules*, 47(21):7588–7596, November 2014. ISSN 0024-9297, 1520-5835. DOI: 10.1021/ma5015403.

[34] Manish Kumar, Mariusz Grzelakowski, Julie Zilles, Mark Clark, and Wolfgang Meier. Highly permeable polymeric membranes based on the incorporation of the functional water channel protein Aquaporin Z. *Proceedings of the National Academy of Sciences*, 104(52):20719–20724, 2007.

[35] Mariusz Grzelakowski, Meron F. Cherenet, Yue-xiao Shen, and Manish Kumar. A framework for accurate evaluation of the promise of aquaporin based biomimetic membranes. *Journal of Membrane Science*, 479:223–231, April 2015. ISSN 03767388. DOI: 10.1016/j.memsci.2015.01.023.

[36] H. Bermúdez, D. A. Hammer, and D. E. Discher. Effect of Bilayer Thickness on Membrane Bending Rigidity. *Langmuir*, 20(3):540–543, February 2004. ISSN 0743-7463, 1520-5827. DOI: 10.1021/la035497f.

[37] Joshua S. Katz, Katherine A. Eisenbrown, Eric D. Johnston, Neha P. Kamat, Jeff Rawson, Michael J. Therien, Jason A. Burdick, and Daniel A. Hammer. Soft biodegradable polymersomes from caprolactone-derived polymers. *Soft Matter*, 8(42):10853–10862, 2012.

[38] Michael L. Wagner and Lukas K. Tamm. Tethered Polymer-Supported Planar Lipid Bilayers for Reconstitution of Integral Membrane Proteins: Silane-Polyethyleneglycol-Lipid as a Cushion and Covalent Linker. *Biophysical Journal*, 79(3):1400–1414, September 2000. ISSN 00063495. DOI: 10.1016/S0006-3495(00)76392-2.

[39] Justyna Kowal, Xiaoyan Zhang, Ionel Adrian Dinu, Cornelia G. Palivan, and Wolfgang Meier. Planar Biomimetic Membranes Based on Amphiphilic Block Copolymers. *ACS Macro Letters*, 3(1):59–63, January 2014. ISSN 2161-1653, 2161-1653. DOI: 10.1021/mz400590c.

[40] Ann-Christine Albertsson and Indra K. Varma. Recent Developments in Ring Opening Polymerization of Lactones for Biomedical Applications. *Biomacromolecules*, 4(6):1466–1486, November 2003. ISSN 1525-7797, 1526-4602. DOI: 10.1021/bm034247a.

[41] Souvik Basak, Vinay Deep Punetha, Ganga Bisht, Satpal Singh Bisht, Nanda Gopal Sahoo, and Jae Whan Cho. Recent Trends of Polymer-Protein Conjugate Application in Biocatalysis: A Review. *Polymer Reviews*, 55(1):163–198, January 2015. ISSN 1558-3724, 1558-3716. DOI: 10.1080/15583724.2014.971371.

[42] Fabian Itel, Ionel Adrian Dinu, Pascal Tanner, Ozana Fischer, and Cornelia G. Palivan. Nanoreactors for Biomedical Applications. In *Frontiers in Nanobiomedical Research*, volume 3, pages 457–508. WORLD SCIENTIFIC, October 2014. ISBN 978-981-4520-64-5 978-981-4520-65-2. DOI: $10.1142/9789814520652_0064$.

[43] Maïté Marguet, Colin Bonduelle, and Sébastien Lecommandoux. Multicompartmentalized polymeric systems: towards biomimetic cellular structure and function. *Chem. Soc. Rev.*, 42(2):512–529, 2013. ISSN 0306-0012, 1460-4744. DOI: 10.1039/C2CS35312A.

[44] H. Aranda-Espinoza, H. Bermudez, F. S. Bates, and D. E. Discher. Electromechanical Limits of Polymersomes. *Physical Review Letters*, 87 (20), October 2001. ISSN 0031-9007, 1079-7114. DOI: 10.1103/PhysRevLett.87.208301.

[45] Harry Bermudez, Aaron K. Brannan, Daniel A. Hammer, Frank S. Bates, and Dennis E. Discher. Molecular Weight Dependence of Polymersome Membrane Structure, Elasticity, and Stability. *Macromolecules*, 35(21):8203–8208, October 2002. ISSN 0024-9297, 1520-5835. DOI: 10.1021/ma020669l.

[46] Zhiliang Cheng, Drew R. Elias, Neha P. Kamat, Eric D. Johnston, Andrei Poloukhtine, Vladimir Popik, Daniel A. Hammer, and Andrew Tsourkas. Improved Tumor Targeting of Polymer-Based Nanovesicles Using Polymer–Lipid Blends. *Bioconjugate Chemistry*, 22(10):2021–2029, October 2011. ISSN 1043-1802, 1520-4812. DOI: 10.1021/bc200214g.

[47] B. M. Discher. Polymersomes: Tough Vesicles Made from Diblock Copolymers. *Science*, 284(5417):1143–1146, May 1999. ISSN 00368075, 10959203. DOI: 10.1126/science.284.5417.1143.

[48] Rumiana Dimova, Said Aranda, Natalya Bezlyepkina, Vesselin Nikolov, Karin A. Riske, and Reinhard Lipowsky. A practical guide to giant vesicles. Probing the membrane nanoregime via optical microscopy. *Journal of Physics: Condensed Matter*, 18(28):S1151, 2006.

[49] Hung-Yu Chang, Yu-Jane Sheng, and Heng-Kwong Tsao. Structural and mechanical characteristics of polymersomes. *Soft Matter*, 10(34):6373, June 2014. ISSN 1744-683X, 1744-6848. DOI: 10.1039/C4SM01092B.

[50] Etienne Cabane, Xiaoyan Zhang, Karolina Langowska, Cornelia G. Palivan, and Wolfgang Meier. Stimuli-Responsive Polymers and Their Applications in Nanomedicine. *Biointerphases*, 7(1):9, December 2012. ISSN 1934-8630, 1559-4106. DOI: 10.1007/s13758-011-0009-3.

[51] Jennifer Bain, Matthew Berry, Catherine Dirks, and Sarah Staniland. Synthesis of ABA Tri-Block Co-Polymer Magnetopolymersomes via Electroporation for Potential Medical Application. *Polymers*, 7(12):2558–2571, December 2015. ISSN 2073-4360. DOI: 10.3390/polym7121529.

[52] Fenghua Meng, Christine Hiemstra, Gerard H. M. Engbers, and Jan Feijen. Biodegradable Polymersomes. *Macromolecules*, 36(9):3004–3006, May 2003. ISSN 0024-9297. DOI: 10.1021/ma034040+.

[53] Camelia Draghici, Justyna Kowal, Alina Darjan, Wolfgang Meier, and Cornelia G. Palivan. "Active Surfaces" Formed by Immobilization of Enzymes on Solid-Supported Polymer Membranes. *Langmuir*, 30 (39):11660–11669, October 2014. ISSN 0743-7463, 1520-5827. DOI: 10.1021/la502841p.

[54] Fabian Itel, Adrian Najer, Cornelia G. Palivan, and Wolfgang Meier. Dynamics of Membrane Proteins within Synthetic Polymer Membranes with Large Hydrophobic Mismatch. *Nano Letters*, 15(6):3871–3878, June 2015. ISSN 1530-6984, 1530-6992. DOI: 10.1021/acs.nanolett.5b00699.

[55] Léa Messager, Jens Gaitzsch, Luca Chierico, and Giuseppe Battaglia. Novel aspects of encapsulation and delivery using polymersomes. *Current Opinion in Pharmacology*, 18:104–111, October 2014. ISSN 14714892. DOI: 10.1016/j.coph.2014.09.017.

[56] Pascal Tanner, Patric Baumann, Ramona Enea, Ozana Onaca, Cornelia Palivan, and Wolfgang Meier. Polymeric Vesicles: From Drug Carriers to Nanoreactors and Artificial Organelles. *Accounts of Chemical Research*, 44(10):1039–1049, October 2011. ISSN 0001-4842, 1520-4898. DOI: 10.1021/ar200036k.

[57] Ozana Onaca-Fischer, Juan Liu, Mark Inglin, and Cornelia G. Palivan. Polymeric Nanocarriers and Nanoreactors: A Survey of Possible Therapeutic Applications. *Current Pharmaceutical Design*, 18(18):2622–2643, April 2012. ISSN 13816128. DOI: 10.2174/138161212800492822.

[58] Katarzyna Kita-Tokarczyk, Julie Grumelard, Thomas Haefele, and Wolfgang Meier. Block copolymer vesicles—using concepts from polymer chemistry to mimic biomembranes. *Polymer*, 46(11):3540–3563, May 2005. ISSN 00323861. DOI: 10.1016/j.polymer.2005.02.083.

[59] Goundla Srinivas, Dennis E. Discher, and Michael L. Klein. Key Roles for Chain Flexibility in Block Copolymer Membranes that Contain Pores or Make Tubes. *Nano Letters*, 5(12):2343–2349, December 2005. ISSN 1530-6984, 1530-6992. DOI: 10.1021/nl051515x.

[60] Corinne Nardin, Sandra Thoeni, Jörg Widmer, Mathias Winterhalter, and Wolfgang Meier. Nanoreactors based on (polymerized) ABA-triblock copolymer vesicles. *Chemical Communications*, (15):1433–1434, 2000. ISSN 13597345, 1364548X. DOI: 10.1039/b004280n.

[61] Alexandra Graff, Caroline Fraysse-Ailhas, Cornelia G. Palivan, Mariusz Grzelakowski, Thorsten Friedrich, Corinne Vebert, Georg Gescheidt, and Wolfgang Meier. Amphiphilic Copolymer Membranes Promote NADH:Ubiquinone Oxidoreductase Activity: Towards an Electron-Transfer Nanodevice. *Macromolecular Chemistry and Physics*, 211(2):229–238, January 2010. ISSN 10221352, 15213935. DOI: 10.1002/macp.200900517.

[62] Mihai Lomora, Martina Garni, Fabian Itel, Pascal Tanner, Mariana Spulber, and Cornelia G. Palivan. Polymersomes with engineered ion selective permeability as stimuli-responsive nanocompartments with preserved architecture. *Biomaterials*, 53:406–414, June 2015. ISSN 01429612. DOI: 10.1016/j.biomaterials.2015.02.080.

[63] Roland Gamsjaeger, Barbara Wimmer, Heike Kahr, Ali Tinazli, Srdjan Picuric, Suman Lata, Robert Tampé, Yves Maulet, Hermann J. Gruber, Peter Hinterdorfer, and Christoph Romanin. Oriented Binding of the His_6-Tagged Carboxyl-Tail of the L-type Ca^{2+} Channel $_1$-Subunit to a New NTA-Functionalized Self-Assembled Monolayer. *Langmuir*, 20(14):5885–5890, July 2004. ISSN 0743-7463, 1520-5827. DOI: 10.1021/la0498206.

[64] Carsten Hoffmann, Guido Gaietta, Alexander Zürn, Stephen R Adams, Sonia Terrillon, Mark H Ellisman, Roger Y Tsien, and Martin J Lohse. Fluorescent labeling of tetracysteine-tagged proteins in intact cells. *Nature Protocols*, 5(10):1666–1677, September 2010. ISSN 1754-2189, 1750-2799. DOI: 10.1038/nprot.2010.129.

[65] Andreas Thess, Silke Hutschenreiter, Matthias Hofmann, Robert Tampé, Wolfgang Baumeister, and Reinhard Guckenberger. Specific Orientation and Two-dimensional Crystallization of the Proteasome at Metal-chelating Lipid Interfaces. *Journal of Biological Chemistry*, 277 (39):36321–36328, September 2002. ISSN 0021-9258, 1083-351X. DOI: 10.1074/jbc.M202145200.

[66] K. Terpe. Overview of tag protein fusions: from molecular and biochemical fundamentals to commercial systems. *Applied Microbiol-*

ogy and Biotechnology, 60(5):523–533, January 2003. ISSN 0175-7598, 1432-0614. DOI: 10.1007/s00253-002-1158-6.

[67] Michael Kruppa and Burkhard König. Reversible Coordinative Bonds in Molecular Recognition. *Chemical Reviews*, 106(9):3520–3560, September 2006. ISSN 0009-2665, 1520-6890. DOI: 10.1021/cr010206y.

[68] Rainer Nehring, Cornelia G. Palivan, Oliver Casse, Pascal Tanner, Jens Tüxen, and Wolfgang Meier. Amphiphilic Diblock Copolymers for Molecular Recognition: MetalNitrilotriacetic Acid Functionalized Vesicles. *Langmuir*, 25(2):1122–1130, January 2009. ISSN 0743-7463, 1520-5827. DOI: 10.1021/la8027308.

[69] Karolina Langowska, Justyna Kowal, Cornelia G. Palivan, and Wolfgang Meier. A general strategy for creating self-defending surfaces for controlled drug production for long periods of time. *Journal of Materials Chemistry B*, 2(29):4684, 2014. ISSN 2050-750X, 2050-7518. DOI: 10.1039/c4tb00277f.

[70] Stefan Egli, Martin G. Nussbaumer, Vimalkumar Balasubramanian, Mohamed Chami, Nico Bruns, Cornelia Palivan, and Wolfgang Meier. Biocompatible Functionalization of Polymersome Surfaces: A New Approach to Surface Immobilization and Cell Targeting Using Polymersomes. *Journal of the American Chemical Society*, 133(12):4476–4483, March 2011. ISSN 0002-7863, 1520-5126. DOI: 10.1021/ja110275f.

[71] Tarun Garg and Amit K. Goyal. Liposomes: Targeted and Controlled Delivery System. *Drug Delivery Letters*, 4(1):62–71, 2014. ISSN 2210-3031.

[72] Abolfazl Akbarzadeh, Rogaie Rezaei-Sadabady, Soodabeh Davaran, Sang Woo Joo, Nosratollah Zarghami, Younes Hanifehpour, Mohammad Samiei, Mohammad Kouhi, and Kazem Nejati-Koshki. Liposome: classification, preparation, and applications. *Nanoscale Research Letters*, 8(1):102, 2013. ISSN 1556-276X. DOI: 10.1186/1556-276X-8-102.

[73] Giuseppina Bozzuto and Agnese Molinari. Liposomes as nanomedical devices. *International Journal of Nanomedicine*, page 975, February 2015. ISSN 1178-2013. DOI: 10.2147/IJN.S68861.

[74] V. Malinova, M. Nallani, W.P. Meier, and E.K. Sinner. Synthetic biology, inspired by synthetic chemistry. *FEBS Letters*, 586(15):2146–2156, July 2012. ISSN 00145793. DOI: 10.1016/j.febslet.2012.05.033.

[75] F. Junge, B. Schneider, S. Reckel, D. Schwarz, V. Dötsch, and F. Bernhard. Large-scale production of functional membrane proteins. *Cellular and Molecular Life Sciences*, 65(11):1729–1755, June 2008. ISSN 1420-682X, 1420-9071. DOI: 10.1007/s00018-008-8067-5.

[76] Thierry Rabilloud. Membrane proteins and proteomics: Love is possible, but so difficult. *ELECTROPHORESIS*, 30(S1):S174–S180, June 2009. ISSN 01730835. DOI: 10.1002/elps.200900050.

[77] Hyo-Jick Choi and Carlo D. Montemagno. Light-Driven Hybrid Bioreactor Based on Protein-Incorporated Polymer Vesicles. *IEEE Transactions On Nanotechnology*, 6(2):171–176, March 2007. ISSN 1536-125X. DOI: 10.1109/TNANO.2007.891822.

[78] Prasad V. Pawar, Shalini V. Gohil, Jay Prakash Jain, and Neeraj Kumar. Functionalized polymersomes for biomedical applications. *Polymer Chemistry*, 4(11):3160, 2013. ISSN 1759-9954, 1759-9962. DOI: 10.1039/c3py00023k.

[79] Adrian Najer, Dalin Wu, Andrej Bieri, Françoise Brand, Cornelia G. Palivan, Hans-Peter Beck, and Wolfgang Meier. Nanomimics of Host Cell Membranes Block Invasion and Expose Invasive Malaria Parasites. *ACS Nano*, 8(12):12560–12571, December 2014. ISSN 1936-0851, 1936-086X. DOI: 10.1021/nn5054206.

[80] Peipei Chen, Min Qiu, Chao Deng, Fenghua Meng, Jian Zhang, Ru Cheng, and Zhiyuan Zhong. pH-Responsive Chimaeric Pepsomes Based on Asymmetric Poly(ethylene glycol)- *b* -Poly(l -leucine)- *b* -Poly(l -glutamic acid) Triblock Copolymer for Efficient Loading and Active Intracellular Delivery of Doxorubicin Hydrochloride. *Biomacromolecules*, 16(4):1322–1330, April 2015. ISSN 1525-7797, 1526-4602. DOI: 10.1021/acs.biomac.5b00113.

[81] Hao Yang, Chuan Zhang, Chang Li, Yong Liu, Yingli An, Rujiang Ma, and Linqi Shi. Glucose-Responsive Polymer Vesicles Templated by -CD/PEG Inclusion Complex. *Biomacromolecules*, 16(4):1372–1381, April 2015. ISSN 1525-7797, 1526-4602. DOI: 10.1021/acs.biomac.5b00155.

[82] P. S. Pramod, Ruchira Shah, Sonali Chaphekar, Nagaraj Balasubramanian, and Manickam Jayakannan. Polysaccharide nanovesicular multidrug carriers for synergistic killing of cancer cells. *Nanoscale*, 6(20):11841–11855, 2014. ISSN 2040-3364, 2040-3372. DOI: 10.1039/C4NR03514C.

[83] Chuncai Zhou, Mingzhi Wang, Kaidian Zou, Jing Chen, Yunqing Zhu, and Jianzhong Du. Antibacterial Polypeptide-Grafted Chitosan-Based Nanocapsules As an "Armed" Carrier of Anticancer and Antiepileptic Drugs. *ACS Macro Letters*, 2(11):1021–1025, November 2013. ISSN 2161-1653, 2161-1653. DOI: 10.1021/mz400480z.

[84] Chin Ken Wong, Alistair J. Laos, Alexander H. Soeriyadi, Jörg Wiedenmann, Paul M. G. Curmi, J. Justin Gooding, Christopher P. Marquis, Martina H. Stenzel, and Pall Thordarson. Polymersomes Prepared from Thermoresponsive Fluorescent Protein-Polymer Bioconjugates: Capture of and Report on Drug and Protein Payloads. *Angewandte Chemie International Edition*, 54(18):5317–5322, April 2015. ISSN 14337851. DOI: 10.1002/anie.201412406.

[85] Soumen Das, Dharmendar Kumar Sharma, Suman Chakrabarty, Arindam Chowdhury, and Sayam Sen Gupta. Bioactive Polymersomes Self-Assembled from Amphiphilic PPO- *Glyco* Polypeptides: Synthesis, Characterization, and Dual-Dye Encapsulation. *Langmuir*, 31(11):3402–3412, March 2015. ISSN 0743-7463, 1520-5827. DOI: 10.1021/la503993e.

[86] Yasutaka Anraku, Akihiro Kishimura, Yuichi Yamasaki, and Kazunori Kataoka. Living Unimodal Growth of Polyion Complex Vesicles via Two-Dimensional Supramolecular Polymerization. *Journal of the American Chemical Society*, 135(4):1423–1429, January 2013. ISSN 0002-7863, 1520-5126. DOI: 10.1021/ja3096587.

[87] Pascal Tanner, Maria Ezhevskaya, Rainer Nehring, Sabine Van Doorslaer, Wolfgang Meier, and Cornelia Palivan. Specific His $_6$ -tag Attachment to Metal-Functionalized Polymersomes Relies on Molecular Recognition. *The Journal of Physical Chemistry B*, 116(33):10113–10124, August 2012. ISSN 1520-6106, 1520-5207. DOI: 10.1021/jp305544v.

[88] Rainer Nehring, Cornelia G. Palivan, Susana Moreno-Flores, Alexandre Mantion, Pascal Tanner, Jose Luis Toca-Herrera, Andreas Thünemann, and Wolfgang Meier. Protein decorated membranes by specific molecular interactions. *Soft Matter*, 6(12):2815, 2010. ISSN 1744-683X, 1744-6848. DOI: 10.1039/c002838j.

[89] Todd O. Pangburn, Frank S. Bates, and Efrosini Kokkoli. Polymersomes functionalized via "click" chemistry with the fibronectin mimetic peptides PR_b and GRGDSP for targeted delivery to cells with different levels of 51 expression. *Soft Matter*, 8(16):4449, 2012. ISSN 1744-683X, 1744-6848. DOI: 10.1039/c2sm06922a.

[90] Daniel Bacinello, Elisabeth Garanger, Daniel Taton, Kam Chui Tam, and Sébastien Lecommandoux. Tailored drug-release from multi-functional polymer-peptide hybrid vesicles. *European Polymer Journal*, 62:363–373, January 2015. ISSN 00143057. DOI: 10.1016/j.eurpolymj.2014.09.001.

[91] J-F. Le Meins, C. Schatz, S. Lecommandoux, and O. Sandre. Hybrid polymer/lipid vesicles: state of the art and future perspectives. *Materials Today*, 16(10):397–402, October 2013. ISSN 13697021. DOI: 10.1016/j.mattod.2013.09.002.

[92] Maud Chemin, Pierre-Marie Brun, Sébastien Lecommandoux, Olivier Sandre, and Jean-François Le Meins. Hybrid polymer/lipid vesicles: fine control of the lipid and polymer distribution in the binary membrane. *Soft Matter*, 8(10):2867, 2012. ISSN 1744-683X, 1744-6848. DOI: 10.1039/c2sm07188f.

[93] Jin Nam, Paul A. Beales, and T. Kyle Vanderlick. Giant Phospholipid/Block Copolymer Hybrid Vesicles: Mixing Behavior and Domain Formation. *Langmuir*, 27(1):1–6, January 2011. ISSN 0743-7463, 1520-5827. DOI: 10.1021/la103428g.

[94] Justyna Kowal, Dalin Wu, Viktoria Mikhalevich, Cornelia G. Palivan, and Wolfgang Meier. Hybrid Polymer–Lipid Films as Platforms for Directed Membrane Protein Insertion. *Langmuir*, 31(17):4868–4877, May 2015. ISSN 0743-7463, 1520-5827. DOI: 10.1021/acs.langmuir.5b00388.

[95] Hans Kiefer. In vitro folding of alpha-helical membrane proteins. *Biochimica et Biophysica Acta (BBA) - Biomembranes*, 1610(1):57–62, February 2003. ISSN 00052736. DOI: 10.1016/S0005-2736(02)00717-4.

[96] Ozana Onaca, Madhavan Nallani, Saskia Ihle, Alexander Schenk, and Ulrich Schwaneberg. Functionalized nanocompartments (Synthosomes): Limitations and prospective applications in industrial biotechnology. *Biotechnology Journal*, 1(7-8):795–805, August 2006. ISSN 1860-6768, 1860-7314. DOI: 10.1002/biot.200600050.

[97] Feng Zhang, Johannes Vierock, Ofer Yizhar, Lief E. Fenno, Satoshi Tsunoda, Arash Kianianmomeni, Matthias Prigge, Andre Berndt, John Cushman, Jürgen Polle, Jon Magnuson, Peter Hegemann, and Karl Deisseroth. The Microbial Opsin Family of Optogenetic Tools. *Cell*, 147(7):1446–1457, December 2011. ISSN 00928674. DOI: 10.1016/j.cell.2011.12.004.

[98] John L. Spudich, Oleg A. Sineshchekov, and Elena G. Govorunova. Mechanism divergence in microbial rhodopsins. *Biochimica et Biophysica Acta (BBA) - Bioenergetics*, 1837(5):546–552, May 2014. ISSN 00052728. DOI: 10.1016/j.bbabio.2013.06.006.

[99] O. Beja. Bacterial Rhodopsin: Evidence for a New Type of Phototrophy in the Sea. *Science*, 289(5486):1902–1906, September 2000. ISSN 00368075, 10959203. DOI: 10.1126/science.289.5486.1902.

[100] Mathias Grote and Maureen A. O'Malley. Enlightening the life sciences: the history of halobacterial and microbial rhodopsin research. *FEMS Microbiology Reviews*, 35(6):1082–1099, November 2011. ISSN 1574-6976. DOI: 10.1111/j.1574-6976.2011.00281.x.

[101] Dieter Oesterhelt and Walther Stoeckenius. Rhodopsin-like Protein from the Purple Membrane of Halobacterium halobium. *Nature New Biology*, 233(39):149–152, September 1971. ISSN 0090-0028. DOI: 10.1038/newbio233149a0.

[102] Matthew J. Ranaghan, Christine T. Schwall, Nathan N. Alder, and Robert R. Birge. Green Proteorhodopsin Reconstituted into Nanoscale Phospholipid Bilayers (Nanodiscs) as Photoactive Monomers. *Journal of the American Chemical Society*, 133(45):18318–18327, November 2011. ISSN 0002-7863, 1520-5126. DOI: 10.1021/ja2070957.

[103] Oded Béjà, Elena N. Spudich, John L. Spudich, Marion Leclerc, and Edward F. DeLong. Proteorhodopsin phototrophy in the ocean. *Nature*, 411(6839):786–789, June 2001. ISSN 0028-0836. DOI: 10.1038/35081051.

[104] Adriana L. Klyszejko, Sarika Shastri, Stefania A. Mari, Helmut Grubmüller, Daniel J. Muller, and Clemens Glaubitz. Folding and Assembly

of Proteorhodopsin. *Journal of Molecular Biology*, 376(1):35–41, February 2008. ISSN 00222836. DOI: 10.1016/j.jmb.2007.11.030.

[105] Christian Bamann, Ernst Bamberg, Josef Wachtveitl, and Clemens Glaubitz. Proteorhodopsin. *Biochimica et Biophysica Acta (BBA) - Bioenergetics*, 1837(5):614–625, May 2014. ISSN 00052728. DOI: 10.1016/j.bbabio.2013.09.010.

[106] Thomas Friedrich, Sven Geibel, Rolf Kalmbach, Igor Chizhov, Kenichi Ataka, Joachim Heberle, Martin Engelhard, and Ernst Bamberg. Proteorhodopsin is a Light-driven Proton Pump with Variable Vectoriality. *Journal of Molecular Biology*, 321(5):821–838, August 2002. ISSN 00222836. DOI: 10.1016/S0022-2836(02)00696-4.

[107] Andrei K. Dioumaev, Jennifer M. Wang, Zoltán Bálint, György Váró, and Janos K. Lanyi. Proton Transport by Proteorhodopsin Requires that the Retinal Schiff Base Counterion Asp-97 Be Anionic †. *Biochemistry*, 42(21):6582–6587, June 2003. ISSN 0006-2960, 1520-4995. DOI: 10.1021/bi034253r.

[108] Sarika Shastri, Janet Vonck, Nicole Pfleger, Winfried Haase, Werner Kuehlbrandt, and Clemens Glaubitz. Proteorhodopsin: Characterisation of 2d crystals by electron microscopy and solid state NMR. *Biochimica et Biophysica Acta (BBA) - Biomembranes*, 1768(12):3012–3019, December 2007. ISSN 00052736. DOI: 10.1016/j.bbamem.2007.10.001.

[109] F. Oesterhelt. Unfolding Pathways of Individual Bacteriorhodopsins. *Science*, 288(5463):143–146, April 2000. ISSN 00368075, 10959203. DOI: 10.1126/science.288.5463.143.

[110] Jean-Louis Rigaud, Bruno Pitard, and Daniel Levy. Reconstitution of membrane proteins into liposomes: application to energy-transducing membrane proteins. *Biochimica et Biophysica Acta (BBA)-Bioenergetics*, 1231(3):223–246, 1995.

[111] Daniel LEvy, Aline Bluzat, Michel Seigneuret, and Jean-Louis Rigaud. A systematic study of liposome and proteoliposome reconstitution involving Bio-Bead-mediated Triton X-100 removal. *Biochimica et Biophysica Acta (BBA)-Biomembranes*, 1025(2):179–190, 1990.

[112] Marie Therese Paternostre, Michel Roux, and Jean Louis Rigaud. Mechanisms of membrane protein insertion into liposomes during reconstitution procedures involving the use of detergents. 1. Solubilization of large unilamellar liposomes (prepared by reverse-phase evaporation) by triton X-100, octyl glucoside, and sodium cholate. *Biochemistry*, 27(8):2668–2677, 1988.

[113] Michel Ollivon, Sylviane Lesieur, Cécile Grabielle-Madelmont, and Maıté Paternostre. Vesicle reconstitution from lipid–detergent mixed micelles. *Biochimica et Biophysica Acta (BBA)-Biomembranes*, 1508(1): 34–50, 2000.

[114] Suzanne M. Kuiper, Madhavan Nallani, Dennis M. Vriezema, Jeroen J. L. M. Cornelissen, Jan C. M. van Hest, Roeland J. M. Nolte, and Alan E.

Rowan. Enzymes containing porous polymersomes as nano reaction vessels for cascade reactions. *Organic & Biomolecular Chemistry*, 6(23): 4315, 2008. ISSN 1477-0520, 1477-0539. DOI: 10.1039/b811196k.

[115] Mariana Spulber, Patric Baumann, Sina S. Saxer, Uwe Pieles, Wolfgang Meier, and Nico Bruns. Poly(*N* -vinylpyrrolidone)-Poly(dimethylsiloxane)-Based Polymersome Nanoreactors for Laccase-Catalyzed Biotransformations. *Biomacromolecules*, 15(4):1469–1475, April 2014. ISSN 1525-7797, 1526-4602. DOI: 10.1021/bm500081j.

[116] David Gräfe, Jens Gaitzsch, Dietmar Appelhans, and Brigitte Voit. Cross-linked polymersomes as nanoreactors for controlled and stabilized single and cascade enzymatic reactions. *Nanoscale*, 6(18):10752–10761, 2014. ISSN 2040-3364, 2040-3372. DOI: 10.1039/C4NR02155J.

[117] Veena Pata, Fariyal Ahmed, Dennis E. Discher, and Nily Dan. Membrane Solubilization by Detergent: Resistance Conferred by Thickness. *Langmuir*, 20(10):3888–3893, May 2004. ISSN 0743-7463, 1520-5827. DOI: 10.1021/la035734e.

[118] Hyo-Jick Choi and Carlo D. Montemagno. Artificial Organelle: ATP Synthesis from Cellular Mimetic Polymersomes. *Nano Letters*, 5 (12):2538–2542, December 2005. ISSN 1530-6984, 1530-6992. DOI: 10.1021/nl051896e.

[119] Miho Yanagisawa, Masayuki Iwamoto, Ayako Kato, Kenichi Yoshikawa, and Shigetoshi Oiki. Oriented Reconstitution of a Membrane Protein in a Giant Unilamellar Vesicle: Experimental Verification with the Potassium Channel KcsA. *Journal of the American Chemical Society*, 133(30):11774–11779, August 2011. ISSN 0002-7863, 1520-5126. DOI: 10.1021/ja2040859.

[120] Daoben Hua, Liangju Kuang, and Hongjun Liang. Self-Directed Reconstitution of Proteorhodopsin with Amphiphilic Block Copolymers Induces the Formation of Hierarchically Ordered Proteopolymer Membrane Arrays. *Journal of the American Chemical Society*, 133(8):2354–2357, March 2011. ISSN 0002-7863, 1520-5126. DOI: 10.1021/ja109796x.

[121] Roxana Stoenescu, Alexandra Graff, and Wolfgang Meier. Asymmetric ABC-Triblock Copolymer Membranes Induce a Directed Insertion of Membrane Proteins. *Macromolecular Bioscience*, 4(10):930–935, October 2004. ISSN 1616-5187, 1616-5195. DOI: 10.1002/mabi.200400065.

[122] John Lawson and John Erjavec. *Experimental Strategies and Data Analysis for Research.* Chapman & Hall, 2014. ISBN 978-1-4665-1217-7. OCLC: 1028111614.

[123] Trevor Laird. Design of Experiments (DoE). *Organic Process Research & Development*, 6(4):337–337, July 2002. ISSN 1083-6160, 1520-586X. DOI: 10.1021/op0255581.

[124] Veronica Czitrom. One-Factor-at-a-Time versus Designed Experiments. *The American Statistician*, 53(2):126–131, May 1999. ISSN 0003-1305, 1537-2731. DOI: 10.1080/00031305.1999.10474445.

[125] D. A. Preece. R. A. Fisher and Experimental Design: A Review. *Biometrics*, 46(4):925, December 1990. ISSN 0006341X. DOI: 10.2307/2532438.

[126] John A. Jacquez. Design of experiments. *Journal of the Franklin Institute*, 335(2):259–279, March 1998. ISSN 00160032. DOI: 10.1016/S0016-0032(97)00004-5.

[127] G. E. P. Box and K. B. Wilson. On the Experimental Attainment of Optimum Conditions. In Samuel Kotz and Norman L. Johnson, editors, *Breakthroughs in Statistics*, pages 270–310. Springer New York, New York, NY, 1992. ISBN 978-0-387-94039-7 978-1-4612-4380-9. DOI: 10.1007/978-1-4612-4380-9$_2$3.

[128] Steven A. Weissman and Neal G. Anderson. Design of Experiments (DoE) and Process Optimization. A Review of Recent Publications. *Organic Process Research & Development*, 19(11):1605–1633, November 2015. ISSN 1083-6160, 1520-586X. DOI: 10.1021/op500169m.

[129] Marcos Almeida Bezerra, Ricardo Erthal Santelli, Eliane Padua Oliveira, Leonardo Silveira Villar, and Luciane Amélia Escaleira. Response surface methodology (RSM) as a tool for optimization in analytical chemistry. *Talanta*, 76(5):965–977, September 2008. ISSN 00399140. DOI: 10.1016/j.talanta.2008.05.019.

[130] Christine M. Anderson-Cook, Connie M. Borror, and Douglas C. Montgomery. Response surface design evaluation and comparison. *Journal of Statistical Planning and Inference*, 139(2):629–641, February 2009. ISSN 03783758. DOI: 10.1016/j.jspi.2008.04.004.

[131] Calyampudi Radhakrishna Rao and Helge Toutenburg. Linear Models. In *Linear Models*, pages 3–18. Springer New York, New York, NY, 1995. ISBN 978-1-4899-0026-5 978-1-4899-0024-1. DOI: 10.1007/978-1-4899-0024-1$_2$.

[132] Xiaoyan Zhang, Wangyang Fu, Cornelia G. Palivan, and Wolfgang Meier. Natural channel protein inserts and functions in a completely artificial, solid-supported bilayer membrane. *Scientific Reports*, 3(1), December 2013. ISSN 2045-2322. DOI: 10.1038/srep02196.

[133] Tillmann Heinisch, Karolina Langowska, Pascal Tanner, Jean-Louis Reymond, Wolfgang Meier, Cornelia Palivan, and Thomas R. Ward. Fluorescence-Based Assay for the Optimization of the Activity of Artificial Transfer Hydrogenase within a Biocompatible Compartment. *ChemCatChem*, 5(3):720–723, March 2013. ISSN 18673880. DOI: 10.1002/cctc.201200834.

[134] Karolina Langowska, Cornelia G. Palivan, and Wolfgang Meier. Polymer nanoreactors shown to produce and release antibiotics locally. *Chem. Commun.*, 49(2):128–130, 2013. ISSN 1359-7345, 1364-548X. DOI: 10.1039/C2CC36345C.

[135] Pavel Broz, Sergey Driamov, Joerg Ziegler, Nadav Ben-Haim, Stephan Marsch, Wolfgang Meier, and Patrick Hunziker. Toward Intelligent

Nanosize Bioreactors: A pH-Switchable, Channel-Equipped, Functional Polymer Nanocontainer. *Nano Letters*, 6(10):2349–2353, October 2006. ISSN 1530-6984, 1530-6992. DOI: 10.1021/nl0619305.

[136] Pascal Tanner, Ozana Onaca, Vimalkumar Balasubramanian, Wolfgang Meier, and Cornelia G. Palivan. Enzymatic Cascade Reactions inside Polymeric Nanocontainers: A Means to Combat Oxidative Stress. *Chemistry - A European Journal*, 17(16):4552–4560, April 2011. ISSN 09476539. DOI: 10.1002/chem.201002782.

[137] Dominik Dobrunz, Adriana C. Toma, Pascal Tanner, Thomas Pfohl, and Cornelia G. Palivan. Polymer Nanoreactors with Dual Functionality: Simultaneous Detoxification of Peroxynitrite and Oxygen Transport. *Langmuir*, 28(45):15889–15899, November 2012. ISSN 0743-7463, 1520-5827. DOI: 10.1021/la302724m.

[138] Madhavan Nallani, Samantha Benito, Ozana Onaca, Alexandra Graff, Marcus Lindemann, Mathias Winterhalter, Wolfgang Meier, and Ulrich Schwaneberg. A nanocompartment system (Synthosome) designed for biotechnological applications. *Journal of Biotechnology*, 123(1):50–59, May 2006. ISSN 01681656. DOI: 10.1016/j.jbiotec.2005.10.025.

[139] StijnF.M. vanDongen, Madhavan Nallani, JeroenJ.L.M. Cornelissen, RoelandJ.M. Nolte, and JanC.M. vanHest. A Three-Enzyme Cascade Reaction through Positional Assembly of Enzymes in a Polymersome Nanoreactor. *Chemistry - A European Journal*, 15(5):1107–1114, January 2009. ISSN 09476539. DOI: 10.1002/chem.200802114.

[140] Muhammad Noor, Tamara Dworeck, Alexander Schenk, Pravin Shinde, Marco Fioroni, and Ulrich Schwaneberg. Polymersome surface decoration by an EGFP fusion protein employing Cecropin A as peptide "anchor". *Journal of Biotechnology*, 157(1):31–37, January 2012. ISSN 01681656. DOI: 10.1016/j.jbiotec.2011.10.005.

[141] Wolfgang Meier, Corinne Nardin, and Mathias Winterhalter. Reconstitution of Channel Proteins in (Polymerized) ABA Triblock Copolymer Membranes. *Angewandte Chemie International Edition*, 39(24):4599–4602, December 2000. ISSN 14337851, 15213773. DOI: 10.1002/1521-3773(20001215)39:24<4599::AID-ANIE4599>3.0.CO;2-Y.

[142] Ozana Onaca, Pransenjit Sarkar, Danilo Roccatano, Thomas Friedrich, Bernard Hauer, Mariusz Grzelakowski, Arcan Güven, Marco Fioroni, and Ulrich Schwaneberg. Functionalized Nanocompartments (Synthosomes) with a Reduction-Triggered Release System. *Angewandte Chemie International Edition*, 47(37):7029–7031, September 2008. ISSN 14337851, 15213773. DOI: 10.1002/anie.200801076.

[143] Sayan Chuanoi, Yasutaka Anraku, Mao Hori, Akihiro Kishimura, and Kazunori Kataoka. Fabrication of Polyion Complex Vesicles with Enhanced Salt and Temperature Resistance and Their Potential Applications as Enzymatic Nanoreactors. *Biomacromolecules*, 15(7):2389–2397, July 2014. ISSN 1525-7797, 1526-4602. DOI: 10.1021/bm500127g.

[144] Ling Lu, Yan Zou, Weijing Yang, Fenghua Meng, Chao Deng, Ru Cheng, and Zhiyuan Zhong. Anisamide-Decorated pH-Sensitive Degradable Chimaeric Polymersomes Mediate Potent and Targeted Protein Delivery to Lung Cancer Cells. *Biomacromolecules*, 16(6):1726–1735, June 2015. ISSN 1525-7797, 1526-4602. DOI: 10.1021/acs.biomac.5b00193.

[145] Pascal Tanner, Vimalkumar Balasubramanian, and Cornelia G. Palivan. Aiding Nature's Organelles: Artificial Peroxisomes Play Their Role. *Nano Letters*, 13(6):2875–2883, June 2013. ISSN 1530-6984, 1530-6992. DOI: 10.1021/nl401215n.

[146] Manish Kumar, Joachim E. O. Habel, Yue-xiao Shen, Wolfgang P. Meier, and Thomas Walz. High-Density Reconstitution of Functional Water Channels into Vesicular and Planar Block Copolymer Membranes. *Journal of the American Chemical Society*, 134(45):18631–18637, November 2012. ISSN 0002-7863, 1520-5126. DOI: 10.1021/ja304721r.

[147] Honglei Wang, Tai-Shung Chung, Yen Wah Tong, Kandiah Jeyaseelan, Arunmozhiarasi Armugam, Zaichun Chen, Minghui Hong, and Wolfgang Meier. Highly Permeable and Selective Pore-Spanning Biomimetic Membrane Embedded with Aquaporin Z. *Small*, 8(8): 1185–1190, April 2012. ISSN 16136810. DOI: 10.1002/smll.201102120.

[148] Mustafa Erbakan, Yue-xiao Shen, Mariusz Grzelakowski, Peter J. Butler, Manish Kumar, and Wayne R. Curtis. Molecular Cloning, Overexpression and Characterization of a Novel Water Channel Protein from Rhodobacter sphaeroides. *PLoS ONE*, 9(1):e86830, January 2014. ISSN 1932-6203. DOI: 10.1371/journal.pone.0086830.

[149] Neha P. Kamat, Myung Han Lee, Daeyeon Lee, and Daniel A. Hammer. Micropipette aspiration of double emulsion-templated polymersomes. *Soft Matter*, 7(21):9863–9866, 2011.

[150] Anthony J. Kim, Mark S. Kaucher, Kevin P. Davis, Mihai Peterca, Mohammad R. Imam, Natalie A. Christian, Dalia H. Levine, Frank S. Bates, Virgil Percec, and Daniel A. Hammer. Proton Transport from Dendritic Helical-Pore-Incorporated Polymersomes. *Advanced Functional Materials*, 19(18):2930–2936, September 2009. ISSN 1616301X, 16163028. DOI: 10.1002/adfm.200900076.

[151] Chiara Martino, Shin-Hyun Kim, Louise Horsfall, Alireza Abbaspourrad, Susan J. Rosser, Jonathan Cooper, and David A. Weitz. Protein Expression, Aggregation, and Triggered Release from Polymersomes as Artificial Cell-like Structures. *Angewandte Chemie International Edition*, 51(26):6416–6420, June 2012. ISSN 14337851. DOI: 10.1002/anie.201201443.

[152] Ho Cheung Shum, Yuan-jin Zhao, Shin-Hyun Kim, and David A. Weitz. Multicompartment Polymersomes from Double Emulsions. *Angewandte Chemie*, 123(7):1686–1689, February 2011. ISSN 00448249. DOI: 10.1002/ange.201006023.

[153] Daniela A. Wilson, Roeland J. M. Nolte, and Jan C. M. van Hest. Autonomous movement of platinum-loaded stomatocytes. *Nature Chemistry*, 4(4):268–274, April 2012. ISSN 1755-4330, 1755-4349. DOI: 10.1038/nchem.1281.

[154] Karmena Jaskiewicz, Antje Larsen, Ingo Lieberwirth, Kaloian Koynov, Wolfgang Meier, George Fytas, Anja Kroeger, and Katharina Landfester. Probing Bioinspired Transport of Nanoparticles into Polymersomes. *Angewandte Chemie*, 124(19):4691–4695, May 2012. ISSN 00448249. DOI: 10.1002/ange.201108421.

[155] Shin-Hyun Kim, Ho Cheung Shum, Jin Woong Kim, Jun-Cheol Cho, and David A. Weitz. Multiple Polymersomes for Programmed Release of Multiple Components. *Journal of the American Chemical Society*, 133 (38):15165–15171, September 2011. ISSN 0002-7863, 1520-5126. DOI: 10.1021/ja205687k.

[156] Ramya Tunuguntla, Mangesh Bangar, Kyunghoon Kim, Pieter Stroeve, Caroline M. Ajo-Franklin, and Aleksandr Noy. Lipid Bilayer Composition Can Influence the Orientation of Proteorhodopsin in Artificial Membranes. *Biophysical Journal*, 105(6):1388–1396, September 2013. ISSN 00063495. DOI: 10.1016/j.bpj.2013.07.043.

[157] Michel Seigneuret and Jean-Louis Rigaud. Use of the fluorescent pH probe pyranine to detect heterogeneous directions of proton movement in bacteriorhodopsin reconstituted large liposomes. *FEBS letters*, 188(1):101–106, 1985.

[158] Michel Seigneuret and Jean Louis Rigaud. Analysis of passive and light-driven ion movements in large bacteriorhodopsin liposomes reconstituted by reverse-phase evaporation. 2. Influence of passive permeability and back-pressure effects upon light-induced proton uptake. *Biochemistry*, 25(21):6723–6730, 1986.

[159] João M. Freire, Marco M. Domingues, Joana Matos, Manuel N. Melo, Ana Salomé Veiga, Nuno C. Santos, and Miguel A. R. B. Castanho. Using zeta-potential measurements to quantify peptide partition to lipid membranes. *European Biophysics Journal*, 40(4):481–487, April 2011. ISSN 0175-7571, 1432-1017. DOI: 10.1007/s00249-010-0661-4.

[160] Daniel Harder, Stephan Hirschi, Zöhre Ucurum, Roland Goers, Wolfgang Meier, Daniel J. Müller, and Dimitrios Fotiadis. Engineering a Chemical Switch into the Light-driven Proton Pump Proteorhodopsin by Cysteine Mutagenesis and Thiol Modification. *Angewandte Chemie*, 128(31):8992–8995, July 2016. ISSN 00448249. DOI: 10.1002/ange.201601537.

[161] Noah Ritzmann, Johannes Thoma, Stephan Hirschi, David Kalbermatter, Dimitrios Fotiadis, and Daniel J. Müller. Fusion Domains Guide the Oriented Insertion of Light-Driven Proton Pumps into Liposomes. *Biophysical Journal*, 113(6):1181–1186, September 2017. ISSN 00063495. DOI: 10.1016/j.bpj.2017.06.022.

[162] J. Philippot, S. Mutaftschiev, and J. P. Liautard. A very mild method allowing the encapsulation of very high amounts of macromolecules into very large (1000 nm) unilamellar liposomes. *Biochimica et Biophysica Acta (BBA)-Biomembranes*, 734(2):137–143, 1983.

[163] Tomaž Einfalt, Roland Goers, Ionel Adrian Dinu, Adrian Najer, Mariana Spulber, Ozana Onaca-Fischer, and Cornelia G. Palivan. Stimuli-Triggered Activity of Nanoreactors by Biomimetic Engineering Polymer Membranes. *Nano Letters*, 15(11):7596–7603, November 2015. ISSN 1530-6984, 1530-6992. DOI: 10.1021/acs.nanolett.5b03386.

[164] C. B. Müller, A. Loman, V. Pacheco, F. Koberling, D. Willbold, W. Richtering, and J. Enderlein. Precise measurement of diffusion by multicolor dual-focus fluorescence correlation spectroscopy. *EPL (Europhysics Letters)*, 83(4):46001, August 2008. ISSN 0295-5075, 1286-4854. DOI: 10.1209/0295-5075/83/46001.

[165] Alice Verchère, Isabelle Broutin, and Martin Picard. Photo-induced proton gradients for the in vitro investigation of bacterial efflux pumps. *Scientific Reports*, 2(1), December 2012. ISSN 2045-2322. DOI: 10.1038/srep00306.

[166] Bradley Jones and Christopher J. Nachtsheim. A class of three-level designs for definitive screening in the presence of second-order effects. *Journal of Quality Technology*, 43(1):1–15, 2011. ISSN 0022-4065.

[167] Bradley Jones and Christopher J. Nachtsheim. Definitive screening designs with added two-level categorical factors. *Journal of Quality Technology*, 45(2):121–129, 2013. ISSN 0022-4065.

[168] John Lawson. *Design and analysis of experiments with R*. Chapman & Hall/CRC texts in statistical science series. CRC Press, Taylor & Francis Group, Boca Raton, 2015. ISBN 978-1-4398-6813-3.

[169] Jifeng Zhang. Protein-Protein Interactions in Salt Solutions. In Weibo Cai, editor, *Protein-Protein Interactions - Computational and Experimental Tools*. InTech, March 2012. ISBN 978-953-51-0397-4. DOI: 10.5772/38056.

[170] Alvaro H. Crevenna, Nikolaus Naredi-Rainer, Don C. Lamb, Roland Wedlich-Söldner, and Joachim Dzubiella. Effects of Hofmeister Ions on the -Helical Structure of Proteins. *Biophysical Journal*, 102(4):907–915, February 2012. ISSN 00063495. DOI: 10.1016/j.bpj.2012.01.035.

[171] R.L. Baldwin. How Hofmeister ion interactions affect protein stability. *Biophysical Journal*, 71(4):2056–2063, October 1996. ISSN 00063495. DOI: 10.1016/S0006-3495(96)79404-3.

[172] Farhana F . Syed. *Citrate Binding to the Membrane Protein Proteorhodopsin*. Dissertation, Syracuse University, Syracuse, 2011.

[173] Matthias Bujara and Sven Panke. Engineering in complex systems. *Current Opinion in Biotechnology*, 21(5):586–591, October 2010. ISSN 09581669. DOI: 10.1016/j.copbio.2010.07.007.

[174] M. Lomora, G. Gunkel-Grabole, S. Mantri, and C. G. Palivan. Biocatalytic nanocompartments for in situ production of glucose-6-phosphate. *Chemical Communications*, 53(73):10148–10151, 2017. ISSN 1359-7345, 1364-548X. DOI: 10.1039/C7CC04739H.

[175] Kasper Renggli, Patric Baumann, Karolina Langowska, Ozana Onaca, Nico Bruns, and Wolfgang Meier. Selective and Responsive Nanoreactors. *Advanced Functional Materials*, 21(7):1241–1259, April 2011. ISSN 1616301X. DOI: 10.1002/adfm.201001563.

[176] Stephan Hirschi, Mirko Stauffer, Daniel Harder, Daniel J. Müller, Wolfgang Meier, and Dimitrios Fotiadis. Engineering and Assembly of Protein Modules into Functional Molecular Systems. *CHIMIA International Journal for Chemistry*, 70(6):398–401, June 2016. ISSN 00094293. DOI: 10.2533/chimia.2016.398.

[177] Thorsten Althoff, Karen M. Davies, Sabrina Schulze, Friederike Joos, and Werner Kühlbrandt. GRecon: A Method for the Lipid Reconstitution of Membrane Proteins. *Angewandte Chemie*, 124(33):8468–8472, August 2012. ISSN 00448249. DOI: 10.1002/ange.201202094.

[178] Joshua Jackman, Wolfgang Knoll, and Nam-Joon Cho. Biotechnology Applications of Tethered Lipid Bilayer Membranes. *Materials*, 5(12): 2637–2657, December 2012. ISSN 1996-1944. DOI: 10.3390/ma5122637.

[179] John Krupinski and Gordon G. Hammes. Steady-state ATP synthesis by bacteriorhodopsin and chloroplast coupling factor co-reconstituted into asolectin vesicles. *Proceedings of the National Academy of Sciences*, 83(12):4233–4237, 1986.

[180] Erik Reimhult and Karthik Kumar. Membrane biosensor platforms using nano- and microporous supports. *Trends in Biotechnology*, 26(2):82–89, February 2008. ISSN 01677799. DOI: 10.1016/j.tibtech.2007.11.004.

[181] Ramya H. Tunuguntla, Mangesh A. Bangar, Kyunghoon Kim, Pieter Stroeve, Costas Grigoropoulos, Caroline M. Ajo-Franklin, and Aleksandr Noy. Bioelectronic Light-Gated Transistors with Biologically Tunable Performance. *Advanced Materials*, 27(5):831–836, February 2015. ISSN 09359648. DOI: 10.1002/adma.201403988.

[182] Samuel Lörcher and Wolfgang Meier. Cosolvent fractionation of PMOXA- b -PDMS- b -PMOXA: Bulk separation of triblocks from multiblocks. *European Polymer Journal*, 88:575–585, March 2017. ISSN 00143057. DOI: 10.1016/j.eurpolymj.2016.12.006.

[183] Hyo-Jick Choi, Hyeseung Lee, and Carlo D Montemagno. Toward hybrid proteo-polymeric vesicles generating a photoinduced proton gradient for biofuel cells. *Nanotechnology*, 16(9):1589–1597, September 2005. ISSN 0957-4484, 1361-6528. DOI: 10.1088/0957-4484/16/9/031.

[184] G. Derringer. Simultaneous optimization of several response variables. *Journal of Quality Technology*, 12(4):214–219, 1980.

[185] Michel Seigneuret and Jean Louis Rigaud. Analysis of passive and light-driven ion movements in large bacteriorhodopsin liposomes reconstituted by reverse-phase evaporation. 1. Factors governing the passive proton permeability of the membrane. *Biochemistry*, 25(21): 6716–6722, 1986.

[186] Hyo-Jick Choi, Jeffrey Germain, and Carlo D Montemagno. Effects of different reconstitution procedures on membrane protein activities in proteopolymersomes. *Nanotechnology*, 17(8):1825–1830, April 2006. ISSN 0957-4484, 1361-6528. DOI: 10.1088/0957-4484/17/8/003.